30306

National Library of Canada / Bibliothèque nationale du Canada

CANADIAN THESES ON MICROFICHE / *THÈSES CANADIENNES SUR MICROFICHE*

NAME OF AUTHOR/*NOM DE L'AUTEUR* Thomas Colin PREDIGER

TITLE OF THESIS/*TITRE DE LA THÈSE* "An optical study of ion and pH effects on phospholipid vesicles"

UNIVERSITY/*UNIVERSITÉ* Simon Fraser University

DEGREE FOR WHICH THESIS WAS PRESENTED/*GRADE POUR LEQUEL CETTE THÈSE FUT PRÉSENTÉE* Master of Science

YEAR THIS DEGREE CONFERRED/*ANNÉE D'OBTENTION DE CE GRADE* 1975

NAME OF SUPERVISOR/*NOM DU DIRECTEUR DE THÈSE* Dr. Konrad Colbow

Permission is hereby granted to the NATIONAL LIBRARY OF CANADA to microfilm this thesis and to lend or sell copies of the film.

The author reserves other publication rights, and neither the thesis nor extensive extracts from it may be printed or otherwise reproduced without the author's written permission.

L'autorisation est, par la présente, accordée à la BIBLIOTHÈQUE NATIONALE DU CANADA de microfilmer cette thèse et de prêter ou de vendre des exemplaires du film.

L'auteur se réserve les autres droits de publication; ni la thèse ni de longs extraits de celle-ci ne doivent être imprimés ou autrement reproduits sans l'autorisation écrite de l'auteur.

DATED/*DATÉ* 21/8/75 SIGNED/*SIGNÉ*

PERMANENT ADDRESS/*RÉSIDENCE FIXE* [redacted]

NL-91 3-74

AN OPTICAL STUDY OF ION AND pH EFFECTS ON PHOSPHOLIPID VESICLES

by

Thomas Colin Prediger

A THESIS SUBMITTED IN PARTIAL FULFILLMENT OF THE REQUIREMENTS FOR THE DEGREE OF

MASTER OF SCIENCE

in the Department

of

BIOLOGICAL SCIENCES

Simon Fraser University

September, 1975

APPROVAL

Name: Thomas Colin Prediger

Degree: Master of Science

Title of Thesis: An Optical Study of Ion and pH Effects on Phospholipid Vesicles

Examining Committee:

Chairman: H.L. Speer

K. Colbow
Senior Supervisor

A.H. Burr

P. Belton

J.S. Barlow

Date Approved: Oct. 14, 1975

PARTIAL COPYRIGHT LICENSE

I hereby grant to Simon Fraser University the right to lend my thesis or dissertation (the title of which is shown below) to users of the Simon Fraser University Library, and to make partial or single copies only for such users or in response to a request from the library of any other university, or other educational institution, on its own behalf or for one of its users. I further agree that permission for multiple copying of this thesis for scholarly purposes may be granted by me or the Dean of Graduate Studies. It is understood that copying or publication of this thesis for financial gain shall not be allowed without my written permission.

Title of Thesis/Dissertation:

"An optical study of ion and pH effects on phospholipid vesicles"

Author:

(signature)

Thomas Colin Prediger

(name)

16/10/75

(date)

ABSTRACT

Sonicated aqueous dispersions of β-γ Dipalmitoyl D-L-Phosphatidyl Choline (DPC) vesicles were studied by means of 90° light scattering and turbidity measurements. Such model membrane studies provide structural and functional information about biological membranes.

The distribution of vesicle sizes of various DPC dispersions was investigated by the turbidity method developed by earlier workers. The time dependence of 90° scattered light intensity was studied as a function of pH for 0 and 10^{-3}M Ca^{+2}. Relative 90° scattered light intensity was studied as a function of temperature in the presence of K^{+} and Ca^{+2}.

Turbidity data were explained in terms of a bimodal vesicle size distribution. The average size of smaller particles was estimated to be 275±25 Å from specific turbidity measurements. The larger particles were estimated to have a size of about 10^{3} Å using the power factor which is obtained experimentally from a logarithmic plot of turbidity as a function of wavelength. The time variation of 90° scattered light is thought to be due to aggregation or fusion of DPC particles. An attempt was made to model the time dependence to reaction rate theory. Vesicle surface charge is believed to determine the rate of aggregation or fusion of vesicles. The study of 90°-scattered-light intensity showed anomalous behaviour as a function of temperature in the presence of K^{+} and Ca^{+2}. This was explained in terms of thermally induced aggregation or fusion of vesicles.

The techniques utilized in this experiment could be of value in determining the physico-chemical conditions which enhance vesicle fusion or aggregation, and possibly help to establish a molecular mechanism for these phenomena. These problems are of fundamental importance to the fusion of biological membranes.

ACKNOWLEDGEMENTS

I wish to thank Dr. K. Colbow for his patient supervision of the research and for his advice and assistance during the preparation of this thesis. Special thanks are set aside for Dr. C.S. Chong for the development of light scattering theory and endless hours of conversation related to the research in this thesis. Also, I wish to thank the other members of the examining committee: Drs. A. Burr, P. Belton, and J. Barlow for their time in examining this thesis.

Several people assisted in the typing of the thesis and the graphical work. I wish to thank Siva Chinniah, Jim Oxten, Silvia Wessel and Lynda Zink for their proficient technical assistance.

I am grateful to Dr. K. Colbow and the Physics Department of Simon Fraser University for their financial assistance during the course of this work.

Deepest gratitude must go to my wife Judie for her patient understanding during this work.

TABLE OF CONTENTS

LIST OF TABLES

LIST OF FIGURES

CHAPTER 1

INTRODUCTION

The structure and function of membranes are highly significant in biological systems. Functions such as passive, active or facilitated transport involve highly specialized membranes. Membranes are also known to play a central role in signal transmission and excitability phenomena. Biological membranes also provide sites for enzymatic, hormonal and drug activities. The elucidation of membrane structure, the organization of component macro-molecules and the studies of their dynamical behaviour have been the subjects of much research for the past few decades.

Membranes have been shown to be composed primarily of two classes of compounds, lipids and proteins. Several attempts have been made to model the geometrical arrangement of these two component classes of molecules in biological membranes. Early investigations by Gorter and Grendal (1925) on monolayers of lipids extracted from erythrocytes indicated that the erythrocyte membrane was bounded by a bilayer of lipid. A similar hypothesis was proposed by Davson and Danielli (1934) to explain some of the permeability properties of the plasma membrane They proposed that membranes consist of a continuous hydrocarbon phase which is contributed by the lipid components of the membrane while proteins are situated exterior to the membrane in

globular or extended form (Fig. 1.1a). Robertson (1957) noting similarities in the electron micrographs of many different types of cell membranes came to conclusions similar to those of earlier authors. Robertson's representation has been termed the unit membrane. Variations in the size of different membranes and the existence of subunits in the plane of the membrane (Sjöstrand 1963) caused several authors (Green, 1966; Korn, 1966; and Parsons, 1967) to criticize the unit membrane hypothesis. New models of membrane structure were proposed by Sjöstrand (1963), Lucy (1964), Benson (1966), Green and Perdue (1966), Wallach and Zahler (1966), Lenhard and Singer (1966), and Hybel and Dorset (1970). However none of these models has enjoyed the wide acceptance of the unit membrane[1].

Current information on the structural organization of biological membranes has been reviewed recently by several authors (Singer 1971, Wallach 1972, Green 1972, Vanderkooi 1972, Singer and Nicholson 1972, Capaldi 1974). The overall packing arrangment of macromolecules in membranes indicated by these studies is of a lipid bilayer which is interrupted by globular protein molecules called intrinsic or integral proteins. These proteins are considered to be amphipathic with a

1. A general review and evaluation of these models may be found in Hendler (1971).

highly polar and a non-polar end (Fig. 1.1a). The polar region is considered to be in contact with the aqueous phase. It contains preferentially polar amino acid residues and covalently bound saccharide residues while the non-polar regions are embedded to varying degrees in the hydrophobic core of the membrane. Extrinsic or peripheral proteins are held at the membrane surface primarily by electrostatic interactions with lipid polar groups. The basic feature of this type of membrane model is its "mosaic" character which allows large fractions of lipids and proteins to be organized independently of each other. Coupled with recent findings that indicate lipids may exist in a bilayer in a fluid state the mosaic model offers the advantage that components of a membrane need not exist in rigidly fixed positions.

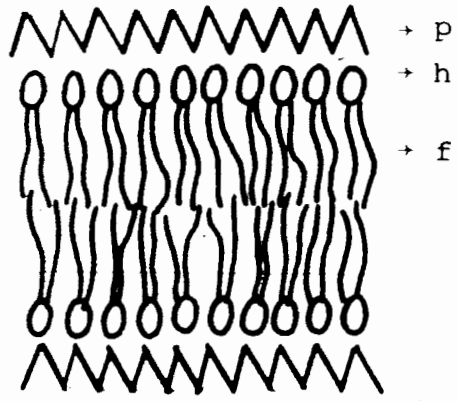

(i) The Davson-Danielli-Robertson model.

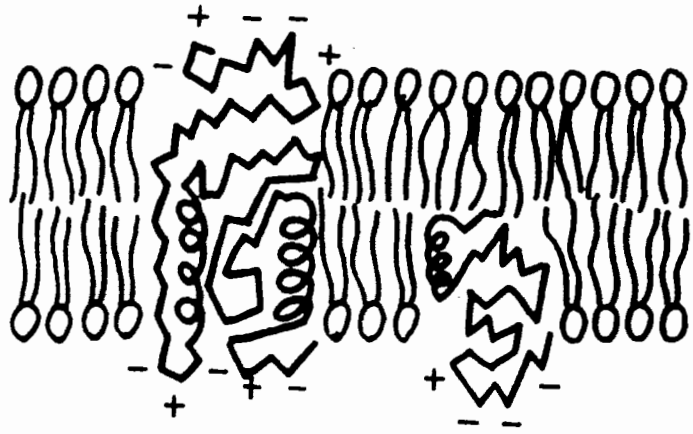

(ii) The fluid mosaic model.

Fig. 1.1a Schematic representations of two membrane models. (i) The Davson-Danielli-Robertson model and (ii) the fluid mosaic model. Symbols p, h and f denote the polypeptide chains of the proteins, the polar head and the fatty acid chains of the phospholipids respectively. The + and - signs represent the ionic residues of the protein (adapted from Singer, 1971).

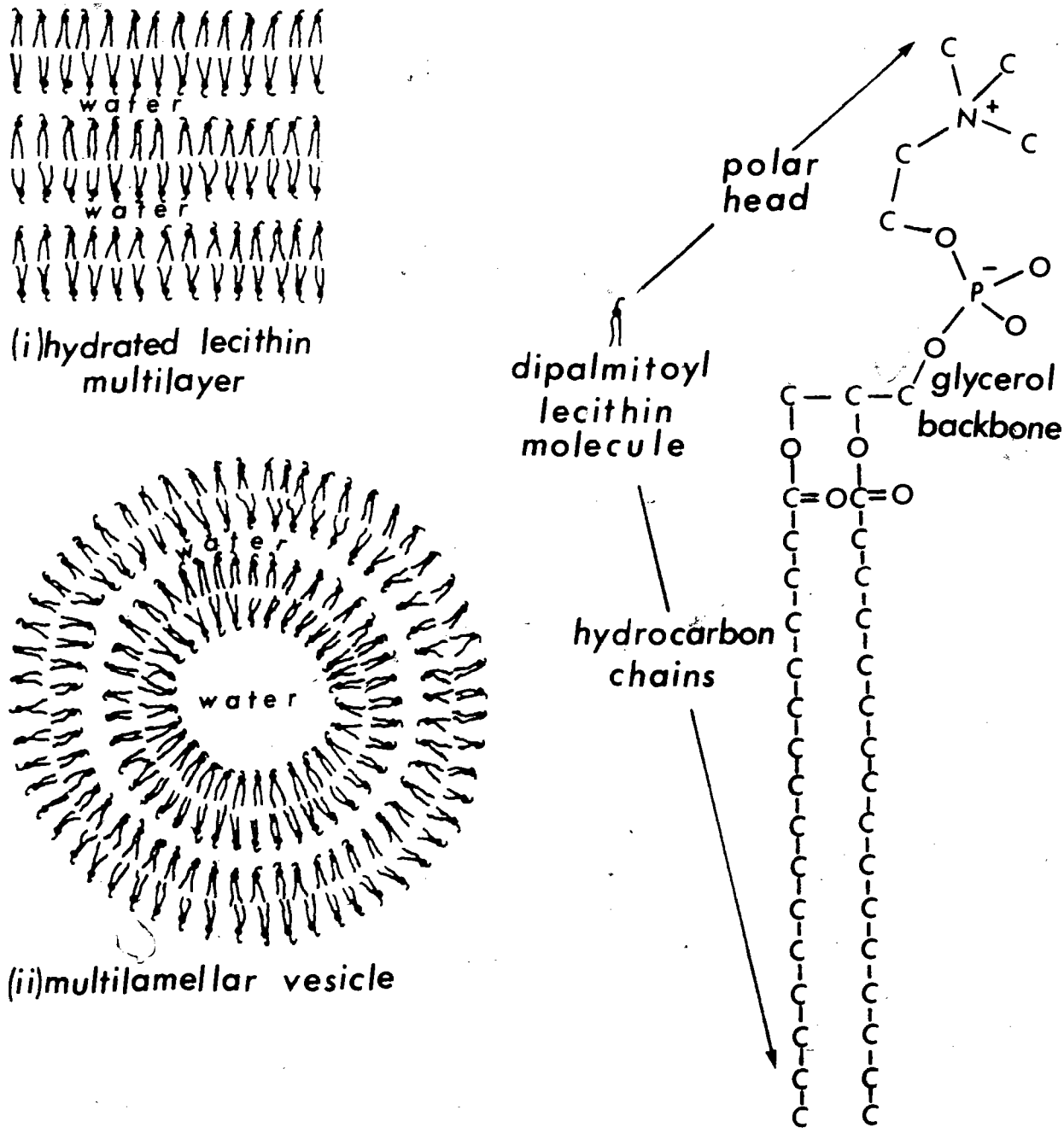

Fig. 1.1b Model membrane systems. (i) Hydrated lecithin multilayer system and (ii) multilamellar lecithin vesicle. The structure of the phospholipid, dipalmitoyl lecithin is shown with the polar group in the gauche conformation. The hydrogen atoms bonded to the carbon atoms are not shown.

Since lipids are known to be basic components of all cell membranes it seems worthwhile studying the properties of model lipid membranes in water in the absence of proteins. Four types of experimental model systems which have received particular attention are monolayers, multilayers, black films and vesicles (Fig. 1.1b).

Monolayers of lipid molecules at an air-water interface can be used to considerable advantage for the evaluation of chemical and physical interactions between molecules. The work of Langmuir (1935) and later, Shah and Schulman (1967) gave interesting results on the interactions of membrane lipids and various ions in the aqueous solution. The obvious drawbacks of this system are that a monolayer consists of only one layer of lipid molcules at an air-water interface and it does not separate two aqueous phases.

Luzzati (1969) used multilayers to study structural parameters and phase transitions of various lipids by means of x-ray diffraction. By varying the water content and the temperature of various lipid systems he was able to obtain phase diagrams and packing arrangments of lipids in various physical situations. Changes in phase were attributed to changes in the packing arrangements of lipid molecules and variations in the mobility of the hydrocarbon chains of the lipids.

Black films (Rudin and Mueller et al. 1964) are produced by dissolving lipid in an organic solvent such as n-decane and spreading this solution over a Teflon hole which separates two aqueous compartments. Capacitance (Hanai et al. 1964) and Optical (Thompson and Huang 1966) measurements showed this film to be of lipid bilayer thickness. While this is a useful system for electrical conductance studies it sometimes gives insufficient sensitivity when larger amounts of materials are required for calorimetry, NMR, ESR, fluorescent probes, electron microscopy and light scattering which are useful techniques to obtain information on phase transitions, molecular conformation and mobility.

A model system which has proven useful when higher sensitivity is required is a suspension of lipid particles in water (Bangham 1968). These suspensions are called vesicles. The lipid used in this thesis was ,β-γDipalmitoyl D-L-α Phosphatidyl Choline called DPC. The choice was based mainly on the fact that a substantial fraction of phospholipids in cell membranes is phosphatidyl choline. The presence of a well documented hydrocarbon chain length (16:0) is important in a model system experiment. In addition DPC has a characteristic thermotropic phase transition at an experimentally convenient temperature (41°C in excess water).

Size and shape are important properties of vesicles whether single-walled or multilamellar. The method of preparation determines the vesicles one obtains. Bangham merely shook the lipid water mixture until a cloudy suspension was obtained. These vesicles were shown to be onion shaped structures. Huang (1969) showed that prolonged sonication followed by treatment on a sepharose column gave vesicles consisting of a single bilayer of lipid separating two aqueous phases. More recently Batzri, Korn (1973) and Colbow (1973) have shown that vesicles of a bilayer nature may be obtained by dissolving a lipid in a polar solvent such as ethanol and injecting the mixture into water. Irrespective of the mode of preparation there is always the problem of determining the size distribution of the suspension which is usually done by electron microscopy. With electron microscopy there is always the question of how much the system may be perturbed by the fixing procedure. Optical techniques such as light scattering which are simple and non-destructive give a detailed specification of a sample one may wish to use in later experiments. However interpretation of optical data such as light scattering has been difficult in the past (Atwood and Saunders 1971, Tinker 1972). Recent progress (Chong 1975, Chong and Colbow to be published) has yielded new methods for interpreting 90° scattered light and turbidity data on vesicles by utilizing the Rayleigh-Gans theory of light scattering which is discussed in Chapter 5. The author has utilized turbidimetry to determine the distribution and size of lipid vesicles prepared by the sonication method.

1.2 DETECTION OF VESICLE FUSION BY LIGHT SCATTERING

Experiments involving the fusion of two black films have been performed by Montal and Muller (1972), Liberman and Nenashev (1972), Badzhinyan et al. (1971) and Neher (1974). This technique is of importance in the construction of asymetric model membranes. It should be possible to obtain information on the kinetics of this fusion process by observation of changes in electrical parameters such as conductance or capacitance as a function of time. Recently Pohl et al. (1973) and Drachev (1974) have incorporated dyes or proteins into black bilayers by the fusion of liposomes with bilayers. This technique may be of further importance in studying vesicle-cell interactions.

The fusion of single compartment vesicles of certain phospholipids has been reported by Taupin and McConnel (1972), Maeda and Ohnishi (1974), Prestegard and Fellmeth (1974) and Papahadopoulas et al. (1973). Although fusion between vesicles may be an oversimplification of events involved in the fusion of intact membranes the results of these recent experiments seems to demonstrate that vesicles will be an extremely valuable model system for the study of membrane fusion. Background on the fusion of biological membranes is discussed in Chapter 2.

Since changes in scattered light intensity are indicative of changes in the size, shape and number of scattering particles it seems reasonable that light scattering and turbidimetry be a worthwhile technique for the investigation of a membrane phenomena such as fusion. Since intact biological membranes are extremely complex the author has confined himself to investigating the intensity of scattered light as a function of time and lipid concentration for DPC vesicles prepared by sonication. Changes in scattered light intensity with time were attributed to fusion or aggregation of vesicles.

While some work has been done on the topic of vesicle fusion, as outlined in an earlier paragraph, little is known of the mechanism by which fusion may take place and factors which affect fusion, such as membrane fluidity and membrane surface charge. Of interest in this thesis is the effect of vesicle surface charge on the time variation of scattered light intensity. Since DPC has a negatively charged phosphate group and a positively charged trimethyl ammonium group variations in vesicle surface charge are obtainable by varying the bulk pH of the vesicle solution. Addition of ions which bind to DPC such as Ca^{+2} provide an alternative method of charging vesicles. The $\Delta S/\Delta t$ values obtained as a function of pH gave interesting results which could be interpreted by comparing the coulombic repulsion energy to vesicle thermal energy. Also of interest was the kinetics of the fusion or aggregation process. An attempt to explain the data in terms of reaction rate theory was made, but much work remains to be done in this regard.

1.3 TEMPERATURE DEPENDENCE OF SCATTERED LIGHT INTENSITY.

Träuble (1971) and Chong (1975) have used 90° light scattering to observe thermotropic lipid phase transitions. Lipid phase transitions are discussed in more detail in Chapter 3.3. By applying the Rayleigh-Gans theory of light scattering to the various structural parameters of DPC, Chong (1975) was able to predict a 30-39% decrease in scattering intensity between 25°C and 50°C. This decrease is in good agreement with the experimental observations of this author, Chong (1975) and earlier workers on vesicle suspensions prepared at temperatures above the phase transition temperature of 41°C in aqueous solutions at pH 6.8 and low ionic strength. We are interested in the effect of ions (specifically K^+ and Ca^{+2}) on these phase transitions. In particular two effects are expected. 1) A slight variation in transition temperature due to binding of ions is expected on the basis of the Guoy theory (Träuble and Eibl 1974). This effect is small for DPC due to the low surface charge on DPC. 2) Even though the surface charge is low the coulombic interactions between vesicles are shown to be sufficient to cause repulsions between vesicles. Variation of temperature increases the thermal energy of vesicles and may cause variations in ion binding (the binding of ions is discussed in 3.4) which in turn may cause fusion or aggregation of vesicles. Strong indications of this behaviour were observed in the presence of K^+ and Ca^{+2} in the vesicle suspension.

CHAPTER 2

MEMBRANE FUSION

2.1 INTRODUCTION

The purpose of this chapter is to provide discussion on the fusion of biological membranes. Though the concern of this thesis is directed towards a model system approach, the author feels that the motivation for this study has its roots in biological membrane phenomena and therefore the biological aspects of the problem should not be ignored.

2.2 IMPORTANCE OF FUSION IN BIOLOGY

Fusion of membranes is an important event in cell biology. Within living cells, membrane fusion is necessary for the incorporation (endocytosis) and subsequent digestion of extracellular material and also for the transport and discharge of intracellular material to the extracellular space (exocytosis). The formation of endocytotic vesicles at the cell surface involves the invagination of a segment of the plasma membrane which must fuse in order to form a closed vesicle. Subsequently the digestion in the endocytotic vesicles involves a series of membrane fusion sequences between these vesicles, lysosomes and Golgi vesicles (Fig. 2.1). Membrane fusion may also play a role in the reverse process of exocytosis in which

fusion takes place at the cell surface between the membrane of the exocytotic vesicle and the plasma membrane. Exocytotic discharge is basic to the process of cell excretion and secretion (Fig. 2.1) and is known to be involved in the release of a wide variety of enzymes, hormones and neurotransmitter substances from a wide variety of cells. Table 2.1 summarizes some tissues which are thought to exhibit these properties. It should be stressed here that there is not universal agreement that exocytosis is the only mechanism by which secretion and digestion are attained. A detailed discussion of this point may be found in (Poste and Allison 1973). Other alternatives to actual fusion which have been suggested and no doubt have applicability in certain situations are summarized in Fig. 2.2 (Smith, 1972). It may be noted however that all these suggestions involve the interaction of a vesicle with a membrane, the difference lying in the mechanism.

Table 2.1: Some Examples of Membrane Fusion in Secretion and Exocytosis Observed by Electron Microscopy.

Tissue	Diameter of Secretory Granule (μm)(microns)	Substance Secreted
Adrenal Medulla	0.2	Catecholamines
Pancreas	0.3	Insulin
Pancreas	1.0	Digestive Enzymes
Mast Cells	0.4	Histamine
Cholinergic Synapses	0.05	Acetylcholine
Adrenergic Synapses	0.08	Noradrenaline

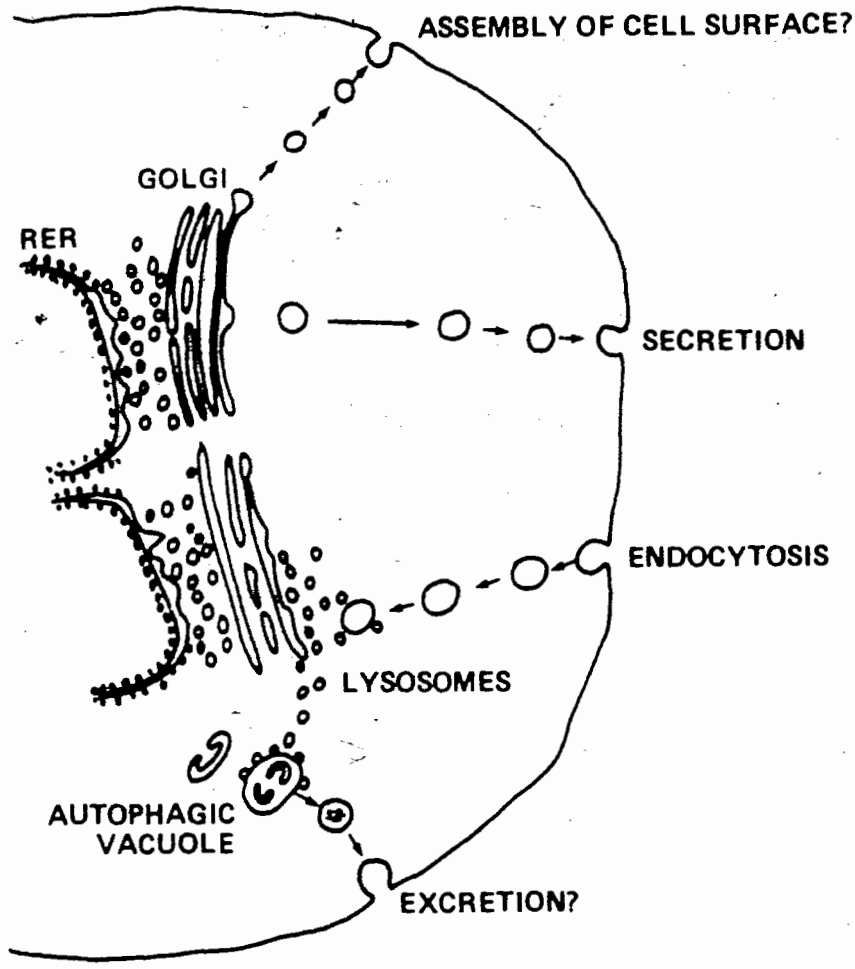

Fig. 2.1 Schematic representation of importance of membrane fusion in the functional relationship between the endoplasmic reticulum, the golgi apparatus and lysosomes and in the entry and release of material from the cell.

The fusion and incorporation of vesicles from the Golgi apparatus into discrete regions of cell membranes may be a common occurance in most, if not all cells and has been suggested as a possible mechanism for obtaining quantitative and qualitative variations in the distribution of materials at the cell surface and for determining specificity on the cell surface (Hirano et al. 1972). Membrane fusion is also felt to be important in the turnover and redistribution of membranes within a cell. Bursts of exocytotic activity involving fusion of secretory granules with the plasma membrane are expected to produce a significant increase in the surface area of the plasma membrane unless mechanisms were available to compensate for the increase. Therefore cycles of exocytosis and endocytosis are thought to provide a mechanism for reutilization and retrieval of membranes (Nagasawa et al. 1970).

Cell fusion is known to occur as a cytotic or cytopathic response to infection with a number of DNA and RNA containing viri. The emergence of virus induced cell fusion as a tool for producing hybrid cells and heterokaryons for the experimental study of genomic and phenotypic regulation, gene mapping and the study of malignancy in cells has shown the need to understand the molecular mechanism of the fusion reaction.

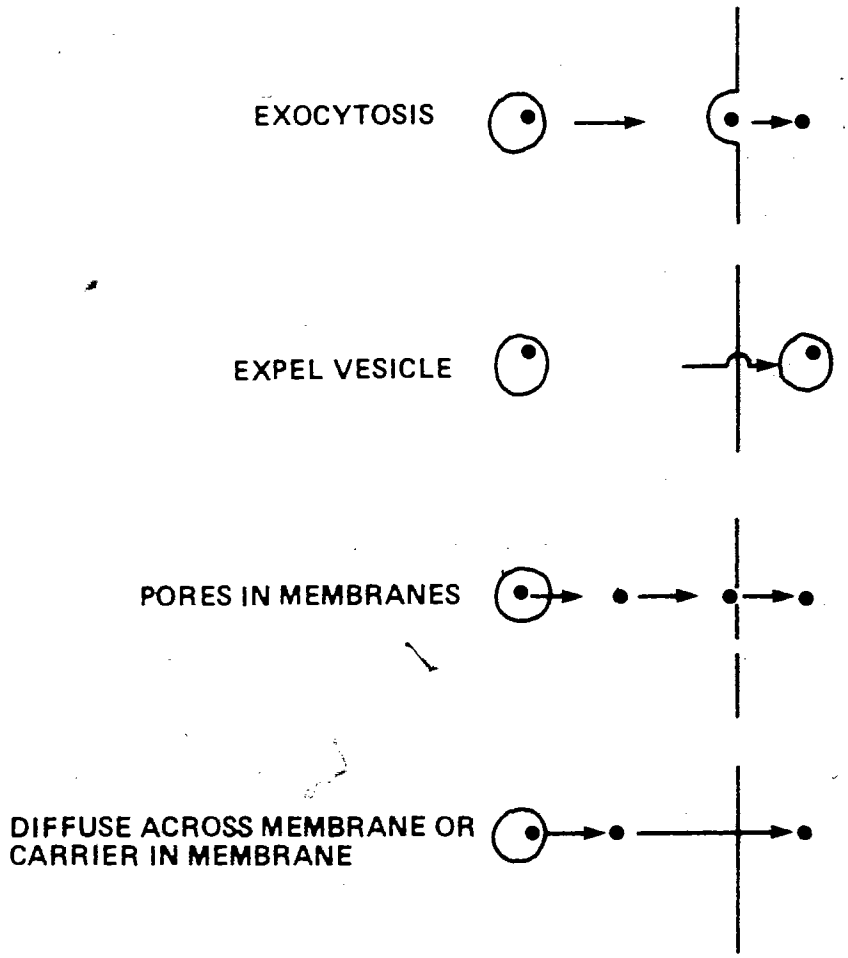

Fig. 2.2 Schematic representation of the possible mechanisms by which material within a secretory vacuole can reach the extracellular space.

2.3 FACTORS WHICH MAY AFFECT MEMBRANE FUSION

Knowledge of the preferred conformations of membrane macromolecules and their motional freedom is necessary for any understanding of the membrane fusion reaction since these factors determine the type of interaction that can occur between macromolecules in adjacent membranes during fusion. The conformational state of macromolecules in membranes has been briefly discussed in Chapter 1 in terms of the fluid mosaic model of membrane structure. This model offers considerable opportunity for rapid changes in the conformation and distribution of membrane macromolecules in response to changes in environment near the membrane.

The motional freedom of membrane macromolecules is clearly of importance in the membrane fusion reaction. No firm conclusions can yet be made concerning the precise identity of the interaction between membrane macromolecules during fusion but it is possible to discuss factors which constrain the motion of membrane components. A discussion of thermal behaviour of lipids will follow in Chapter 3.3. The motional freedom and spatial arrangement of proteins is thought to be sensitive to the relative fluidity of the lipid matrix. A fluid lipid matrix facilitates the lateral diffusion of membrane components. It is possible that this lateral diffusion might provide a sensitive mechanism for rapid structural rearrangements of membranes in response to change in the environment close to the membrane.

Membrane fusion requires that membranes be brought into opposition at molecular distances. The fact that cells are charged suggests the existence of electrostatic interactions between membranes. The fact that all vertebrate cells carry a net negative charge (Weiss 1967) suggests that electrostatic interactions between cells would be repulsive at large distances (several cell diameters). The other primary interaction is the short range interaction the London-Van der Waals force, which is attractive. An excellent review of the theory of electrodynamics applied to Biology is found in Parsegian (1974). Although these are exact physical theories their application to membranes has been limited due to uncertainties in membrane structure. Suffice it to say that contact is determined by the charge distributions on membranes over entire surfaces and in small domains. However we do not know the charge distribution.

The ability of membranes to fuse is also affected by the local ion concentration specifically Ca^{+2}, Mg^{+2} , ATP and ATPase activity. This is discussed in the next section.

2.4 A POSSIBLE SCHEME FOR MEMBRANE FUSION

Poste and Allison (1973) postulate that membrane fusion, whether it be cell-cell fusion or vesicle-cell fusion, may be thought of as a four stage reaction.

The first stage is a direct molecular contact between membranes. As mentioned earlier the electrodynamic approach to determining membrane contact is useful only when one knows the distribution of

charge on the surface. Other factors which are believed to influence cell contact have been suggested by various authors. These may be natural tissue specific "aggregating" factors (Henkert et al. 1973), synthetic polymers (Brooks, 1973), or polyelectrolytes (Katchalsky et al. 1959). Divalent cations are believed to sit between negative acid groups on opposing surfaces (Steinburg 1962). There can be extensive hydrogen bonding between cell surface dipoles holding onto other cells or onto an artificial substrate. Enzyme substrate complexing may occur between adjacent surfaces (Roth 1973). Binding between antibodies and antigenic sites may take place. Electrostatic attraction between surfaces of unlike charge may arise in some cases while long-range electrodynamic attractive forces may act at longer distances (Curtis 1962). The degree to which some or all of these possibilities are applicable in real life is unknown. What is important here is that contact is necessary for fusion to take place.

The second stage in the reaction is the induction stage. This stage is considered to require displacement of Ca^{+2} and ATP from the membranes. This statement is based on widespread findings which demonstrate that fusion is dependent upon an active energy source and the presence of Ca^{+2}, but is inhibited by high concentrations of Ca^{+2}, Mg^{+2} and ATP at both the cellular and subcellular level. It has been postulated that fusion is similar at the cellular and subcellular level (Poste and Allison 1974).

Further evidence supporting this hypothesis is the observation that ATPase is necessary for the removal of membrane bound Ca^{+2}.

This is expected to increase the fluidity of the membranes. As mentioned earlier changes in membrane fluidity imparts different motional freedom to membrane components. Little work has been done relating membrane fluidity with fusion capacity.

The third stage in the reaction is the fusion itself. This involves the formation of stable linkages between macromolecules in neighbouring membranes. Membrane fluidity is thought to be important here for two reasons. First, increased motional freedom of macromolecules due to Ca^{+2} displacement is expected to increase the chance for successful interactions between molecules in opposed membranes. Secondly, a fluid structure would encourage rapid intermixing of components during fusion. Lucy (1970) suggests that fusion occurs by interdigitation of micelles in adjacent membranes. This hypothesis seems unacceptable since there is no evidence in support of lipid micelles in physiological conditions. It also ignores the likelihood that intrinsic proteins are involved in the fusion reaction.

The last stage is stabilization of the membrane which is thought to be the reverse of stage 2, the replacement of Ca^{+2} and ATP to the membrane.

An important deficiency in this scheme is the lack of a stimulus for each of these stages. What stimulus is there to promote cell contact? What stimulates membranes to release ATP and Ca^{+2}? In stage 4, how does Ca^{+2} and ATP bind to the membrane? There are a number of agents which are known to enhance membrane fusion.

Lysolecithin (Lucy 1970) is often mentioned as a candidate for triggering the fusion reaction by enhancement of micellization of lipid in membranes. However many other lipophilic and lipolytic agents have been shown to induce fusion. These include retinol, oleic acid, glycerol mono-oleate, sucrose monolaurate, DL-sphingosine sulphate, sorbitan monolaurate and phospholipase C. There seems to be no solid evidence to confirm lysolecithin as a fusion initiator. Another notion on how fusion is initiated is that of Poste and Allison (1971). Formation of minimum primary contacts between opposed membranes may be sufficient to initiate the fusion reaction. Surface contact between membranes is expected to alter the orientation of charged groups and dipolar groups within membranes. Changes in charge and dipolar orientation would be expected to produce conformational changes of some membrane macromolecules. These conformational changes may account for changes in Ca^{+2} binding in stage 2. Though much of this discussion is speculative in nature and the experimental evidence for various stages scarce, this model may be subjected to experiment and is therefore worth considering.

2.5 EXPERIMENTAL MODELS FOR MEMBRANE FUSION

Most of the information obtained on membrane fusion has been through observations of the cellular processes in which fusion occurs. Direct experimental study of the fusion reaction has been frustrated by the lack of suitable systems in which events in the membrane may be evaluated at the molecular level.

Cell fusion "in vitro" has been advanced as a potential model for the study of membrane fusion. Although the actual fusion of two cells takes place very rapidly, the number of cells fusing at any time is very low and fusion assessed in terms of the whole system is extended over several hours with still only a small percentage of cells fusing. Although certain cell fusion viruses (Harris H. 1970) may enhance this process, this technique is far from perfected. The study of factors which influence the extent of the fusion reaction and gross aspects of control and regulation are undoubtedly useful but cannot yet provide precise information on the molecular changes in membranes. One example of virus induced cell fusion which may overcome these criticisms is the fusion of lipid enveloped virus such as the Sendai virus with the plasma membranes of cells "in vitro" which occurs in the first stage of virus infection (Apostolov and Poste 1972).

It seems reasonable that systems of lower complexity should be useful in this type of study. The use of artificial membrane systems prepared from components known to occur naturally in membranes would appear to offer such possibilities. An attempt to model this behaviour is part of the concern of this thesis.

CHAPTER 3

VESICLES

3.1 METHODS OF PREPARATION

Earlier methods of preparing lipid water suspensions consisted of dissolving a known amount of lipid in chloroform. A known volume of solution could then be evaporated over dry N_2. An aqueous solution was added and the mixture was shaken until a cloudy suspension was obtained (Bangham and Horne 1964). The micro-structure of these suspensions was shown to be the smectic mesophase or onion structure by x-ray diffraction and electron microscopic techniques (Stoeckenius, Schulman and Prince 1960). The size distribution of vesicles produced in this manner was highly variable thus making certain types of experiments, such as transport studies, very difficult to perform. Therefore, more refined methods were required.

Prolonged ultrasonic treatment of lipids in water followed by a secondary treatment, such as column chromatography (Huang 1969, Sheetz and Chan 1972), has been shown by electron microscopy and sedimentation velocity experiments to produce a nearly homogenous distribution of single bilayer vesicles of an average diameter of about 250 Å. The efficiency of this procedure has been shown to depend upon sonication time (Atwood and Saunders 1965), salt concentration (Sheetz and Chan 1972) and the temperature at which the

sonication takes place (Chapman 1974). It has also been suggested that chromatography may influence the vesicles aggregation. Furthermore, the pretreatment for electron microscopy may be open to the criticism that the method of treatment may not produce a true replica of the vesicles. Despite these criticisms and the difficulties involved in obtaining a homogenous distribution of vesicles, sonication followed by secondary treatment remains the most widely utilized method of vesicle preparation.

A more recent method for making vesicles involves the dissolving of a bilayer forming lipid in a water soluble organic solvent such as ethanol. The ethanol lipid solution is injected into water with a Hamilton syringe. This procedure gives lipid water suspensions which are indistinguishable from those obtained by other methods provided the ethanol concentration is sufficiently small (less than 10% by weight; Batzri and Korn 1973, Colbow 1973). The average size of these vesicles was estimated to be about 250 Å by electron microscopy. Vesicles prepared by this method must be concentrated usually by ultrafiltration before they are useful in other experiments. This method has not yet been implemented as extensively as the sonication method for vesicle preparation, but may prove useful in future.

3.2 THERMAL BEHAVIOUR OF LIPIDS IN WATER

As mentioned in the previous chapter, the conformations and physical states of membrane macromolecules influences membrane phenomena such as fusion. Thus it seems reasonable to devise methods

for studying these properties in model systems. Factors which influence properties of lipids are temperature, degree of saturation, and hydrocarbon chain lengths.

The capillary melting points of anhydrous lipids are quite high (diacyl phosphatidylethanolamine 200°C, phosphatidyl cholines 230°C). These values are independent of both the chain length and the degree of unsaturation of the fatty acid residue associated with the phospholipid. These melting points can be compared with those of other long chain molecules. The melting points of fatty acids containing the same length of hydrocarbon chain are much lower (stearic acid 69.7°C). On the other hand, the capillary melting point of sodium stearate is 300°C. The high capillary melting points are therefore consistent with the occurrence of ionic linkages existing in the crystal associated with the polar groups of the phospholipid. The higher melting points of the sodium soaps, compared with the phospholipids, suggest that there is greater ionic character associated with the polar groups of these molecules. In addition to the capillary melting point, a number of other thermotropic phase changes occur. These thermotropic phase changes have been demonstrated by a wide variety of physical techniques (Chapman 1974). The main conclusions of these various studies are as follows. Firstly, even with fully saturated phospholipids some molecular motion occurs in the solid. Secondly, when the phospholipid is heated to a higher temperature, it reaches a transition point where a marked endothermic change occurs and the lipid hydrocarbon chains exhibit a

much higher degree of molecular motion. For phospholipids containing shorter chain lengths or unsaturated bonds, those marked endothermic phase transitions occur at lower temperatures. The temperatures at which these transitions occur parallel the behaviour of the melting point of the related fatty acids. The transition temperatures are high for the fully saturated long chain phospholipids and are lower when there is a double bond present. This variation of transtion temperature seems to imply that this phase transition is primarily associated with a melting of the hydrocarbon chains of the phospholipids which is a reflection of the dispersion forces between the chains.

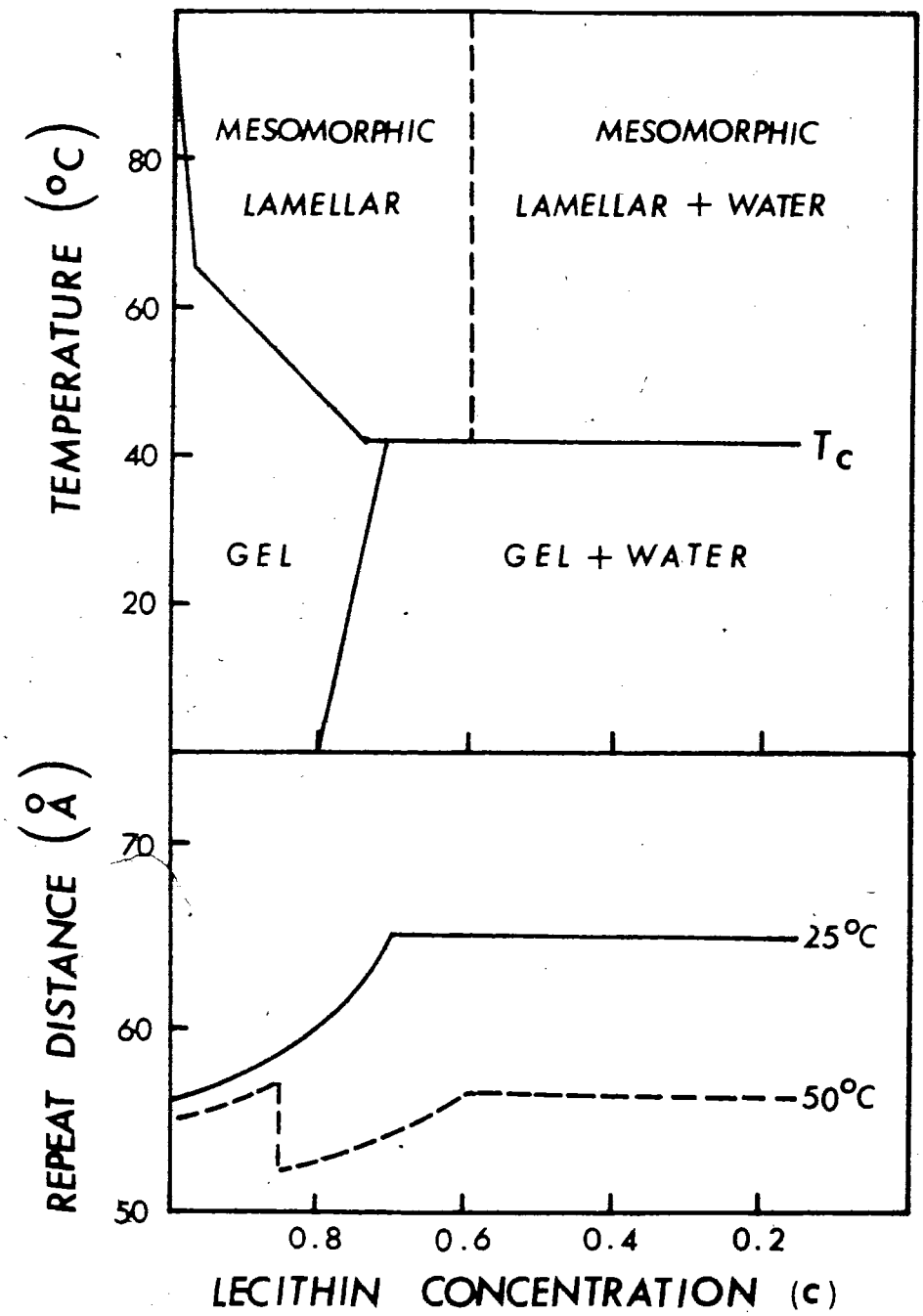

Fig. 3.1 The phase behaviour of dipalmitoyl lecithin-water system. (adapted from Chapman et al. 1967).

Since biological membranes exist in an aqueous environment it is important to study the effects of water on lipid systems. Small amounts of water are known to have unusual effects upon the mesomorphic behaviour of phospholipids. Fig. 3.1 shows the phase diagram of the 1,2 dipalmitoyl-1-phosphatidyl choline-water system (Chapman et al. 1967). It is seen that on the addition of water the transition temperature of the phospholipid is lowered to a certain limiting value T_c which is independent of addition of more water. Above T_c the phosphatidyl choline water system exists in a mesomorphic lamellar phase consisting of bimolecular layers of lipid molecules separated by layers of water. The long hydrocarbon chains of the lecithin molecules are in a fluid state and the polar groups are on the surface separating the lipid water layers. The composition of the system at maximum hydration is about 40% water. On addition of more than 40% water the system dissociates into two phases, the mesomorphic lamellar phase and the water phase. When the phosphatidyl choline/water system is cooled below the T_c line, the hydrocarbon chains adopt an ordered packing. The structure of this phase is also lamellar. The large amount of bound water taken up by the phosphatidyl cholines (about 20%) which does not form ice below $0^{o}C$ is probably due to the formation of a hydrate structure associated with the polar groups. In dispersions of synthetic lipids this phase transition has been observed by a variety of physical techniques such as x-ray diffraction (Luzzati 1968), differential thermal analysis (Chapman et al. 1967), dilatometry (Träuble and Haynes 1971), ESR

(Hubbel and McConnell 1971), NMR (Barker et al. 1972; Lee et al. 1972) and laser Raman investigations (Lippert and Peticolas 1971). Most recently, the phase transition has been revealed by several convenient optical methods using 90° light scattering, absorption, or fluorescent probing (Träuble 1971; Säckmann and Trauble 1972; Colbow 1973; Chong 1975). As a result of these studies, it became apparent that below the transition temperature T_c, which is characteristic for each lipid, the hydrocarbon chains in the bilayer are in the all-trans conformation forming a hexagonal closely packed array. The transition is accompanied by a loss of order in the two dimensional lattice, a sudden increase in chain mobility, a lateral expansion in the plane of the membrane and a net increase in volume per lipid molecule. The fluid state, $T>T_c$, permits rapid lateral diffusion of the lipid molecules in the plane of the membrane. The transition is highly co-operative and therefore, a large number of lipid molecules in a continous phase are a prerequisite for its occurence. For dipalmitoyl-phosphatidyl choline this temperature has been measured to be 41°C.

In addition to the usual 41°C phase transition a second phase transition at about 34°C (which we term the pretransition) has been observed by fluorescent probing (Colbow 1973), calorimetry (Hinz and Sturtevant 1972), NMR (Sheetz and Chan 1972) and dilatometry (Nagle 1974). The nature of this phenomena is not well understood but it has been suggested to be due to the realignment of lipid polar groups (Colbow 1973; Ladbrook and Chapman 1969). A discussion of polar group configurations appears in the next section.

Lipid phase transitions have been detected in Mycoplasma laidlawii, Micrcooccus lysodeicticus and mammalian membranes by differential scanning calorimetry (Steim et al. 1969; Reinert and Steim 1970; Melchior et al. 1970; Ashe and Steim 1971; Blazyk and Steim 1972). In Mycoplasma membranes Engleman (1970, 1971) and Abramson and Pisetsky (1972) have detected thermal transitions by x-ray diffraction and turbidimetry. It is not surprising that lipid phase transitions are detected in living organisms, but yet it must be noted that most organisms are remarkably stable with respect to temperature, thus it would seem that thermally induced phase transitions do not play a role in most living systems. However, ions binding to the polar groups may affect membrane fluidity (Träuble and Eible 1973). Organisms which are capable of altering hydrocarbon chain length or degree of saturation may be capable of changing phase transition temperature in their membranes. The degree to which proteins affect membrane fluidity has not been studied to any great extent. It is suspected that protein configurations are partly controlled by the state of lipid molecules in membranes. Lipid vesicles would seem to be a good model for studying the methods by which phase transition may be induced in membranes.

3.3 INTERACTIONS OF IONS WITH LIPID VESICLES

The binding of alkali and alkaline earth metals by lipids was suggested by some of the earliest investigators of lipid chemistry (Koch and Pike 1910). The first quantitative study of sodium and

potassium binding by cephalin was reported by Christensen and Hastings (1940). Recently investigators have again emphasized the importance of this type of metal binding in biological systems. There are indications that such metal chelation is important in lipoprotein formation, cation transport and other biochemical processes such as membrane fusion.

The binding of ions to monolayers of various lecithins such as dioleoyl, egg and dipalmitoyl phosphatidyl choline has been studied extensively by Shah and Schulman (1965a, 1965b, 1967) by means of the Langmuir technique and surface potential measurements. This work showed that ions such as K^+ and Ca^{+2} were able to bind to the polar head of lipid molecules. The degree of binding was found to be proportional to the degree of saturation of the hydrocarbon chains (Fig. 3.2) which is important in the packing of lipid molecules. At large molecular separations (due to unsaturated hydrocarbon chains) water and hydrated monovalent ions compete for binding sites with Ca^{+2}. As the intermolecular distance decreases one Ca^{+2} shared between two phosphate groups binds more readily than two monovalent ions. The highly saturated lipids such as DPC were found to bind divalent cations more readily than highly unsaturated lecithins.

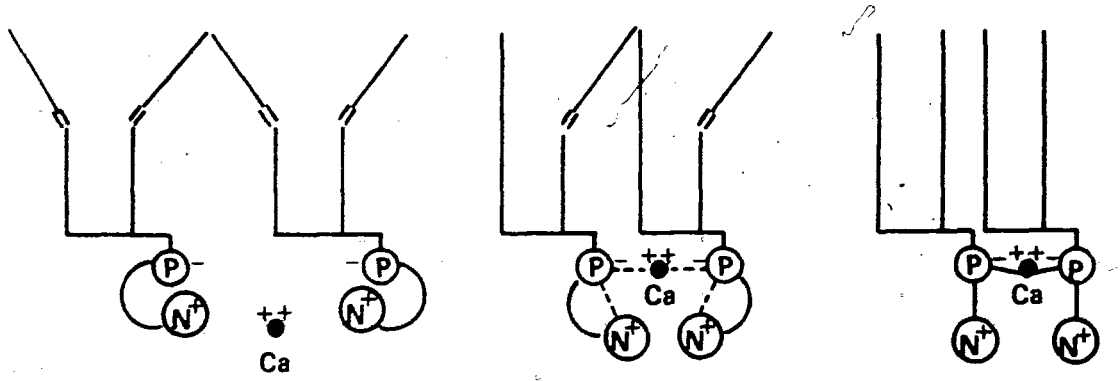

Fig. 3.2 The effect of hydrocarbon chain saturation and internal salt linkage on binding of ions.

The binding of ions cannot be explained on the basis of intermolecular spacing alone, as has been shown by varying the head groups of lipids with the same hydrocarbon chains. Also occurring are internal salt linkages (Fig. 3.2) between the phosphate group and the trimethyl ammonium which inhibit the binding of ions on the polar group of lipids. The strength of this salt linkage is dependent upon the degree of saturation of the hydrocarbon chains. The polar groups of highly unsaturated lipids have lower ionic repulsion between like charges allowing the salt linkage to occur more readily. Highly unsaturated lipids have high interionic repulsions, thus one way the dipoles may align themselves is perpendicular to the layer, thus minimizing the internal linkage. High salt concentration is also capable of breaking this linkage by internal neutralization of oppositely charged groups of adjacent molecules. Ca^{+2} seems to be more effective than Na^{+} in discharging the salt linkage. It is not

known how well these concepts will apply to vesicles since parameters related to intermolecular spacing and state of compression are not as well defined as in monolayers.

It is believed that at low pH's a phospholipid such as dipalmitoyl phosphatidyl choline is protonated at the phosphorous head group and dissociates according to

$$-PO_4H \overset{K_1}{\rightleftharpoons} -PO_4^- + H^+ \qquad 4.1$$

The bulk pK_1 of this reaction was found to be 1.40 (Seimya and Ohki 1972). At higher pH the methyl ammonium group must absorb a hydroxide:

$$N(CH_3)_3^+ \ldots . OH^- \overset{K_2}{\rightleftharpoons} N(CH_3)_3^+ + OH^- \qquad 4.2$$

An estimate of pK_2 by Joos and Carr (1967) is 11.6. Molecular salt formation is thought to occur:

$$-PO_4^- + N(CH_3)_3^+ \overset{K_3}{\rightleftharpoons} N(CH_3)_3^+ \ldots . -PO_4^- \qquad 4.3$$

K_3 was measured by Seimya and Ohki (1972) to be 8.85×10^2.
Ca^{+2} binds to the negatively charged phosphate group:

$$Ca^{+2} + 2\ (-PO_4^-) \overset{K_4}{\rightleftharpoons} Ca(-PO_4)_2 \qquad 4.4$$

K_4 was measured to be 6.41×10^5. No quantitative data for the binding of monovalent cations have been found in the literature. This scheme agrees qualitatively with what was said in the preceding paragraph. High Ca^{+2} concentration causes chelation of Ca^{+2} with the lipid phosphate while low Ca^{+2} concentration would allow the formation of the internal salt linkage. The internal salt linkage is further controlled by the pH which controls the charge on the lipid groups. It is expected that the internal salt linkage would be strongly in effect for the pH range 4-7 since most authors quote this as the isolelectric range of phosphatidyl choline. However, measurements of resistance and dielectric breakdown potentials for black films as a function of pH show strong peaks at pH 4 (Ohki 1969). These results are best understood if one assumes this is the isoelectric point of the lipid. One may criticize this work since the degree of saturation of the hydrocarbon chains is not specified, thus equilibrium constants measured by different authors and different techniques are not as meaningful as they could be.

The binding of ions to lipids should affect the phase transition of lipids (Träuble and Eible 1973), high surface charge causes repulsions between polar groups, which cause bilayer expansion, thus allowing the hydrocarbons more motional freedom. Low surface charge results in tighter packing of lipids and therefore less motional freedom for the hydrocarbon chains. Träuble's expression for the change in T_c is

$$\Delta T_c = \frac{-2RT}{\Delta S} \left[\frac{\Delta f}{f_1} - \frac{\Delta f^2}{f_1 f_2} \right] \alpha \qquad 4.5$$

where R is the universal gas constant, T is the absolute temperature, ΔS is the entropy change during the phase transition, f_1 is the area per molcule for $T > T_c$, f_2 is the area per molecule for $T > T_c$, $\Delta f = f_2 - f_1$ and α is the degree of dissociation of the phosphate groups. Assuming f_1 and f_2 are relatively independent of lipid charge, which may not be true, Eqn. 4.5 predicts that the transition temperature is a function of the degree of dissociation of the lipid polar groups. The significance of the phenomena is that changes in pH or ion concentration in the external medium are capable of inducing phase transitions on membranes. This may be of critical importance to recent theories on nerve excitation and sensory transduction where cation induced structural changes in biomembranes are believed to exist. This theory has shown good quantitative agreement for simple lipids such as phosphatidic acid. However, more complex polar groups such as phosphoryl choline and ethanolamine may carry positive and negative charges simultaneously which means estimates of surface charge require assumptions about the conformations of the polar groups. To date no reliable method for accurately determining polar group conformation as a function of pH or ion concentration is available.

Since the binding of ions to lipids is a function of pH and ion

concentration one expects the aggregation and/or fusion of vesicles to be dependent upon these parameters. Fusion of phospholipid vesicles has been demonstrated by NMR (Taupin and McConnell 1972), PMR (Prestegard and Fellmeth 1974), gel filtration, electronmicroscopy, and differential scanning calorimetry (Papahadjopoulos et al. 1973). These studies report that vesicle fusion is enhanced at temperatures greater than T_c, or with Ca^{+2} shared between negatively charged lipids. However, no mechanism has been established for fusion of model membranes. Light scattering, which gives information on the size and shape of vesicles, is believed to be a technique which may prove useful in studying these problems.

CHAPTER 4

EXPERIMENTAL

4.1 MATERIALS

Synthetic DPC was purchased from Sigma Chemical Company. Thin layer chromatography showed only one spot and the lipid was used without further purification. All water used was double distilled and stored in Pyrex glassware. The ionic strength of this water was assumed to be very small in comparison to what was added to water before an experiment since the electrical resistance of the water was measured to be 10-100 MΩ . Other reagents used in the experiment were CH_3Cl, CH_2O, $CaCl_2 . 2H_2O$, KOH, KCl and HCl. All chemicals used in this study were spectrograde.

4.2 SAMPLE PREPARATION

A desired amount of DPC (usually about 50 mg.) was weighed on a Mettler H20 balance. The DPC was dissolved in sufficient CH_3Cl to obtain a 25 mg/ml solution of DPC in CH_3Cl and immediately refrigerated at about 2°C until required. A known amount of this solution, usually .08ml or 2mg was placed via a number 710 Hamilton syringe into a clean dry silica glass tube. This solution was placed in a warm dry chamber in which N_2 gas was gently blown over the

solution to evaporate the CH_3Cl and leave a uniform thin film of DPC on the bottom of the tube. When the film appeared to be a white powder it was assumed that no CH_3Cl remained in the DPC.

About 50 aqueous solutions ranging in concentration from 10^{-4}M to 10^{-1}M of appropriate ion content were mixed, the pH being adjusted by addition of appropriate volumes of KOH or HCl. pH measurements were taken on an Accumet model 320 expanded scale research pH meter equipped with a Fisher 13-639-92 combination pH electrode. To the dried DPC film was added 4 mls of the prepared solution. This mixture was placed in a water jacket heated to $50\pm3^{\circ}C$ and sonicated for 30 minutes by a Biosonic IV sonicator equipped with a low power probe. The samples were placed without further treatment into the sample holder and cooled to $25^{\circ}C$ in about 3-5 minutes, after which measurements commenced.

4.3 SCATTERING MEASUREMENTS

A diagram of the apparatus used for 90° light scattering measurements is shown in Fig. 4.1. The light source was a PEK 100-watt mercury vapour lamp type 112-2118. A QC91 Corning glass filter which transmits below 400 nm was used in combination with an Oriel 400 interference filter which eliminated the fluorescence of the glass filter. The only spectral lines detectable with this pair are the 366 nm, 368 nm doublet and 404 nm. The light was chopped at 80 hertz and focused on the slit of a Jarell Ash grating spectrometer

(Spec 1 in Fig. 4.1) which was adjusted to pass 366 nm light. The emerging beam was split by a quartz slide into a reference beam I_1 and sampling beam I_2. I_1 was directed onto an RCA 331 photomultiplier, and the photocurrent fed into a PAR JB-5 phase lock amplifier. The amplifier output was fed through an operational amplifier manifold, which corrects the differential output of the JB-5 to a signal directly proportional to the input, into channel 1 of a 23 M1P Philbrick Multiplier Divider. The beam I_2 was collimated and reflected to the sample. The light scattered from the sample at 90^{o} was focused onto Spectrometer II (Spex Industry). Spec II was adjusted to the wavelength of the light incident on the sample. The spectrometer exit was equipped with an ITT photomultiplier. The photomultiplier output was fed into a PAR HR-8 phase lock amplifier which gave an output e_2 directly proportional to the input. The amplifier output is fed into channel 2 of the multiplier divider. The quotient (e_2/e_1) is computed by the divider circuit and the divider output was fed into a strip chart recorder. By dividing (e_2/e_1), the effect of variations in source intensity on scattered intensity I_2 was eliminated since both I_1 and I_2 would vary by the same fraction.

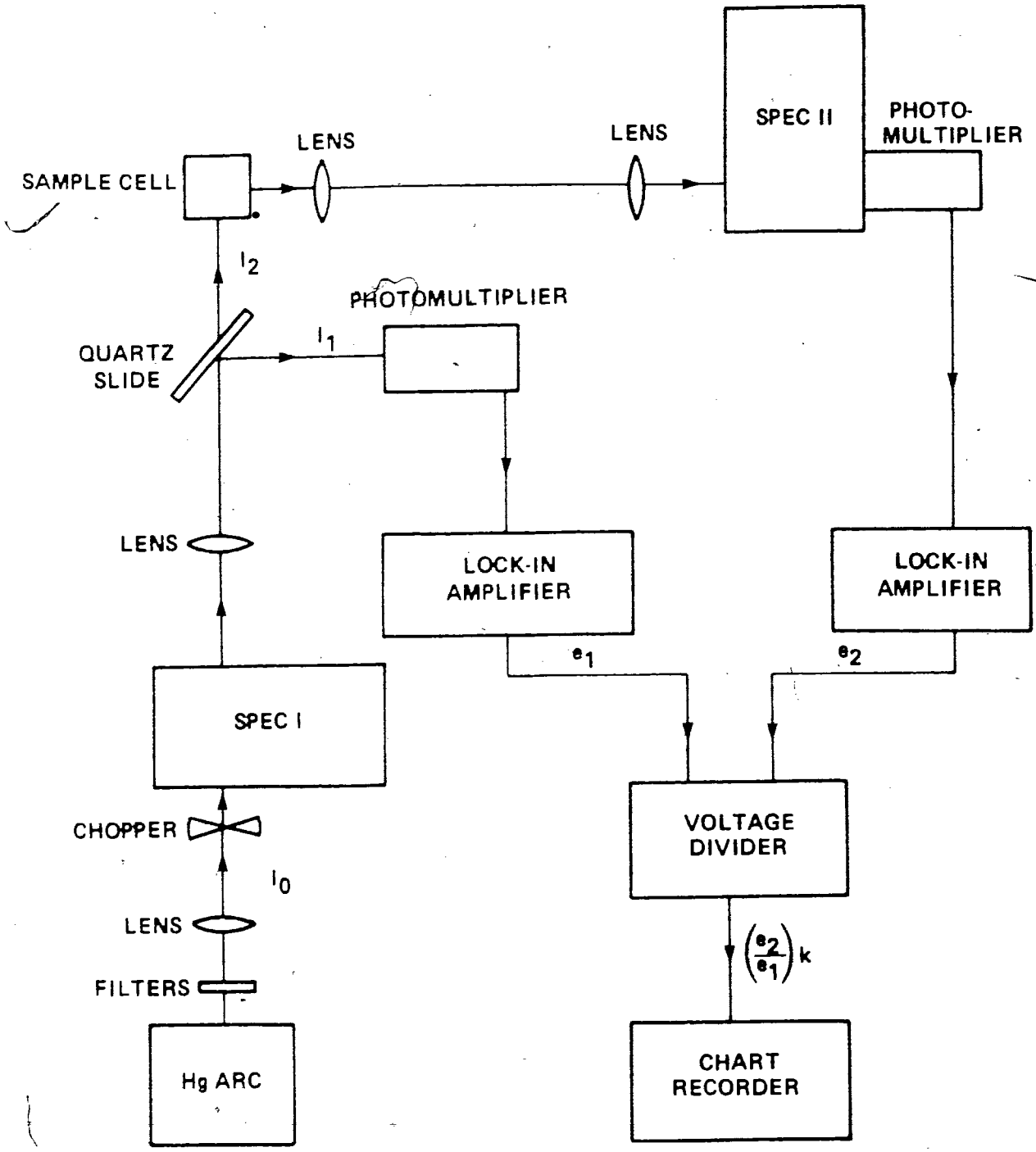

Fig. 4.1 Experimental Setup

The only optical path for light to reach the slit of Spectrometer II was from the light source. All sources of stray light were carefully eliminated by placing the apparatus in a blackened box.

4.4 TURBIDITY MEASUREMENTS

Turbidity measurements were made on a Cary 14 spectrophotometer at 25°C as a function of wavelength in the range of 340 to 550 nm. All measurements were made with respect to a water blank.

4.5 TEMPERATURE CONTROL AND MEASUREMENT

Samples contained in a quartz cuvette were placed in a brass sample holder equipped with a water circulation jacket. The sample holder was machined so the tight fit between the quartz cuvette and the water jacket would give an excellent thermal contact. The temperature of the sample holder was controlled by a Haake circulation pump which permitted one to either maintain a constant temperature or a temperature continually varying at a controlled rate. The experimental accuracy of temperatures measured in this work is estimated to be ± .25°C.

In experiments where a continuous variation of temperature was desired, a lag was noted between the temperature of the water in the pump and the sample temperature. Thus the sample temperature was always lower (about 0.5 to 2°C) than the pump temperature.

Therefore it was necessary to calibrate the system so that the pump temperature could be corrected to a true sample temperature. This method is reasonable as long as one scans in the same temperature range and at the same rate. An alternative method would be to place a thermocouple in each sample and continually record the thermal voltage but this would not really be any more efficient than the method employed.

To calibrate the pump-sample temperature difference, a Fenwal GD 25 P2 glass thermistor was placed in the quartz cuvette in the sample holder while the temperature was varied continuously from 25°C to 62°C at an average rate of 3/4 degree per minute. The resistance of the thermistor as a function of temperature was monitored on a 4470 Dana digital volt-ohm meter while the pump temperature was monitored with a thermometer. The results are plotted in Fig. 4.2a. The resistance temperature characteristic of the thermistor was previously determined by placing the thermistor and a thermometer close together in a heating bath and recording resistance and temperature in this case. These results are also plotted in Fig. 4.2a. As one may observe, the two curves indicate that the sample temperature lags the pump temperature by up to 2°C. A plot of true temperature versus pump temperature is shown in Fig. 4.2b which is used for the calibration.

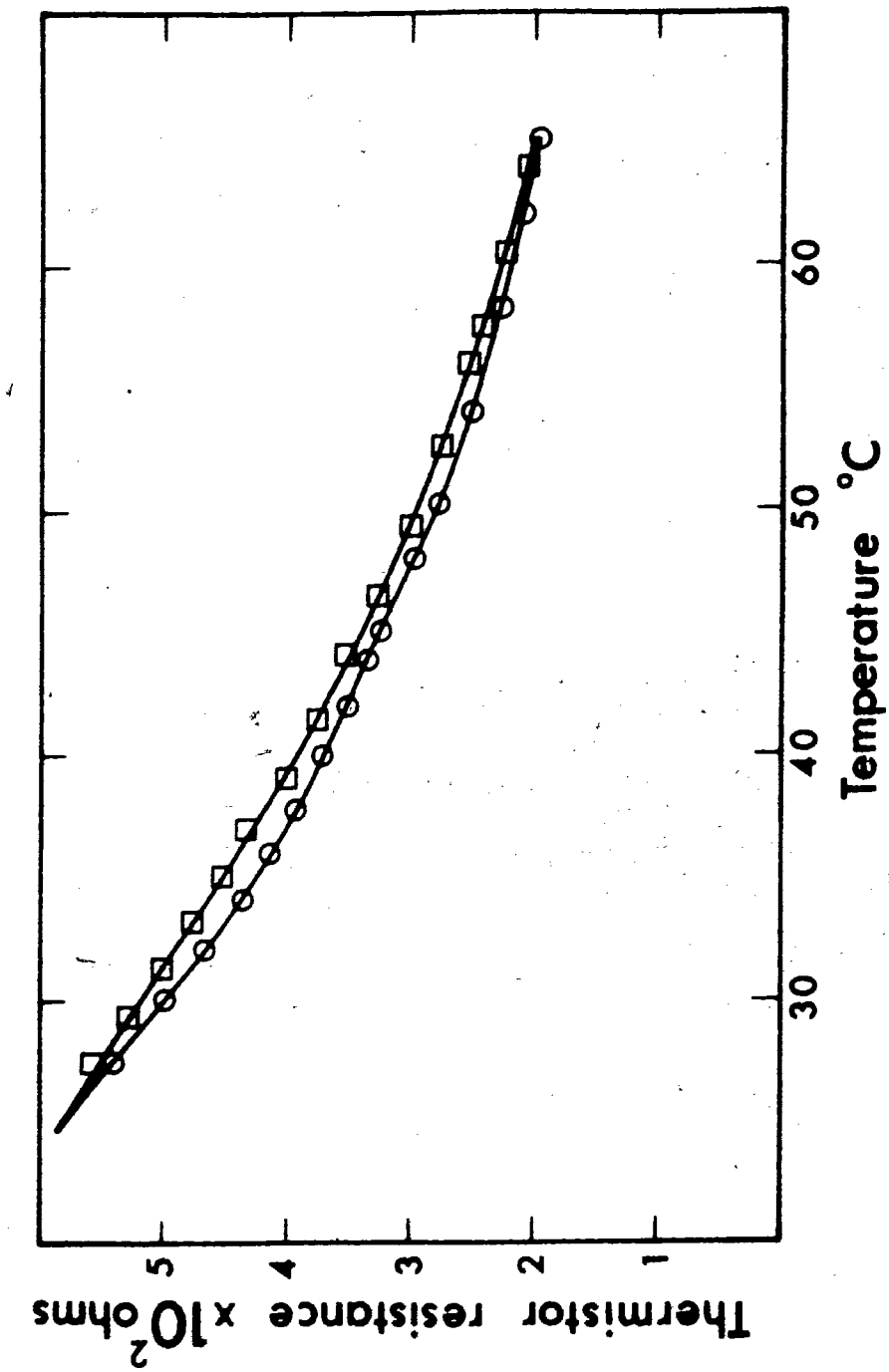

Fig. 4.2a Calibration of pump, sample temperature gradient; O sample temperature, □ pump temperature.

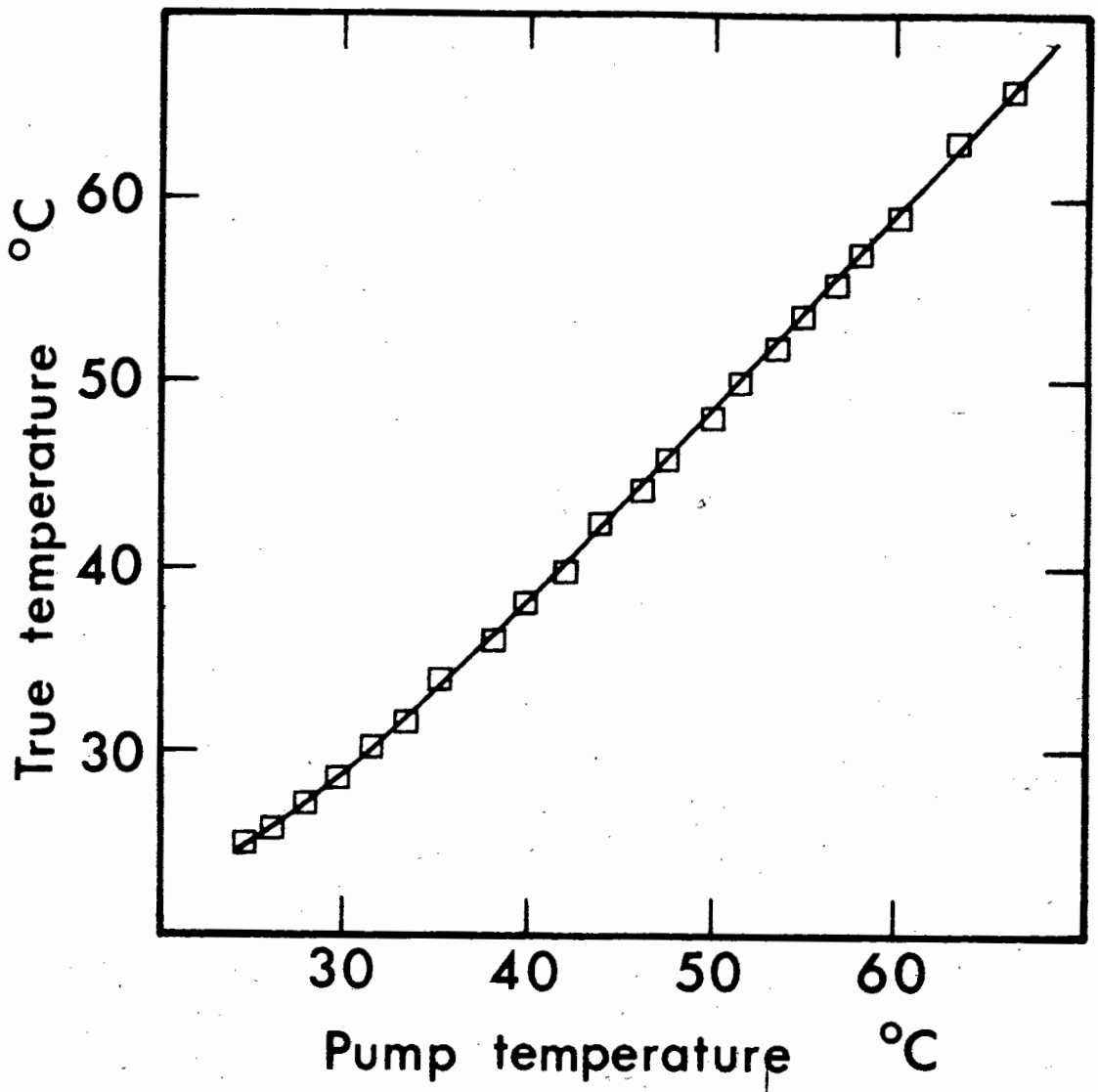

Fig. 4.2b Curve obtained by taking constant thermistor resistance in Fig. 4.2a.

CHAPTER 5

SCATTERING OF LIGHT BY LECITHIN DISPERSIONS

5.1 INTRODUCTION

The scientific study of light scattering commenced over a century ago. The scattering of light by very small particles was investigated by Tyndall in 1869 and is sometimes referred to as the Tyndall effect. This was followed by Lord Rayleigh's theoretical work (1881) and scattering by particles of sizes much smaller than the wavelength of the scattered light is frequently referred to as Rayleigh scattering. Approximate theory for particles with dimensions comparable to the wavelength of the incident radiation was developed by Rayleigh (1914), Debye (1915) and later by Gans (1925). This type of scattering is called Rayleigh-Gans scattering or Rayleigh-Debye scattering. The problem was solved in a rigorous fashion for spheres of arbitrary size by Mie (1908) and independently by Debye (1909) and is commonly referred to as the Mie theory.[1]

Light scattering methods have often been used to determine the sizes and shapes of cells, subcellular particles and phospholipids dispersed in water. Koch (1961) employed the Rayleigh-Gans

FOOTNOTE [1]. The reader is referred to an excellent book on scattering of light by Kerker (1969).

approximation of light scattering to estimate the size of mitochondria and the bacteria Escherichia coli. Physiochemical differences between fragments of plasma membrane and endoplasmic reticulum were studied by Wallach et al. (1966) using turbidity measurements. Atwood and Saunders (1965) studied changes in the size and shape of egg lecithin aggregates subjected to varying lengths of time of sonication by means of light scattering. The presence of thermotropic phase transitions in both natural and model membranes dispersed in water have also been observed by light scattering and turbidimetric methods. Abramson (1971) observed a decrease in turbidity of an aqueous dispersion of dipalmitoyl lecithin in the range of 24° to 33°C and a sharp decrease at the transition temperature of 41°C. A sharp decrease in scattered light intensity at the phase transition was also observed for isolated phospholipids, and membranes of the fatty acid auxotroph of Escherichia coli supplemented with different fatty acids in the growth medium (Overath and Träuble, 1973).

Theoretical studies of light scattering by phospholipid dispersions have been made on the assumption of a spherical shell model for the lipid vesicle (Seufert, 1970; Tinker, 1972). Such a model is applicable to the microvesicles prepared by the method of Huang (1969). However, for normal preparations of phospholipid dispersions, electron micrographs often reveal onion-shaped multilamellar liposomes of various sizes ranging from a few microns

down to a fraction of a micron (Bangham and Horne, 1964; Chapman et al., 1968). Aggregates of liposomes were often observed, however the sizes and shapes of the lecithin particles observed in the electron micrographs depended on the different techniques used for examination of the specimen (Colbow, 1974). Light scattering methods offer a distinct advantage, since the system under study can be observed in situ without significant perturbation.

This chapter is organized into two parts. In Section 5.2, Rayleigh scattering and the Rayleigh-Gans theory are presented.[2] I have calculated the scattered light intensity, turbidity and other useful quantities as a function of particle size for a system of particles of the same size (i.e. monodispersed).

FOOTNOTE[2]. The theory presented is based on the treatment of Chong (1975).

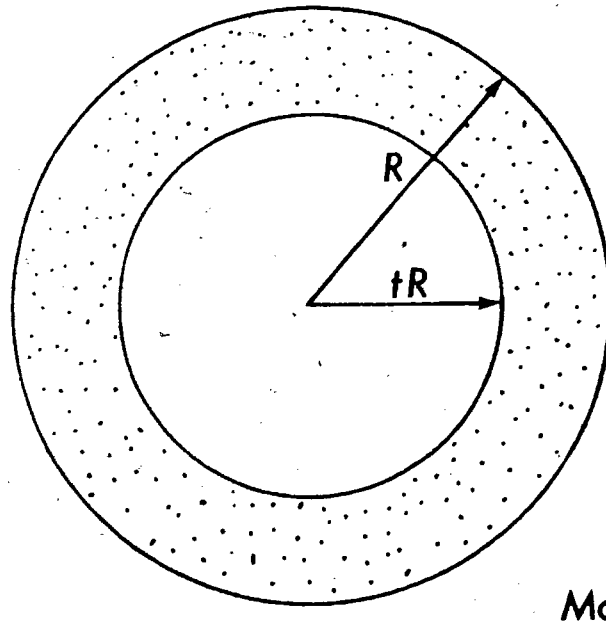

Model 1
Single lipid shell vesicle

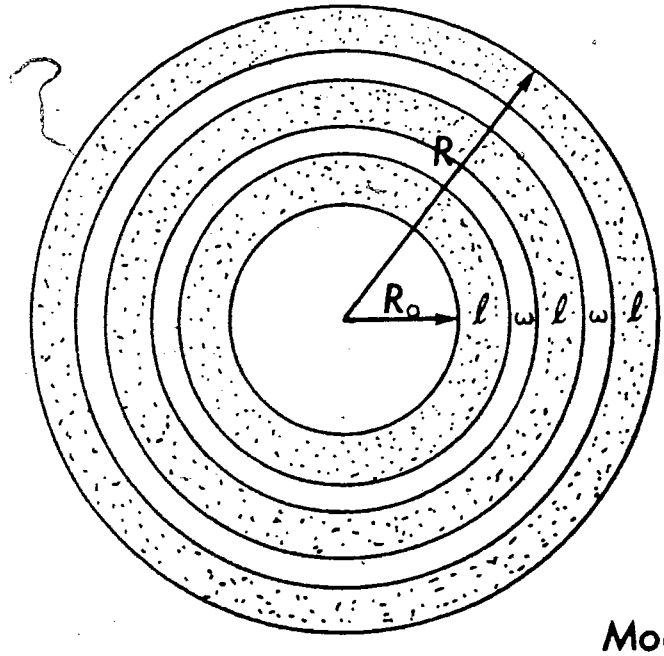

Model 2
Multilamellar vesicle

Fig. 5.1 Models of lecithin vesicle structure.

5.2 THEORY OF LIGHT SCATTERING

Based on the work of earlier workers who showed DPC vesicle diameters to vary from 250 Å to several microns, I have attempted to apply the Rayleigh-Gans theory of light scattering. I shall first consider Rayleigh scattering which applies to particles much smaller than the wavelength of the incident light, and then the Rayleigh-Gans approximation which is applicable to particles of size comparable to the wavelength of the incident radiation.

(a) Rayleigh Scattering

The intensity of light scattered by an isotropic particle in vacuum, smaller in size in comparison to the wavelength of incident light, as first pointed out by Rayleigh (1881) is given by

$$S(\theta) = \frac{(1 + \cos^2\theta)\, q^4 \alpha^2}{2r^2} I_o \qquad (5.1)$$

where $q = 2\pi/\lambda$, λ is the wavelength of the incident light in vacuum, θ is the angle of observation measured from the incident beam, r is the distance of observation, α is the polarizability of the particle and I_o is the intensity of the natural incident light. The term 1 in the bracket corresponds to the component perpendicular to the scattering plane and the term $\cos^2\theta$ corresponds to the component parallel to the scattering plane which is defined by the direction of the incident light and the scattered beam.

For a homogeneous dielectric sphere of dielectric constant ϵ_o immersed in a medium of dielectric constant ϵ, the polarizability α is given by (Bottcher, 1952; p 51)

$$\alpha = \frac{3V(\epsilon_o - \epsilon)}{4\pi(\epsilon_o + 2\epsilon)} \qquad (5.2)$$

where V is the volume of the particle. In the optical frequency region, we replace the dielectric constants by the refractive indices and we obtain for N isotropic spheres/unit volume, the intensity scattered per unit volume of solution

$$S(\theta) = \frac{9\pi^2 V^2 N n^4 (m^2-1)^2}{2r^2\lambda^4 \quad (m^2+1)^2}(1+\cos^2\theta) I_o \qquad (5.3)$$

m is the relative refractive index given by the ratio n_o/n, where n_o is the refractive index of the particle and n is that of the medium.

Integrating over the surface of a sphere of radius r yields the total light scattered

$$S = \frac{24\pi^3 V^2 N n^4 (m^2-1)^2}{\lambda^4 \quad (m^2+2)^2} I_o \qquad (5.4)$$

Similar to the Beer-Lambert's law for absorption, the transmitted light intensity I_T is written as

$$I_T = I_o \exp(-\tau l) \quad \text{or} \quad I_T = I_o\, 10^{-Al} \tag{5.5}$$

where τ the attenuation constant is called the turbidity, l is the pathlength and A the absorbance of the sample is the quantity measured with the spectrophotometer. It is readily seen that

$$\tau = 2.303A = \frac{24\pi^3 V^2 N n^4 (m^2-1)^2}{\lambda^4 \quad (m^2+2)^2} \tag{5.6}$$

(b) Rayleigh-Gans Theory

When a particle has a linear dimension comparable to the incident light wavelength, wavelets from different parts of the particle interfere. More light is scattered in the forward direction. Rayleigh (1914), and Gans (1925) considered the interference of light scattered from different parts of the particle but neglected the phase changes in light traversing the particle. The criteria necessary for the approximation are:

(1) The refractive index of the particle is close to that of the medium, i.e. $|m-1| \ll 1$

(2) The phase shift through the particle is small, i.e.

$$4\pi R(m-1)n/\lambda \ll 1$$

Under such conditions, the scattered light is reduced by the scattering factor $P(\theta)$, which for spherically symmetric particles with continuous scattering elements, is given by the square of the form factor (see e.g. Kerker, 1969, p 423)

$$f = \frac{\int 4\pi r^2 \, G(r) \, (\sin kr)/kr \; dr}{\int 4\pi r^2 \, G(r) \, dr} \qquad (5.7)$$

where $k = (4\pi \sin\theta/2)n/\lambda$ and $G(r)$ is the radial distribution function. Consequently, the turbidity is modified by the dissipation factor

$$Q = 3/8 \int P(\theta)(1+\cos^2\theta) \sin\theta \, d\theta \qquad (5.8)$$

$P(\theta)$ can be written in simple analytic forms for some common particle shapes. These expressions are: For a sphere (Rayleigh, 1914),

$$P(\theta) = \left[\frac{3}{x^3} (\sin x - x \cos x)\right]^2, \quad x = \frac{4\pi nR \sin\theta/2}{\lambda} \qquad (5.9)$$

For a shell of thickness (1-t) R (Oster and Riley, 1952),

$$P(\theta) = \frac{3}{(1-t^3)x^3}(\sin x - x\cos x + tx\cos x - \sin t\,x)$$

$$x = \frac{4\pi n R \sin\theta/2}{\lambda} \qquad (5.10)$$

For a rod of length L (Neugebauer, 1943),

$$P(\theta) = \frac{1}{x}\int \frac{\sin w\, dw}{w} - \frac{(\sin x)^2}{x} \quad x = \frac{2\pi L \sin\theta/2}{\lambda} \qquad (5.11)$$

The expressions for $P(\theta)$ in the case of the sphere and shell can be directly obtained from Eqn.7 taking $G(r) = 1$ for $tR<r<R$ and $G(r) = 0$ elsewhere. In the case of multilamellar structure, I take the model of concentric shells of lecithin enclosing water between the shells (Fig. 5.1). Let the thickness of the lecithin shell be l and that of the water w. Likewise from Eqn.7,

$$f = \frac{4\pi}{k^3 V}\sum_{j=1}^{y} \sin kx_j - \sin k(x_j-l) + k(x_j-l)\cos k(x_j-l)$$

$$-k\,x_j \cos kx_j\, l \qquad (5.12)$$

where $x_j = R_o + (j-1)\,w + jl$, y is the total number of lecithin shells and R_o is the radius of the central core of enclosed water. V is the total volume of lecithin material in the structure and is given by

$$V = \frac{4\pi}{3}\sum_{j=1}^{y} [x_j^3 - (x_j - 1)^3] \qquad (5.13)$$

In order to express $S(\theta)$ and τ in terms of more directly measureable parameters we use the treatment of Yi and MacDonald (1973) which states that the refractive index of a dispersion n_s is a linear function of concentration.

$$n_s = n_w + W\, dn/dW \qquad (5.14)$$

where n_w is the refractive index of water, W is the weight fraction of lecithin and dn/dW is the refractive index increment with respect to changes in weight fraction.

The concentration c (in gm/ml) is related to the weight fraction W and the density of the dispersion ρ_s by Eqn. 5.15

$$c = \rho_s W \qquad (5.15)$$

The density of lecithin $\rho_l = 1.056$ (Sheetz and Chan, 1972) and thus ρ_s, the density of the dispersion, differs only slightly from unity for the range of lecithin concentration which is of interest. Thus to a good approximation,

$$dn/dW = \rho_s\, dn/dc \qquad (5.16)$$

and the numerical value of dn/dc is only slightly less than that of dn/dW. Equation 5.14 may now be written in the form

$$n_s = n_w + c\, dn/dc \qquad (5.17)$$

Setting $n=n_w$, $m=n_s/n_w$ we obtain

$$n(m-1) = (1/V)\, M\, dn/dc \qquad (5.18)$$

where M is the anhydrous mass of a single particle, c the concentration of DPC and dn/dc is the measured refractive index increment. Thus, with c=MN, we finally get the expressions for the specific intensity and the specific turbidity

$$\frac{S(\theta)}{c} = \frac{9\pi^2 n^3 V}{2\, r^2 \lambda^4}\left(\frac{dn}{dc}\right)\frac{(m+1)^2(m-1)\ (1+\cos^2\theta)\ P(\theta)\ I_o}{(m^2+2)^2} \qquad (5.19)$$

$$\frac{\tau}{c} = \frac{24\pi^3 n^3 V}{\lambda^4}\left(\frac{dn}{dc}\right)\frac{(m+1)^2(m-1)}{(m^2+2)^2}\ Q \qquad (5.20)$$

Power dependence of τ on λ

From Eqn. 5.20, we obtain the derivative

$$-\frac{d \log \tau}{d \log \lambda} = 4 - d \log Q/d \log\lambda - d \log B/d \log\lambda$$

$$= 4 - \beta - \gamma \qquad (5.21)$$

where $$B = \frac{n^3(m+1)^2(m-1)}{(m^2+2)^2}\, dn/dc$$

$$\beta = d \log Q/d \log\lambda \ , \ \gamma = d \log B/d \log\lambda \ . \qquad (5.22)$$

Clearly β for a given wavelength depends only on the dimension D of the scattering particle. It has been computed by Doty and Steiner (1950) for rods and spheres of size range $0 < nD/\lambda < 0.8$. We shall compute β for shells of various thickness and the onion-shaped structure. It is useful to note the limiting cases of β for large D. Koch (1961) showed that for a sphere $\beta = 2$, for a long rod $\beta = 1$ and for a thin spherical shell $\beta = 1.83$.

γ is estimated from a plot of log B versus log λ using measurements of refractive indices of water and dispersions of different concentrations. For DPC, Chong (1975) has estimated n = 1.347, dn/dc = .160, m = 1.120 and $\gamma = 0.32$ at $\lambda = 366$ nm.

I have computed the quantities $P(\theta)$, Q, $S(90^{o})/c$, β and τ/c for both the models shown in Fig. 5.1 for monodisperse systems. The choice of l and W in the second model (multilamellar vesicle) was based on the electron micrograph observations of Bangham and Horne (1964). The lipid thickness l was chosen to be 45 Å while the water thickness was 20 Å. The computations and graphical plots are presented in the Appendix section. The results obtained for the first model (single lecithin shell model) are in Appendix 1 and those obtained from the multilamellar model are put in Appendix 2.

As mentioned earlier, the single shell model is a good model for lecithin dispersions with a small vesicle size parameter. It is of interest to note from Tables A1.4 and A2.4 that the β values calculated for both models are not much different when the particles are sufficiently large and have the same water core radius and the

same size. However, from Tables A1.5 and A2.5, the turbidity for the second model is about 0.6 of that of the first model. In view of the multilamellar structure, one should have used an effective relative refractive index in the calculation of turbidity for model 1. From Eqn. 5.20, one finds that a change in the relative refractive index changes the turbidity mainly through the term (m-1). A choice of m = 1.07 for the effective relative refractive index would give the ratio of 0.6 for the turbidities.

I shall now describe the procedure for the estimation of size and structure of lecithin particles in a monodisperse system. The turbidity of the dispersion is first obtained for a range of wavelengths (300 nm to 650 nm) using a conventional spectrophotometer. A log-log plot of the turbidity against wavelength is then obtained. The gradient of the curve at 366 nm is found and β can then be calculated from Eqn. 5.17 knowing the value of λ. The specific turbidity at 366 nm can also be calculated knowing both the turbidity at 366 nm and the concentration of lecithin in the dispersion (c is in mg/ml). Tables A1.4 and A1.5 (or A2.4 and A2.5) are then examined. The size parameter which gives the best match of the measured values of both β and τ/c to the calculated values then provides a reasonable estimate of the mean size and structure of the lecithin particles in the dispersion. Interpolation of the calculated values may be necessary to obtain good matching.

If a good match of the measured and calculated values of both β and τ/c cannot be found, the particles are assumed to have a wide

range of sizes and the calculations obtained for the polydisperse system will have to be used. Polydispersity is briefly discussed in Chapter 6.

The specific 90^{o} scattered light intensity was not used to provide estimation of the sizes of the particles for three reasons. Firstly, the scattered light intensity measurements were not absolute measurements and the instrument calibration had not been made. Secondly, the oscillatory nature of $S(90^{o})/c$ as a function of the size parameter limits its usefulness. The third reason concerns the range of validity of the Rayleigh-Gans approximation. It was shown for solid spheres (see Kerker (1969, p 427) that τ/c agreed with the more rigorous Mie Theory to within 10% for values of nR/λ up to 1.5 whereas the range of validity for the scattered light intensity decreased rapidly for increasing angle of scattering. Although no calculations have been performed, we shall assume that the above conclusion is applicable to the multilamellar structure. 90^{o} scattered light intensity measurements would be more useful if the size distribution is sufficiently narrow and the size parameter is less than 0.2.

The oscillatory region of the scattering factor $P(\theta)$ can be avoided by working with low angle scattering. We shall briefly describe in this subsection, a useful method for determining particle sizes utilizing the angular variation of scattering close to the forward direction.

For small θ, one can write (see Kerker, 1969, p 433)

$$P(\theta) = 1 - \frac{16\pi^2 n^2 \ R_g^2 \ \sin^2\theta/2}{3\lambda^2} \qquad (5.23)$$

where R_g is the radius of gyration of the particle. We shall rewrite Eqn. 5.18 in the form

$$\frac{S(\theta)}{c} = \frac{9 \ \pi^2 n^2 M_o}{2 \quad r^2 \lambda^4 N_o} \left(\frac{dn}{dc}\right)^2 \frac{(m+1)^2 \ P(\theta) \ (1+\cos^2\theta) \ Io}{(m^2+2)^2} \qquad (5.24)$$

where $M_o = N_o M$ is the molecular weight of the lecithin particle, N_o is Avagadro's number and M is the anhydrous mass of the particle used in Eqn. 5.18.

Defining

$$K = \frac{9 \ \pi^2 n^2}{2 \ \lambda^4 N_o} \left(\frac{dn}{dc}\right)^2 \frac{(m+1)^2 \ (1+\cos^2\theta)}{(m^2+2)^2} \qquad (5.25)$$

and the Rayleigh ratio

$$R = \frac{S(\theta) \ r^2}{Io} \qquad (5.26)$$

I obtain the relationship

$$\frac{Kc}{R} = \frac{1}{M_o P(\theta)} \qquad (5.27)$$

If concentration fluctuations are taken into account, the right hand side of Eqn. 5.25 is modified. We then get (see Kerker, 1969, p 434 and p 507)

$$\frac{Kc}{R} = \frac{1}{M_o P(\theta)} + \frac{2Bc}{P(\theta)} \qquad (5.28)$$

where B is the second virial coefficient.

In the limit of $c \rightarrow o$, we can neglect the concentration fluctuations. From Eqn. 21 and 25 we get

$$\frac{Kc}{R} = \frac{1}{Mo}\left(1 + \frac{16\pi^2 n^2 \ R_g^2 \sin^2\theta/2}{3\lambda^2}\right) \qquad (5.29)$$

On the other hand, in the limit $\theta \rightarrow o$ (forward direction), we get

$$\frac{Kc}{R} = \left(\frac{1}{Mo} + 2Bc\right)\frac{1}{P(\theta)} \qquad (5.30)$$

The molecular weight M_o, the radius of gyration R_g and the second virial coefficient B can be evaluated from a Zimm plot (Zimm, 1948) in which Kc/R is plotted against $[\sin^2(\theta/2) + gc]$ where g is arbitrarily chosen to provide a convenient spread of data. M_o is obtained from the interception of the plot in the limit $\theta \rightarrow 0$ and B is the slope. Having found M_o, R_g is obtained from the slope in the limit $c \rightarrow o$.

The Zimm-plot method provides a distinct advantage over the turbidity method of size estimation since it leads to a measure of both M_o and R_g independent of any assumptions regarding the shape of the particle. However, instrumental calibration and precise measurements of angles are necessary to give good results. Since the specialized instrumentation was not available, the Zimm-plot method could not be employed. It is felt that the turbidity method offers a reasonable alternative to the Zimm method of determining particle size.

CHAPTER 6

RESULTS AND DISCUSSION

6.1 DETERMINATION OF VESICLE SIZE BY THE TURBIDITY METHOD

The purpose of this section is to determine the size distribution of vesicles used in this experiment. The specific turbidity τ/c and the power factor β were obtained from our experimental data using Eqns. 5.6 and 5.21. The results are summarized in Table 6.1. It is impossible to find a size parameter for these suspensions which matches the specific turbidity and the power factor. The β values give relatively large values of x while the τ/c values give much smaller values of x. To see this, one need only observe that for ϕ = 0, and pH 5.8, τ/c is .387 while β is 1.55. Examining Table A1.5 one sees that for τ/c = .387, x is approximately .1 for r_i/r_o = .7. It is easily shown that R is approximately 270 Å, which is roughly the size of bilayer vesicles quoted by other authors. However, examining Table A1.4 for β = 1.55 gives a size parameter of about .3 which corresponds to R = 800 Å. Larger values of R are also possible due to the oscillitory nature of β. A summary of τ/c, β and estimates of vesicle size is given in Table 6.1. In all cases the τ/c indicates a smaller particle size than the smallest size possible for the corresponding β.

Table 6.1

λ = 366 nm. Size parameters obtained from single shell model $x = nR/\lambda$.

$\phi = \frac{[Ca^{+2}]}{[DPC]}$	pH $\pm$ .1	β	$x(\beta)$ (min)	τ/c	$x(\tau/c)$	$R(\tau/c)$ Å
0	5.8	1.55	.2700	.387	.1023	277.4
.15	5.8	1.24	.2141	.322	.0831	225.3
.73	5.8	2.01	1.0807	.160	.0743	201.4
1.46	5.8	1.88	.9969	.276	.1302	353.0
14.60	5.8	2.28	1.1926	.294	.1302	353.0
0.00	10.2	2.01	1.0807	.316	.0800	216.9
.15	10.2	1.25	.2141	.552	.1023	277.3
.73	10.2	1.64	.2980	.138	.0660	179.0
1.46	10.2	2.18	1.1087	.276	.0743	201.4
14.60	10.2	2.59	-	1.790	.1582	428.9

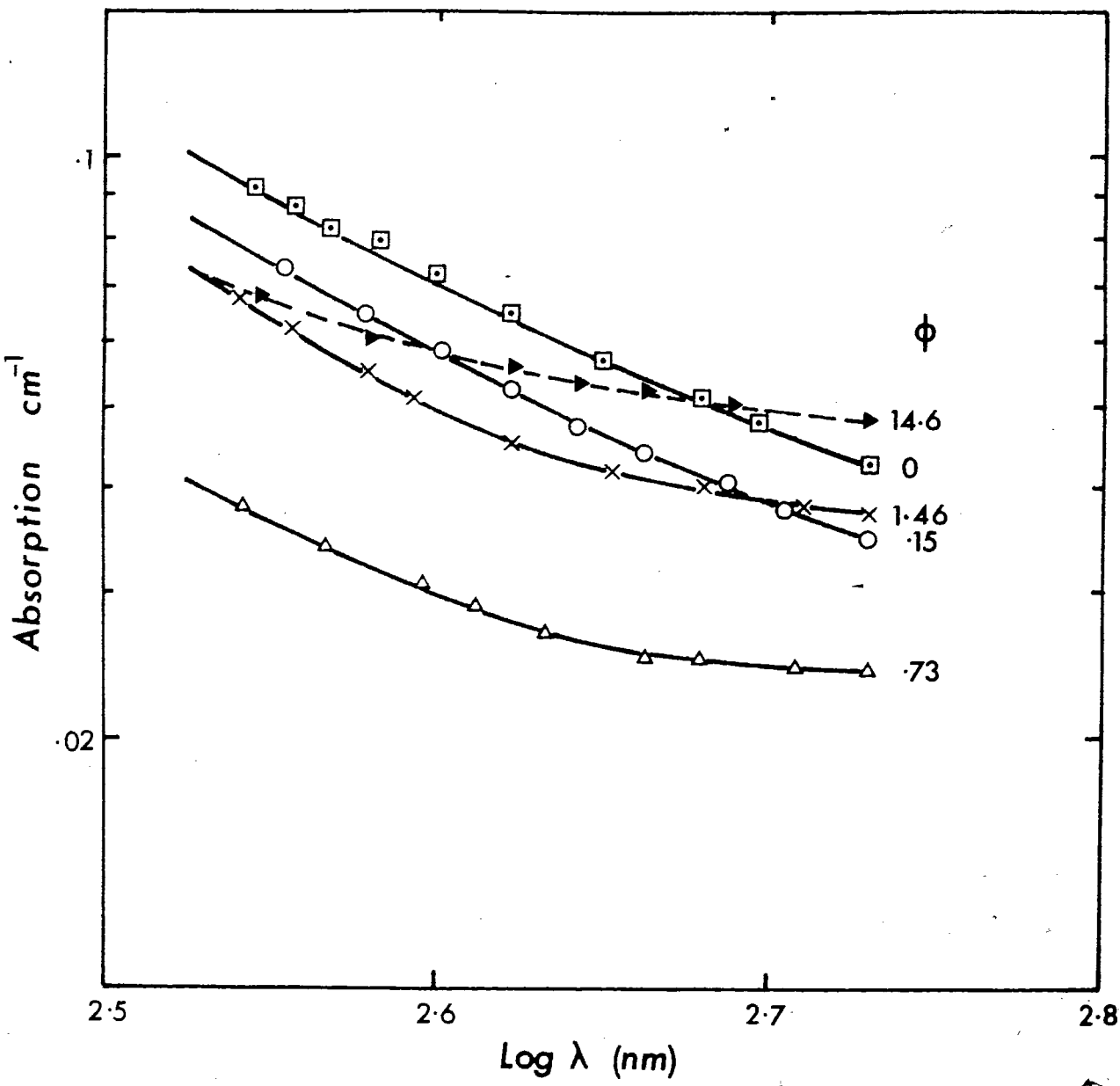

Fig. 6.1a Absorption as a function of log λ for various Ca^{+2} concentrations. $\phi = [Ca^{+2}]/[DPC]$, pH = 6.0, [DPC] = 6.84×10^{-4} M

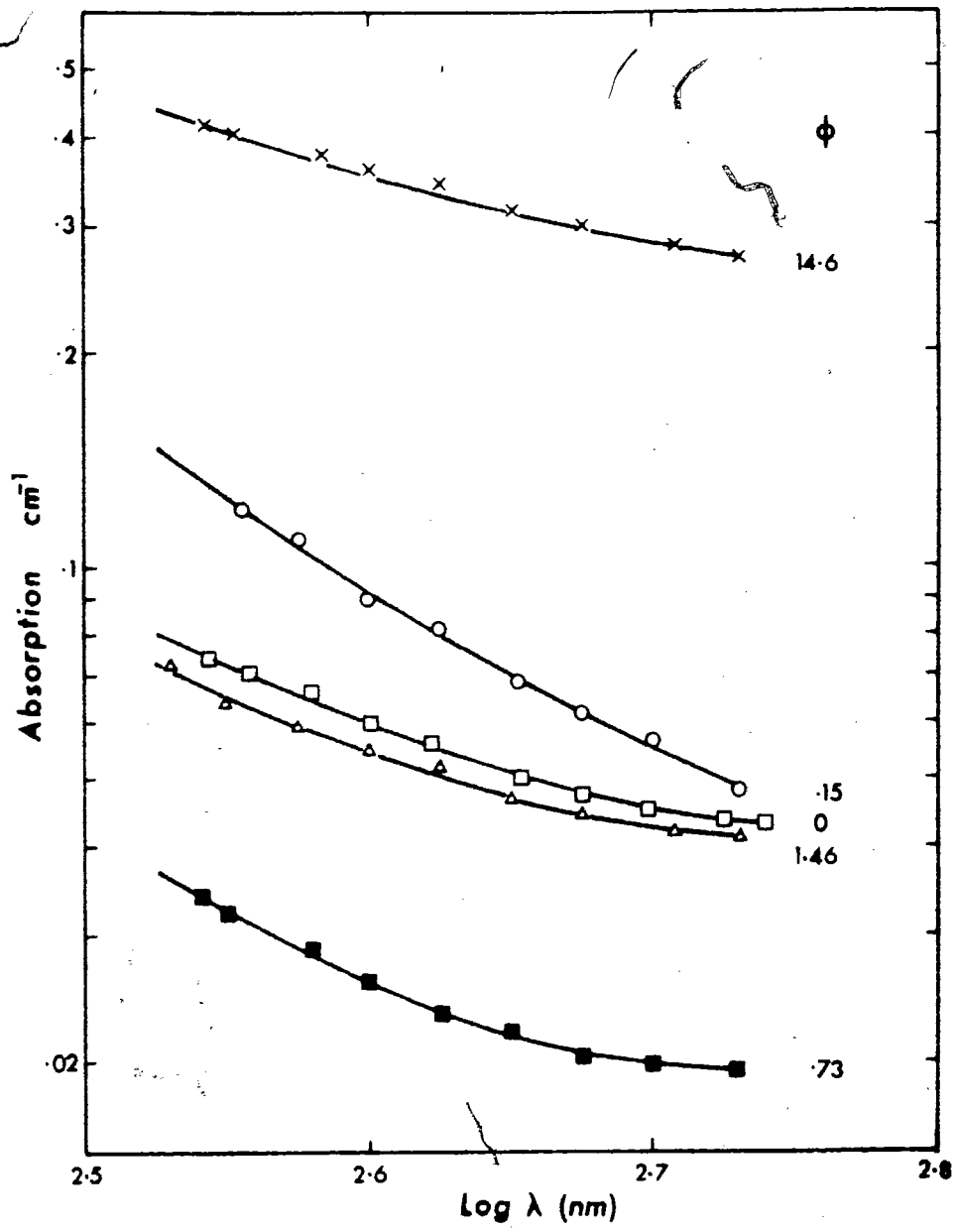

Fig. 6.1b Absorption as a function of log λ for various Ca^{+2} concentrations. $\phi = [Ca^{+2}]/[DPC]$, pH = 10.2, [DPC] = 6.84×10^{-4}M

The previous data is understandable if one assumes that a polydisperse distribution of vesicle sizes exists. Let the weight concentration of lecithin particles of a given size parameter x_j be c_j. The size parameter is a dimensionless variable given by nR_j/λ where R_j is the radius of the j'th particle. If c is the total lipid concentration of lecithin in the dispersion, then $f_j = c_j/c$ is the weight fraction of lecithin particles of size x_j. One notes that

$$\tau/c = \sum f_j \tau_j \quad ; \; S(90^o)/c = \sum f_j S_j$$

$$\frac{-d \log \tau}{d \log \lambda} = 4 - \gamma - \sum f_j \beta_j / (\tau/c)$$

$$= 4 - \gamma - \beta_s \qquad 6.1$$

One may see from Eqn. 6.1, that since β_s depends only on the size of particles and not the number, β_s should be sensitive to the presence of a few large particles, while τ/c may be dominated by a large percentage of smaller vesicles. If this is true, then τ/c should be a more reliable estimate of the size of particles in suspension. One way to explain this data, is to postulate that there are two particle size distributions in the suspension, f_1 being the weight fraction of smaller vesicles, and f_2 being the weight fraction of larger particles as estimated from the β values.

$$\tau/c = f_1\tau_1 + f_2\tau_2 \qquad 6.2$$

If $f_1 >> f_2$ then the specific turbidity must be dominated by the smaller particles. A possible reason for the existence of a small fraction of larger particles, may be that the sonication introduces some metallic particles into the suspension, or large lipid aggregates are present due to incomplete sonication. In earlier experiments metal particles were not a problem, but since these sonicator probes decay, metal particles may have been a problem in later experiments on turbidimetry. The existence of some larger lipid particles is in agreement with the work of Huang (1969).

Another way of discussing this problem is to assume that there is a continuous distribution of particle sizes. Naturally occuring populations are frequently skewed. We shall assume that the distribution of the lecithin particles behaves similar to the electron micrograph observations (Seufert 1970; Sheetz and Chan, 1972). A satisfactory choice of a skewed distribution function is the lognormal distribution (see Kerker, 1969, p 353).

$$f(x) = \frac{1}{\sqrt{2\pi}\, x\sigma} \left(\exp - \left[\frac{(\ln x/x_m)^2}{2\sigma^2} \right] \right) \qquad 6.3$$

In this distribution, it is $\ln x_m$ rather than x which is normally distributed. The mean value of $\ln x$ is $\ln x_m$ and σ is the standard deviation. x_m is the geometric mean of all x values. Some lognormal distribution curves are shown in Fig. 6.2a, for various values of σ and x_m placed into Eqn. 6.3.

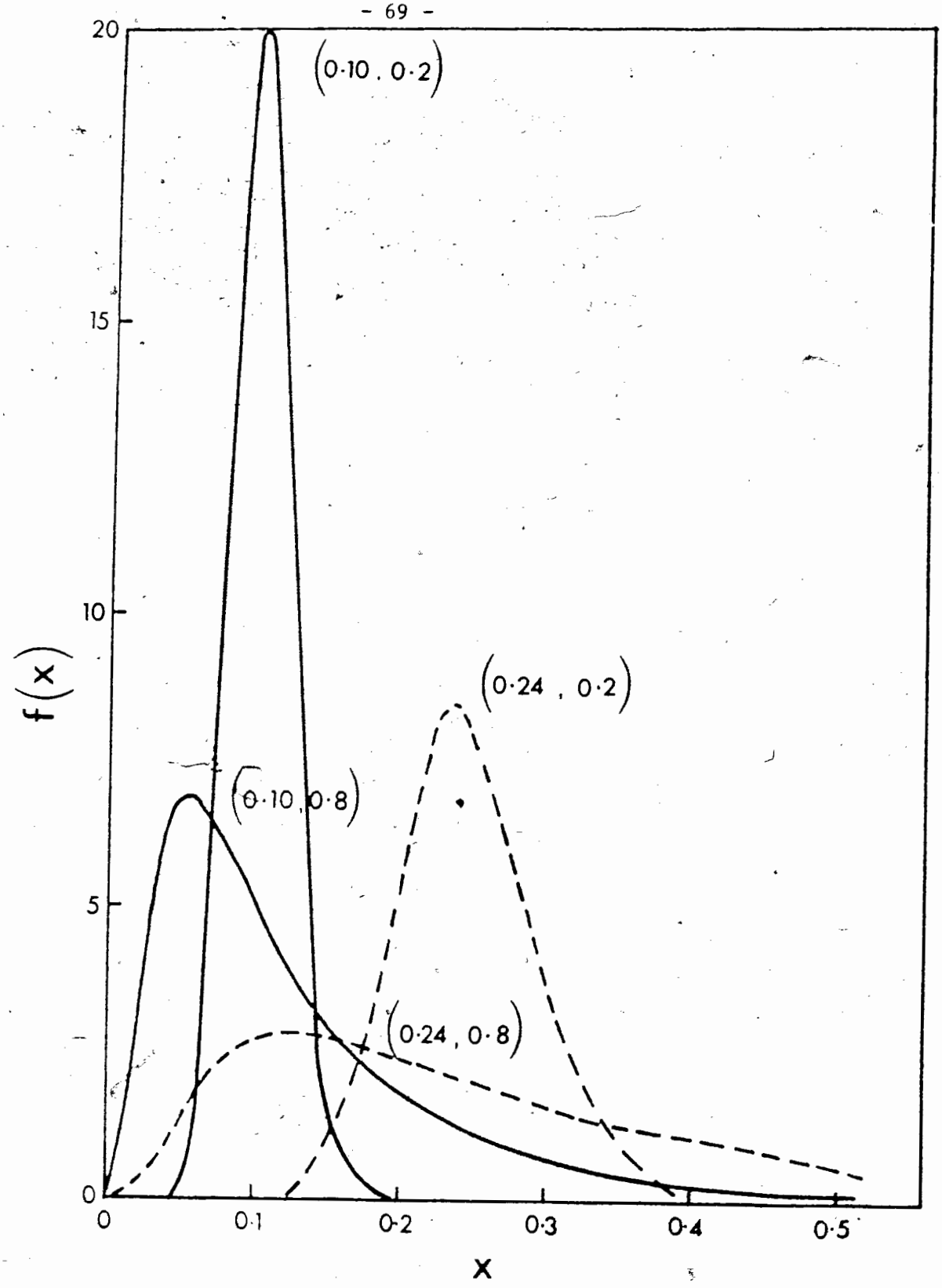

Fig. 6.2a Some lognormal distribution curves. Each pair of numbers denotes the geometric mean x_m and the standard deviation σ of the distribution.

The summations in Eqn. 6.1 are then replaced by integration. However, in the computer calculation, the procedure is still that of a summation. f_j is simply replaced by $f(x)\,\Delta x$ which gives the fraction of particles with sizes between $x - 1/2\Delta x$ and $x + 1/2\,\Delta x$. We shall now discuss the computations of such quantities as τ/c and β for polydispersed systems.

The quantities τ/c and β_s are calculated using Eqn. 6.1 for a variety of lognormal distributions. We shall call these values the effective turbidity and effective power factor respectively. The τj and βj values are those which are already calculated for the monodisperse system. We have only computed the effective values at 436 nm for the multilamellar model with no central water core. Taking into account the enclosed volume of water in the aqueous core, the correction is minimal. The results of the computations are shown in Fig. 6.2b and 6.2c.

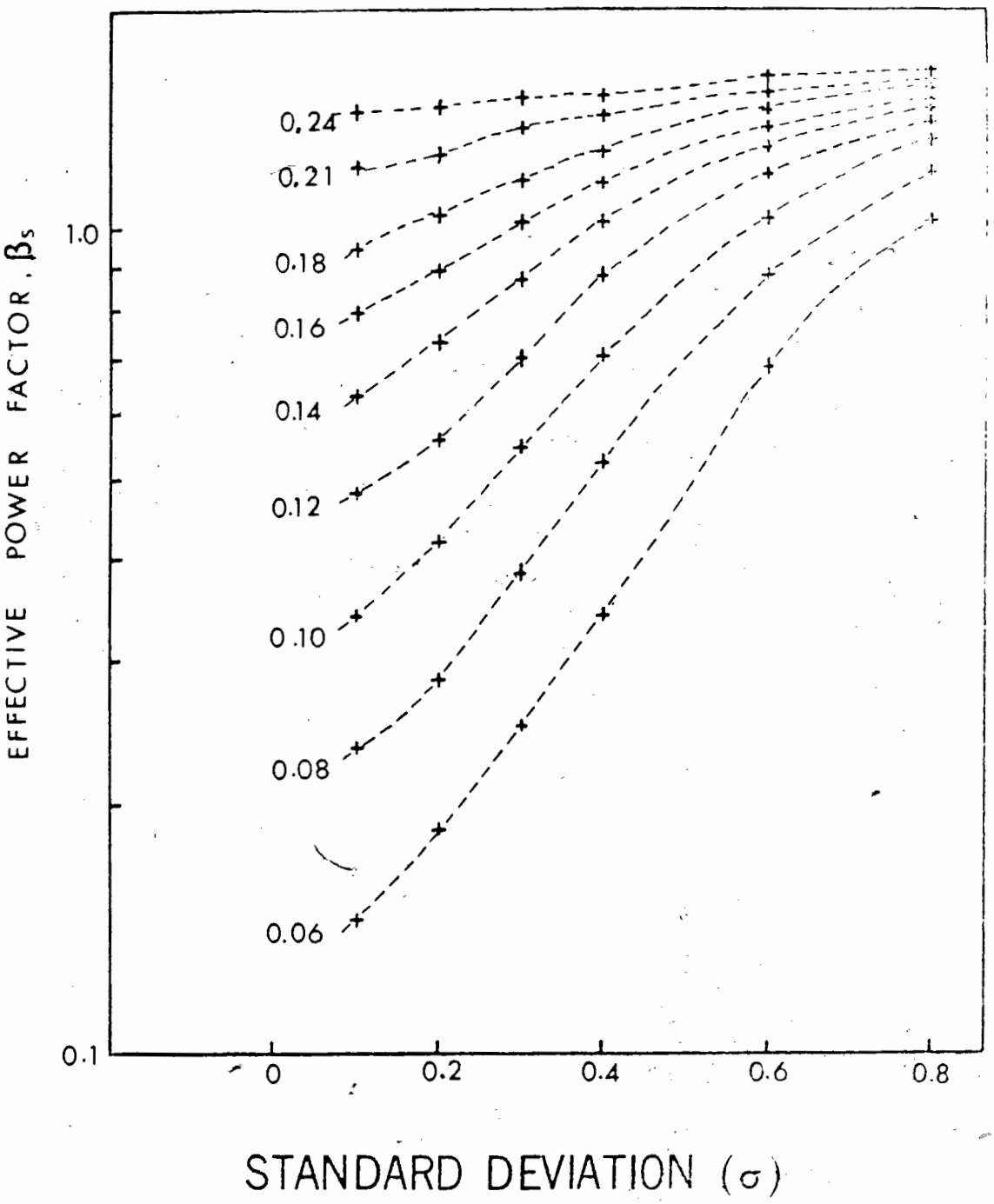

Fig. 6.2b Variation of effective power factor for different lognormal distributions of a theoretical vesicle suspension. The numbers beside the curve denote the geometric mean x_m of the lecithin size distributions.

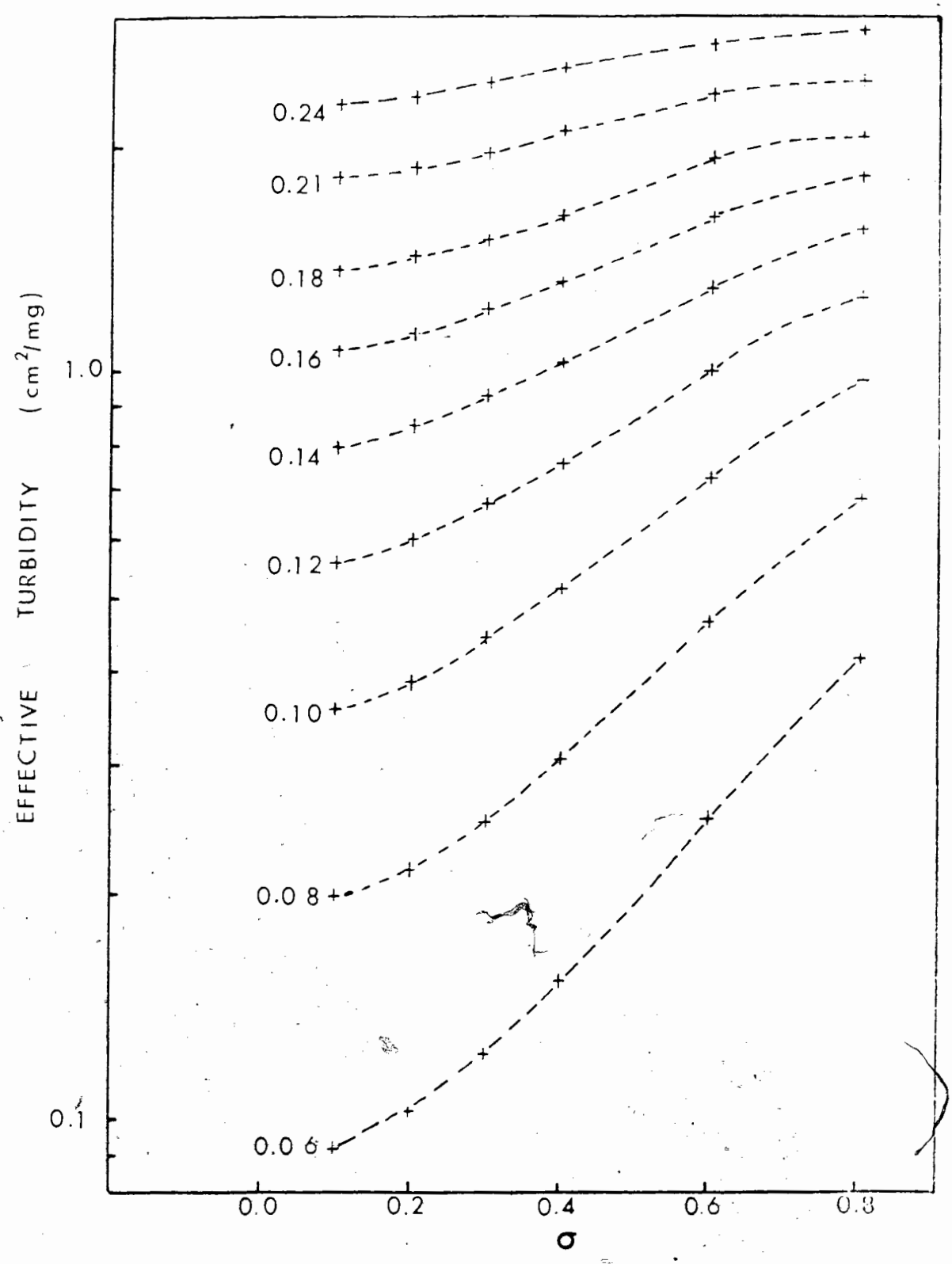

Fig. 6.2c Variation of effective turbidity for different lognormal distributions of a theoretical vesicle suspension. The numbers beside the curves denote the geometric mean x_m of the size distributions.

To estimate the distribution of the lecithin particles in the dispersion, the experimental values of τ/c and β_s are first obtained as described previously. The experimental values are then matched against those values given in Fig. 6.2b and 6.2c. It may then be possible to obtain a reasonable estimate of the distribution of lecithin particles in the dispersion, if the distribution is log-normal.

In computing Fig. 6.2b and 6.2c, the multilamellar model with lipid layer thickness l = 45 Å and water layer thickness w = 25 Å has been implicitly assumed. This is a reasonable assumption on the basis of both electron micrograph observations and x-ray diffraction studies.

It can be seen that a match of β and τ/c for a size parameter cannot be made with the log-normal distributions calculated. For example, in Table 6.1 τ/c = .387 and β = 1.55, one notes that for the τ/c value a size parameter x_m of less than or equal .1 is obtained with various standard deviations. A β value of 1.55 corresponds to a size parameter x_m which is at least twice as large as that obtained from τ/c. Thus a single log-normal distribution does not seem to be present. Thus it seems reasonable that the earlier suggestion of a bimodal distribution of particle sizes is more probable with the very large particles being a small percentage of metallic residue from the sonicator tip, or large lipid particles due to incomplete sonication.

If we assume the τ/c measurements give an estimate of the size of the largest fraction of particles in the suspension, I estimate the

average size of smaller vesicles to be 277 ± 25 Å in diameter where 25 Å is the standard deviation of the measurements. This agrees reasonably well with the 250 Å size estimates of other workers (Huang, 1969, Batzri and Korn, 1973; Sheetz and Chan, 1972) for single bilayer vesicles. In these calculations the lipid thickness is assumed to remain the same while the size of the aqueous core varies.

The measurements indicate particles whose sizes range from 580 Å to 3200 Å. It is stressed that these were the smallest possible sizes that were taken from the tables in Appendix 1 so that the size might actually be much larger. Two possible reasons for this have already been discussed. To prepare monodisperse vesicle suspensions one should follow up the sonication with some secondary treatment such as sepharose chromatography, ultra centrifugation or filtration. However, as will be seen in the next section, secondary treatments are not desirable for all experiments and the purpose behind this section was to estimate the size of vesicles used in this experiment.

6.2 TIME DEPENDENCE OF 90° SCATTERED LIGHT

Observations on Hg 366 nm light scattered at 90° indicates that $S(90^{\circ})$ is a function of time which depends upon parameters such as lipid concentration, pH and Ca^{+2} concentration. These factors were studied for suspensions prepared as described in Chapter 4. The

experiments were carried out at 25°C. Changes in scattered light intensity are thought by the author to be indicative of vesicle fusion or aggregation processes.

To understand why $S(90^{o})$ may be a function of time, one recalls from Eqn. 6.1 that the specific scattering $S/c = \sum f_j S_j$. Noting that the weight fraction of the j'th particle size f_j is c_j/c, 6.1 may be rewritten as

$$S(t) = \sum c_j(t)\, S_j$$

$$\frac{dS}{dt} = \sum \frac{d\, c_j(t)}{dt}\, S_j \qquad 6.4$$

The S_j's are functions of size only, therefore they need not be differentiated with respect to time. If one treats a vesicle suspension as if it were made up of a discrete number of particle sizes and hypothesizes a rate mechanism by which the number of vesicles of a given size varies with time, then it is possible to determine any c_j as a function of time and hence the specific scattering can be determined explicitly as a function of time. The simplest possible example of this treatment is to assume a bimodal particle distribution with particles of concentrations c_1 and c_2 respectively. In analogy with Chapter 6.1, c_1 corresponds to the concentration of small (275 Å) single walled vesicles and c_2 would correspond to larger multilamellar (10^3 Å) vesicles.

Assuming the simplest possible rate law $c_1 \xrightarrow{k_1} c_2$ where at t= o, $c_1 = c_o$, and c_2 = o, it is straightforward to show;

$$c_1 = c_o S_1 \exp - k_1 t; \quad c_2 = c_o S_2 (1-\exp-k_1 t) \qquad 6.5$$

Knowing the time dependence of c_1 and c_2 one may write

$$S = c_o S_1 \exp - k_1 t + c_o S_2 (1-\exp-k_1 t)$$

$$\frac{dS}{dt} = c_o k_1 (S_2-S_1) \exp - k_1 t \qquad 6.6$$

Factors which complicate this mechanism are numerous. The precise distribution of particles is not known in our experiments but a bimodal distribution is likely from the discussion in Section 6.1. The molecularity of the rate processes involved are obviously more complex than indicated in Eqn. 6.5. Other rate processes which seem likely to be important are $nc_1 \rightarrow c_j$ where n is usually 1, 2 or 3. Also, mixed rates such as $c_1 + c_j \rightarrow c_k$ would become important for larger times t. Of greater interest to this work than the full details of the mechanism, are the effects of externally controlled parameters such as lipid concentration, pH and Ca^{+2} concentration on S and dS/dt.

Fig. 6.3a shows the effect of lipid concentration on dS/dt for two pH values. dS/dt was measured 1 hr. after the samples were cooled to 25°C. A straight line of unit slope was drawn through the experimental points. For low lipid concentrations ($<10^{-3}$M) this line fits the experimental data. Measurements at much lower concentrations are difficult due to signal to noise ratio problems. Thus at low lipid concentrations the value of dS/dt is proportional to lipid concentration. This is indicative of the presence of a first order rate process.

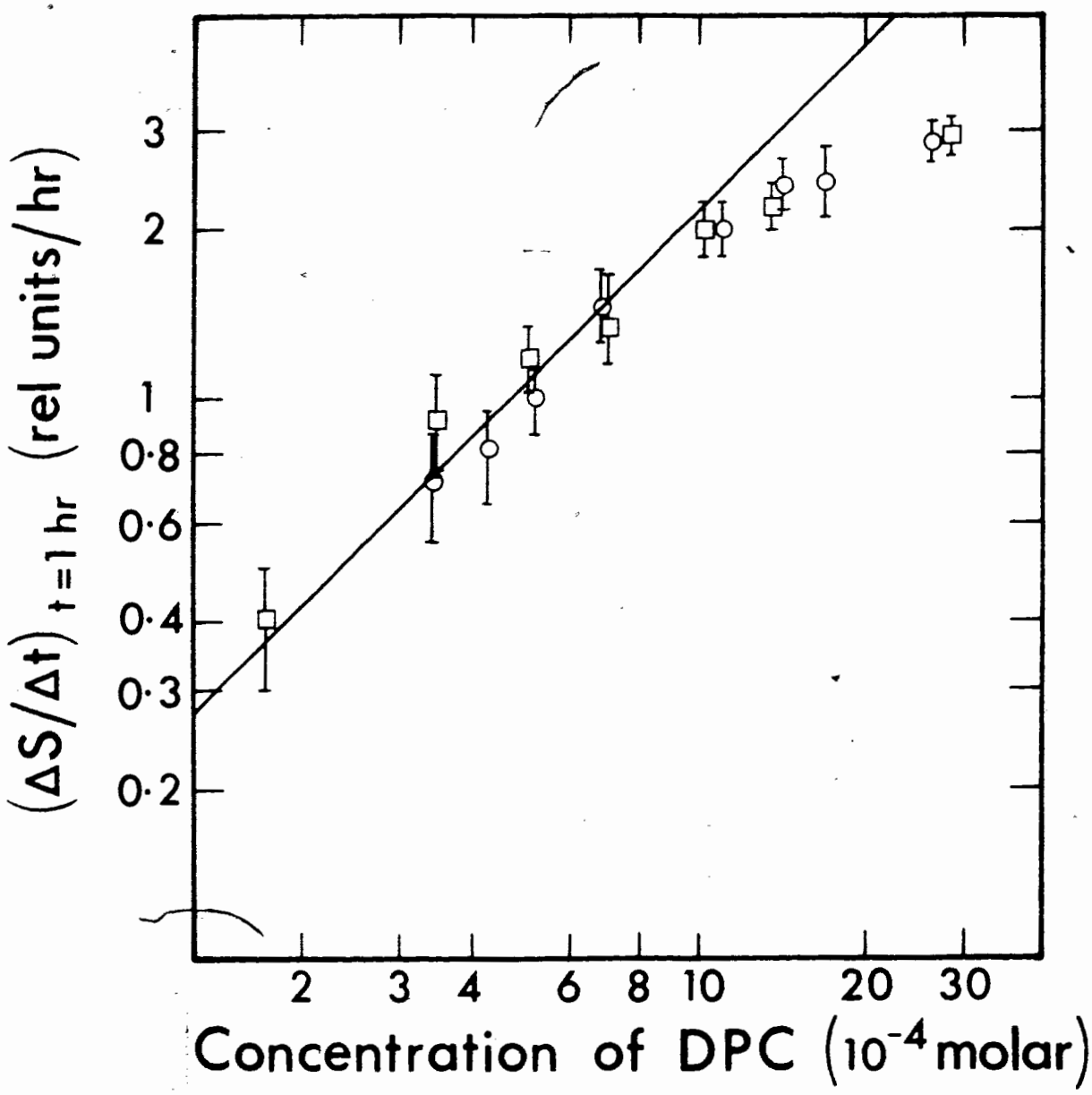

Fig. 6.3a Time rate of change of scattering intensity (relative units/hr.) as a function of DPC concentration for two pH values. □ pH 5.1, ○ pH 5.8.

A conclusion one may draw from the linear dependence of $\Delta S/\Delta t$ on DPC concentration is that for low lipid concentrations a highly homogenous vesicle distribution is obtained. Another is that there is a first order rate process present. At higher lipid concentrations the slope indicates the power is less than one. Two reasons for this behaviour are believed to exist. First, since all these samples were sonicated for the same length of time, samples of higher lipid concentration contain a larger fraction of large vesicles, therefore are less sensitive to changes in scattering due to fusion or aggregation of small vesicles. Second, higher lipid concentrations may give rise to multiple scattering of photons which should decrease light intensity. Another kinetic study in the literature by Maeda and Ohnishi (1974) utilized E.S.R. spectra of 12-nitroxide stearic acid labelled lipids to study mixing of lipid molecules. Their data indicated that a similar dependence existed between lipid concentration and rate of fusion.

Fig. 6.3b shows the scattered light intensity $S(90^{o})$ as a function of time t for samples prepared at various pH values $S(90^{o})$, plotted on a logarithmic scale. The sharp increase in $S(90^{o})$ during the first five minutes is due to the cooling of the samples from $50^{o}C$ to $25^{o}C$. For $t > 5$ min. all curves are linear with respect to time with slopes varying with the bulk pH of the suspension. Since log dS/dt is a linear function of time, t and dS/dt is a positive decreasing function of time, one concludes that a rate law of the form;

$$\frac{dS}{dt} \propto k \exp - kt \qquad 6.7$$

must exist where k is a rate constant which describes the overall time behaviour of the system. If one agrees that a change in $S(90^{o})$ with time must indicate either fusion or aggregation of vesicles, then k must be related to the degree of dissociation of the lipid polar groups.

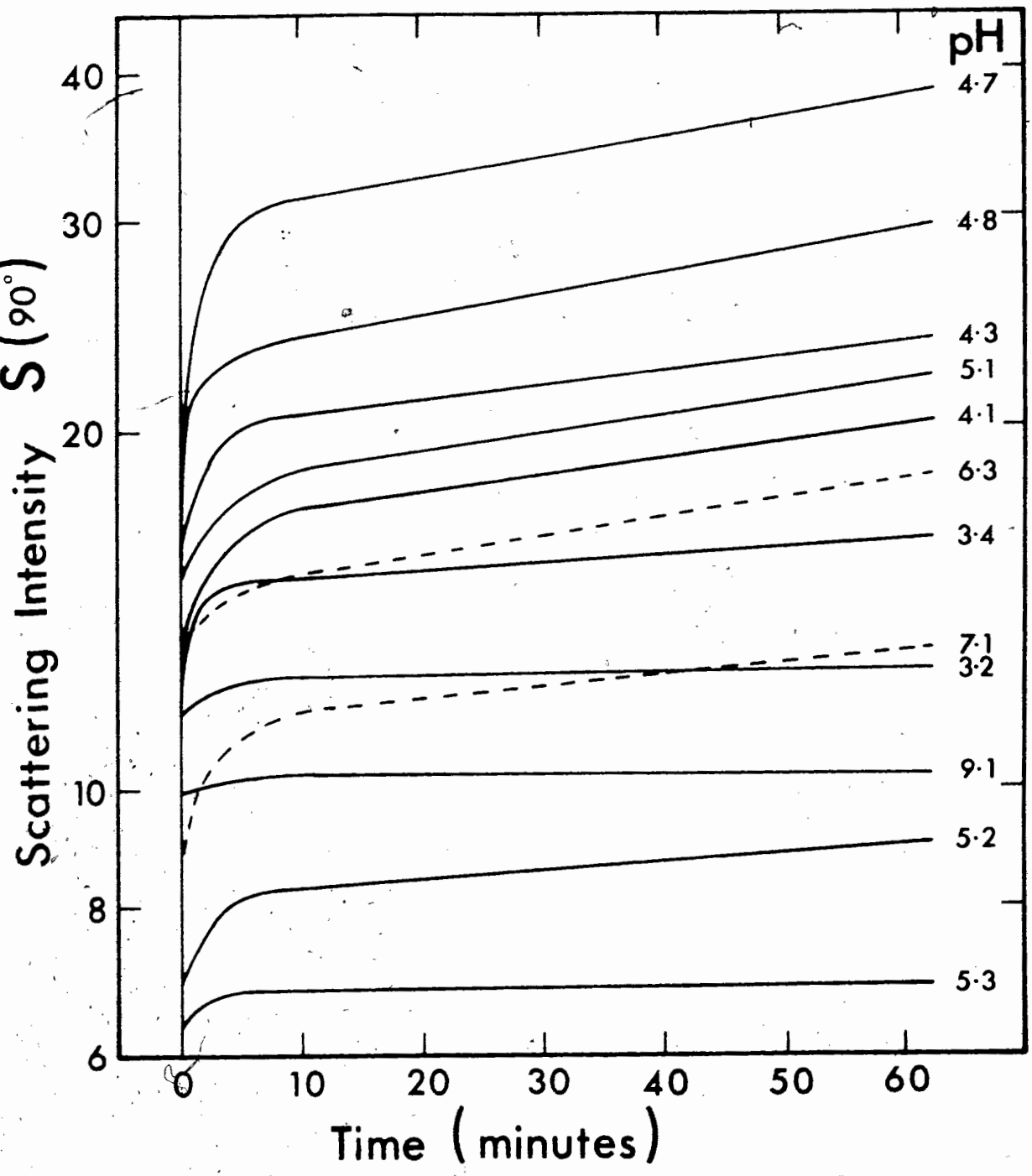

Fig. 6.3b Scattering intensity (relative units) as a function of time for various pH values.

Fig. 6.3c shows dS/dt as a function of pH for various times after sonication. As one can see, $\Delta S/\Delta t$ decreases for increasing t at a given pH. This is expected if dS/dt is proportional to k exp-kt. More interesting are the maxima and minima which are observed in Fig. 6.3c. This is interpreted as a variation in the rate constant k as the degree of dissociation of DPC molecules changes. Recalling from Eqn. 4.3.1 that the phosphate group of DPC can bind a proton where pK_1 is 1.40 for the bulk solution, we write

$$pK_1 = pH - \frac{\log[PO_4^-]}{[HPO_4]_+} \qquad 6.8$$

We recall the equilibrium constant for the formation of the internal salt linkage K_3 is 8.85×10^2. For pH < 3 the measured value of $\Delta S/\Delta t$ is very low for all time t.

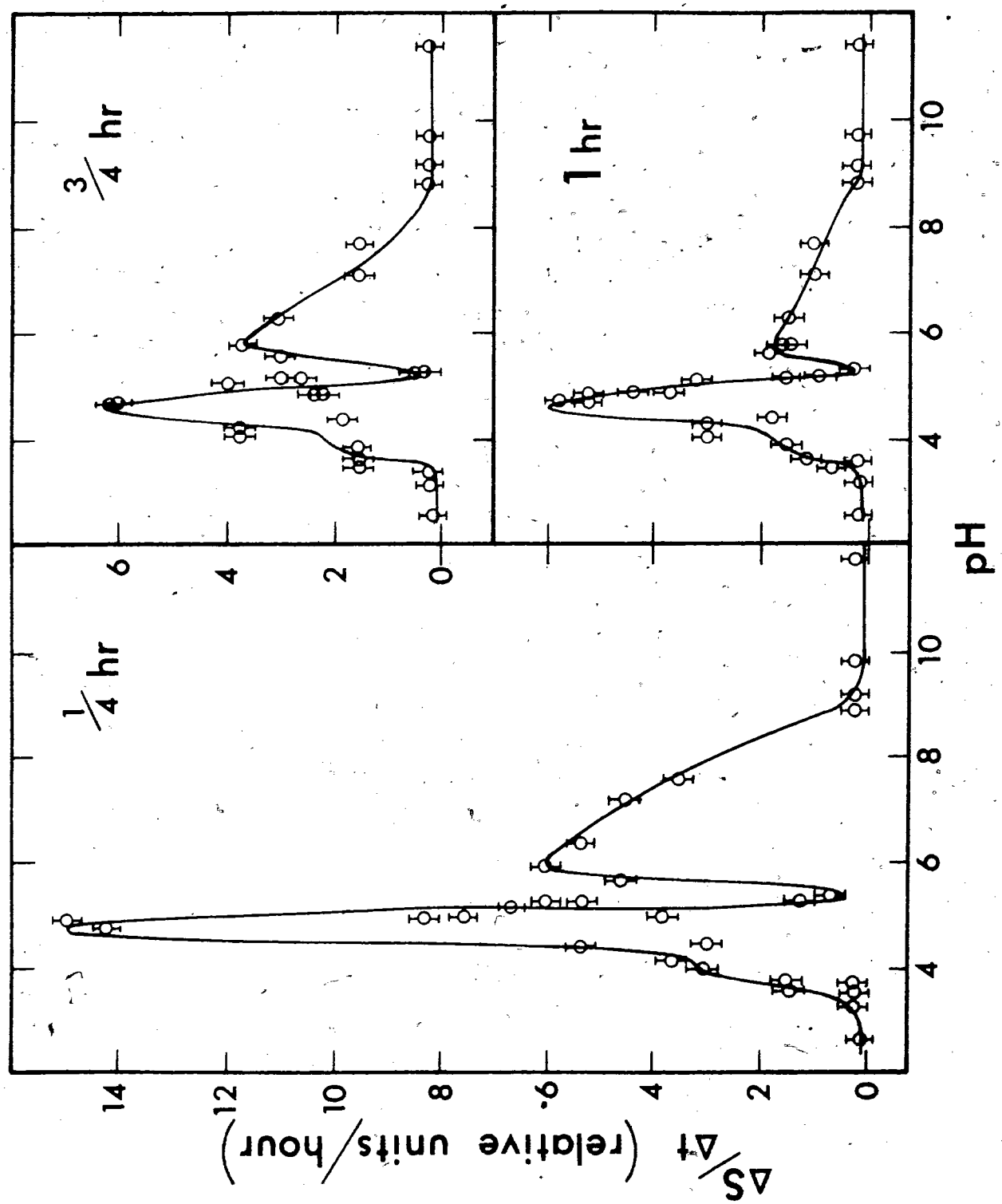

Fig. 6.3c Time rate of change of scattering intensity (relative units/hr.) as a function of pH for various times.

It is easily shown that at pH 3 99.5% of the lipid molecules are dissociated into PO_4^- and may form internal salt linkages with the trimethylammonium group. 0.5% of the lipid molecules are protonated, thus they will carry a net positive charge of $q = 1.6 \times 10^{-19}$ coulombs. Accepting that the molecular weight of bilayer vesicles is 2.1×10^6 (Huang, 1965) and noting that the molecular weight of DPC is 734, it is easily seen that there are approximately 2.86×10^4 lipid molecules per vesicle. The average number of charged lipids per vesicle is about 140. Assuming these charges to be uniformly distributed on a sphere of radius 275 Å and immobile, the electrostatic repulsive energy between two vesicles 1000 Å apart in pure water is approximately given by

$$E_R = q_1 q_2 / 4\pi\epsilon r_{12} = 5.5 \times 10^{-12} \text{ ergs} \qquad 6.9$$

where q_1 and q_2 are the charges on the two vesicles r_{12} is the center to center distance between the vesicles and ϵ is the dielectric constant of water. The thermal energy E_t per vesicle for dilute suspensions at room temperature (298°K) is

$$E_t = 3/2\ kT = 6.18 \times 10^{-14} \text{ ergs.} \qquad 6.10$$

where T is the absolute temperature (298°K) and k is Boltzmann's constant (1.38×10^{-16} erg/°K). When $E_t/E_R > 1$ the vesicles have sufficient thermal energy to overcome the electrostatic energy

barrier and fusion or aggregation may take place. From Eqns. 6.9 and 6.10 $E_t/E_R = 0.011$ at 10^3 Å. Decreasing r_{12} or increasing the surface charge on the vesicles will decrease Et/E_R further. Thus at pH < 3 few collisions are expected to occur, which permit fusion or aggregation, because of the high surface charge on the vesicles. There are several factors which may modify the assumptions made in this treatment. The charge on the lipid is not totally immobile. Lateral diffusion of lipid molecules is dependent on membrane fluidity. Since this experiment was performed at 25°C the author would expect diffusion of charges to be at a minimum. For $T > T_c$ charges may diffuse rapidly through lateral diffusion. The vesicles are expected to act similar to conducting spheres. The charge distribution will become nonuniform so as to relax the electrostatic repulsions. Since $T < T_c$ and diffusion of charges is small the initial treatment is thought to be sufficient. The surface charge is screened by counter ions (Cl^-), but it is believed that these had only a small effect since solutions of low ionic strength were utilized. Van der Waals forces which are attractive and proportional to r^{-6} will be negligible at larger distances (since electrostatic forces are proportional to r^{-2}), but at shorter distances will dominate the electrostatic forces. For Et/ER < 1 Van der Waals interactions should be negligible. At pH 4 $\Delta S/\Delta t$ rises very sharply to a peak which occurs at pH 4.8. At pH 4.8 the fraction of charged lipids is 6.3×10^{-4} which is an average of 17.6 charges/vesicle. Et/ER in this case is 1.77 which means the thermal

energy of vesicles is suficient to overcome electrostatic repulsions. Thus $\Delta S/\Delta t$ is expected to increase due to fusion or aggregation. The minimum at pH 5.5 is more difficult to explain. The surface charge is smaller than in the previous cases, thus Et/ER > 1 which, according to theory should enhance $\Delta S/\Delta t$. It is believed internal salt binding may explain the minimum. A second peak which decreases with increasing pH is observed at pH 5.9. For pH > 8.5 $\Delta S/\Delta t$ becomes small. This is thought to be due to the equilibrium of Eqn. 4.3.2 which charges vesicles by absorption of OH^- ions on the trimethylammonium groups. The pK_2 for this reaction is 11.6. One has for pK_2

$$pK_2 = pH + \log \frac{[N(CH_3)_3{}^+....]_o}{[N(CH_3)_3{}^+....OH^-]_-} \qquad 6.11$$

where the dissociation of a proton is considered physically equivalent to the binding of an hydroxide ion. Lipids with headgroups such as serine or ethanolamine simply lose a proton in basic solution, but since choline has no dissociable proton on the trimethylammonium group, it must absorb an hydroxide in highly basic solutions. If α is the fraction of uncharged lipids then

$$\alpha = \frac{10^{(pK_2-pH)}}{1+10^{(pK_2-pH)}} \qquad 6.12$$

For pH 10, α is .975 which means the fraction of charged vesicles is .025. This corresponds to about 700 charges making E_t/E_R 4.48 x 10^{-4}. Thus above pH 10 $\Delta S/\Delta t$ should be small since the surface charge is high. Below pH 10 the surface charge decreases rapidly and E_t/E_R increases. $\Delta S/\Delta t$ increases as expected.

Fig. 6.3d shows the effect of 10^{-3}M Ca $Cl_2.2H_2O$ in the aqueous media on $\Delta S/\Delta t$ as a function of pH. Basically the same behaviour as in Fig. 6.3c is noted in Fig. 6.3d. The first peak is shifted to a lower pH (4). The minimum in Fig. 6.3d is much broader than that in Fig. 6.3c (4.8 to 6.0) and the second peak is steeper and narrower than in Fig. 6.3c. To understand this one must note that for low pH $[H^+] >> [OH^-]$ reactions 4.1, 4.2 and 4.4 will be in competition. The amount of PO_4^- available to interact with Ca^{+2} or to form an internal salt linkage is controlled by the pH of the suspension. For high $[H^+]$ vesicles become charged according to Eqn. 4.3.1. Increasing $[H^+]$ 10 times will cause $[PO_4^-]$ to decrease by a factor of 10. The amount of bound Ca^{+2} is expected to decrease by a factor of 100 according to Eqn. 4.4, thus low pH's should reduce Ca^{+2} binding and internal salt linkage and increase surface charge by protonation of PO_4^-. The overall effect of this, modified by counter ions and charge mobility, should tend to decrease aggregation or fusion of vesicles. The binding of Ca^{+2} to neutral lipid molecules should impart a positive charge. If there is some pH where Ca^{+2} may begin binding to vesicles, then one might expect a decrease in $\Delta S/\Delta t$. Increasing the pH further should cause

vesicles to accumulate negative charge (OH^-) which would cancel the positive charges of Ca^{+2}. Neutral vesicles should then be free to collide thus increasing $\Delta S/\Delta t$. Increasing the pH further causes an excess of negative charge thus reducing $\Delta S/\Delta t$ by increased electrostatic repulsions. To successfully apply this reasoning K_4 must be less than the value indicated to explain low Ca^{+2} binding at lower pH values. The value for K_4 quoted from Seimiya and Ohki (1972) was for phosphatidyl ethanolamine, which has a dissociable proton ($pK_2 = 7.5$), which would lower the potential barrier experienced by cations, thus binding to the phosphate groups should readily occur. In the case of DPC there is no dissociable proton on the trimethylammonium group thus an hydroxide must bind according to Eqn. 4.2. Prior to this, the trimethylammonium group would tend to strongly repel cations, thus Ca^{+2} binding would be relatively low at physiological pH. The findings of Joos and Carr (1967) indicate that Ca^{+2} does not bind to phosphatidyl choline below pH 10. Work by Ohki (1969) on the resistance of black films as a function of pH and Ca^{+2} concentration showed behaviour remarkably similar to that observed in Figs. 6.3c and 6.3d. As the pH was increased the electrical resistance increased to pH 4.4 where R was a maximum. This was attributed to minimum charge on the dipoles (isoelectric point). Above this pH the resistance decreased up to a pH of 10 where stable films could no longer be formed. In the presence of $Ca\ Cl_2$ this behaviour was modified as the peak was eliminated and the resistance rose steadily. This difference could be attributed only to the

binding of Ca^{+2} to the black film. Thus there is a difference of opinion among authors on the binding properties of Ca^{+2} to phosphatidyl choline. This difference is more easily understood if as mentioned in Section 3.4 the degree of saturation is important to the way in which ions bind to lipids. This information is summarized in Fig. 3.2. Completely saturated chains at $T < T_c$ pack closer and bind Ca^{+2} more readily. Work by previous authors often stated that phosphatidyl choline was used, without making reference to the degree of saturation of hydrocarbon chains. This may account for variations in experimental results. The author's work indicates that there is some Ca^{+2} binding at pH values as low as 4.5. Applying K_4 to the equilibrium conditions set out in Chapter 3 one might expect a greater effect on the data in Fig. 6.3d. Since this is not the case, K_4 must be smaller than the figure obtained in the literature.

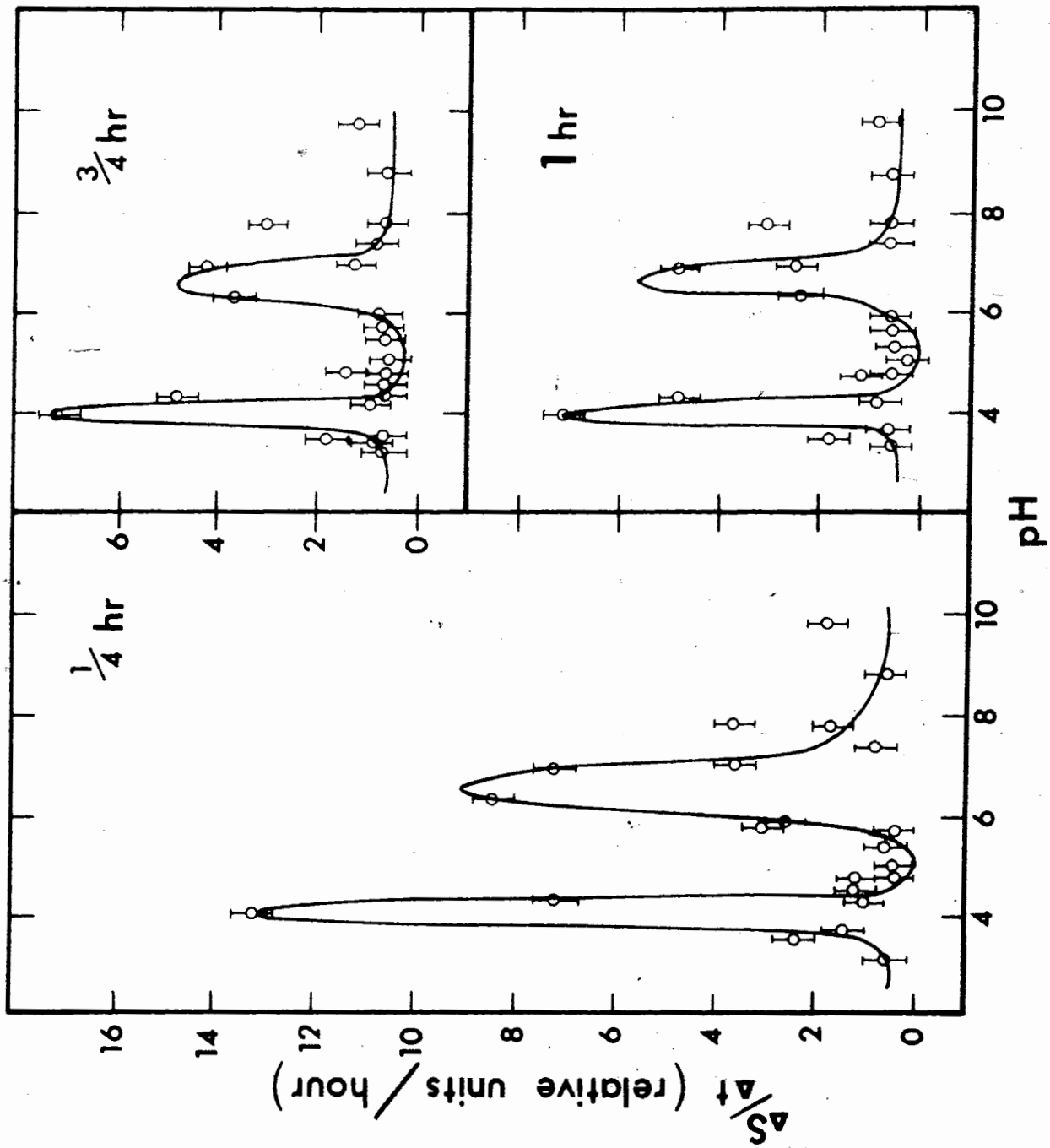

Fig. 6.3d Time rate of change of scattering intensity (relative units/hr.) as a function of pH for various times in 10^{-3} M Ca^{+2} solution.

6.3 TEMPERATURE DEPENDENCE OF SCATTERED LIGHT INTENSITY

Thermotropic phase transitions of lipids have been discussed in Section 3.3. Recalling Eqn. 5.19

one notes that changes in temperature may cause changes in V, dn/dc, m and $P(\theta)$ which cause $S(90^{o})$ to change. The percentage change in scattering between two temperatures is given by the sum of percentage changes in these variables. The observations of Sheetz and Chan (1972) indicate a 3% increase in the volume of the vesicles. The work of Chapman et al. (1967) shows the lipid layer thickness l decreases from 45 Å to 40 Å, while the water layer thickness w increases from 25 Å to 30 Å when the temperature is increased above T_c. Chong (1975) has shown that $P(\theta)$ should decrease anywhere from 2% to 10% depending on the vesicle radius and aqueous core radius. The average decrease was shown to be about 7%. Yi and MacDonald (1973) and Chong (1975) have shown that the term dn/dc decreases by about 16% from 25°C to 50°C. Change in the relative refractive index m leads to an additional change in the scattering primarily through a change in the term (m-1) giving a further decrease of 15%. Thus the expected decrease in scattering should range from 30% to 39%, depending upon $P(\theta)$. In addition, a slow decrease in $S(90^{o})$ is predicted by dn/dc and m terms above and below the phase transition. Large variations from this behaviour are noted in Fig. 6.4a and 6.4b for samples prepared in solution of high ion concentration. ϕ is the ratio of ion concentration to lipid concentration. The lipid concentration in all cases was 6.84×10^{-4}M.

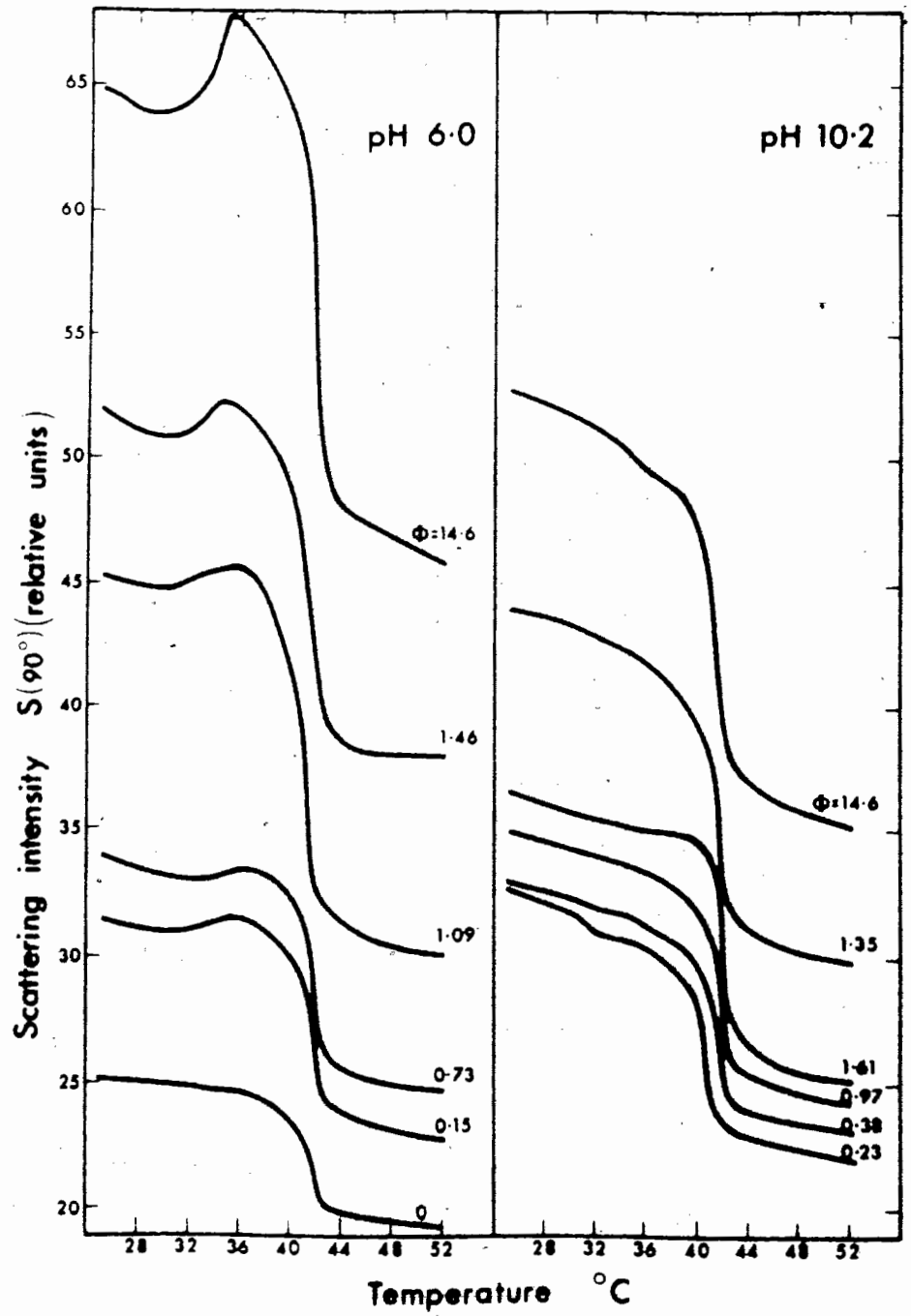

Fig. 6.4a Scattering intensity (relative units) as a function of temperature for various K^+ concentrations for two pH values. ϕ = $[K^+]/[DPC]$, [DPC] = 6.84×10^{-4} M.

Fig. 6.4a shows $S(90^{o})$ as a function of temperature for various mole fractions of K^{+}. K^{+} is added before sonication, therefore is expected to be uniformly distributed in the aqueous solution. For ϕ = 0 and pH 6 we observe a smooth curve with a sharp transition at $41.5^{o}C$. A slight change in slope is also noted at about $33^{o}C$ which may be the pretransition reported by other authors (see Section 3.3). Between $25^{o}C$ and $50^{o}C$ the scattering intensity decreases by 28%, slightly less than that predicted by theory. For pH 10.2 and ϕ = .23 a change of 30.8% is noted and a much sharper drop in $S(90^{o})$ at $32^{o}C$. On increasing the KCl content of the pH 6 samples there is an increase in scattering intensity between $32^{o}C$ and $38^{o}C$ which increases with increasing KCl concentration. The percent decrease in scattered light intensity between $25^{o}C$ and $50^{o}C$ remains near the limits proposed in the theory. This information is summarized in Table 6.2.

Table 6.2

Summary of changes in scattered light intensity for various K^+ concentrations.

$\phi = \frac{[K^+]}{[DPC]}$	pH ± .1	$\frac{[S(25)-S(36)]10^2}{S(25)}$	$\frac{[S(25)-S(50)]10^2}{S(25)}$
0.00	6.0	1.90	25
.15	6.0	0.00	28
.73	6.0	1.75	25
1.09	6.0	-.44	34
1.46	6.0	-.38	27
14.60	6.0	-3.80	30
.23	10.2	7.30	33
.38	10.2	6.30	31
.96	10.2	4.80	29
1.33	10.2	5.20	27
1.60	10.2	6.20	33
14.60	10.2	4.40	33

This behaviour is not observed at pH 10.2 where S always decreases in the 25°C to 36°C range. Some of the pH 10.2 curves show what may be pretransition type behaviour, but this change is very small and may not be experimentally significant. For pH 6 the percent decrease in S between 25°C and 50°C is on average 28% which is slightly lower than predicted by theory. For pH 10.2 this figure is on average 31% which is within the predictions of theory. Higher values of ϕ seem to cause higher initial levels of scattering. It is believed that high concentration of KCl increases screening of charge and hence reduces repulsions between vesicles causing larger vesicles to form initially. This effect is the same at pH 6 and pH 10.2. The bumps on the pH 6 curves are best explained if there is some change in aggregation properties of vesicles which is triggered by temperature. The fact that this change occurs in a region where the pretransition has been observed leads one to hypothesize that some dipolar rearrangements may be occuring. If temperature causes the disruption of the internal salt linkage , a corresponding rearrangement in local ion concentrations is feasible. Counter ions will cancel free charge on the dipoles proportional to the ion concentration, causing aggregation of vesicles due to low electrostatic repulsions (kT is also increased due to higher temperature). At pH 10.2 one does not see this effect because the internal salt linkage is broken by the high pH which charges the vesicles.

Fig. 6.4b shows S(90°) as a function of temperature for pH values of 6.0 and 10.2 for vesicles prepared in solutions of various

Ca^{+2} concentrations. The percentage change in scattered light intensity between 25°C, and 36°C and 25°C and 50°C are summarized in Table 6.3. ϕ is the ratio of Ca^{+2} concentration to lipid concentration. The lipid concentration is kept constant at 6.84 x 10^{-4}M. Examination of Fig. 6.4b and Table 6.3 shows the percent decrease in scattered light intensity is less than predicted by theory for the 41° transition by about 4% on average for pH 6. The decrease in S(90°) between 25°C and 36°C shows anomalous behaviour at pH 10.2 but not at 6.0. For pH 10.2 the 41° transition shows highly anomalous behaviour. If one assumes that a small percentage of Ca^{+2} is bound at pH 6 then it is expected that some lipid molecules would be held in a more rigid structure. The parameters which decrease S would be affected less due to the binding of Ca^{+2}. This agrees with the notion that Ca^{+2} stabilizes membrane structures. At pH 10.2 the thermal behaviour of the lipid suspensions is highly anomalous. A larger degree of Ca^{+2} binding at this pH is expected due to presence of a net negative charge on some vesicles which should lower electrostatic repulsion of cations. By Eqn. 6.12 the fraction of negatively charged lipid molecules is expected to be .036 assuming pK_2 is 11.6. A lower pK_2 would increase this fraction and thus increase the degree of Ca^{+2} binding. The presence of small amounts of Ca^{+2} cause a sharp anomoly in the 25°C to 36°C region. The greatest effect in this region is noted at ϕ = .4 to .5. This effect is interesting since one Ca^{+2} binds with two PO_4^-. Increasing the concentration of Ca^{+2} further

causes the anomoly to shift to higher temperatures. It is believed that this is a mass action effect. The higher Ca^{+2} concentration causes the equilibrium described by Eqn. 4.4 to shift further to the right. The unpredicted rise in scattering intensity is attributed to aggregation or fusion of vesicles. No mechanism for this anomaly is proven in this data but the author suggests that the breaking of Ca^{+2}, PO_4^- bonds might cause aggregation of vesicles. No variations in T_c with ion concentration are observed in these experiments. It is felt this is due to low surface charge (charges of order 1 per lipid molecule are necessary to change T_c by Eqn. 4.5).

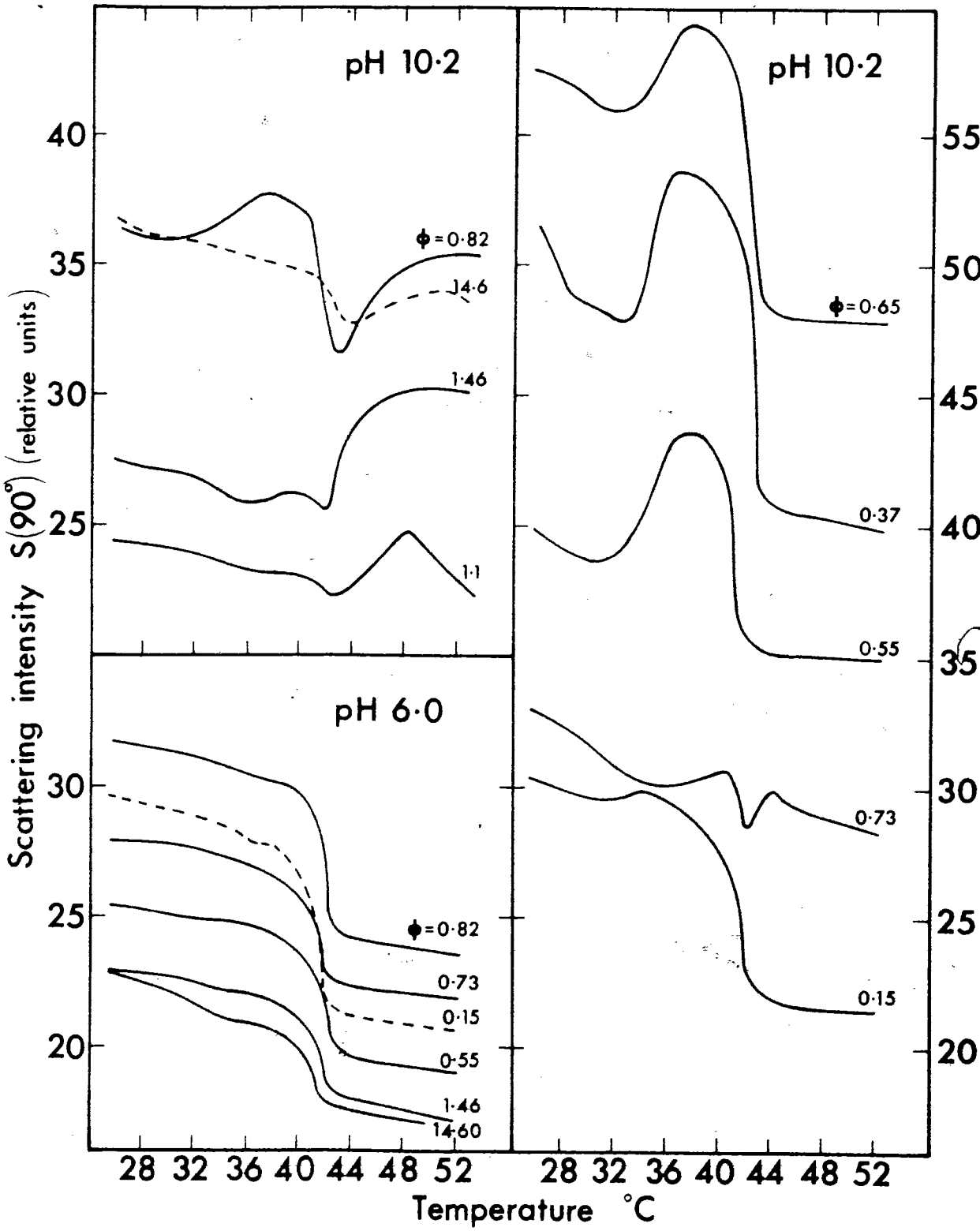

Fig. 6.4b Scattering intensity (relative units) as a function of temperature for various Ca^{+2} concentrations for two pH values, ϕ = $[Ca^{+2}]/[DPC]$, [DPC] = 6.84×10^{-4} M.

Table 6.3

Percentage change in scattered light intensities for various Ca^{+2} concentrations.

$\phi = \frac{[Ca^{+2}]}{[DPC]}$	pH ± .1	$\frac{[S(25)-S(36)]10^2}{S(25)}$	$\frac{[S(25)-S(50)]10^2}{S(25)}$
.15	6.0	6.15	30
.55	6.0	2.8	24
.73	6.0	3.2	21
.82	6.0	4.4	25
1.46	6.0	6.3	26
14.6	6.0	9.1	26
.15	10.2	2.6	26
.37	10.2	-4.5	22
.55	10.2	-8.5	12
.65	10.2	-3.0	17
.73	10.2	9.0	14.5
.82	10.2	-3.6	2.7
1.1	10.2	4.5	5.3
1.46	10.2	5.8	-9.8
14.6	10.2	3.3	7.4
.23[1]	10.2	-8.0	22.5
.22[1]	10.2	-1.2	27.7
.40[1]	10.2	-13.0	27.0

1. Other measurements taken but not shown on Fig. 6.4b

6.4 DISCUSSION OF RESULTS

The results in Section 6.1 are explained in terms of a bimodal distribution of particle sizes. Small vesicles of diameter 275 Å are obtained by sonication in addition to a fraction of larger particles which are present due to incomplete sonication of lipids and the presence of particles from the sonicator probe. A single narrow distribution could be obtained by methods such as ultracentrifugation, chromatography, and ultrafiltration. However, studies involving scattering intensity as a function of time make secondary treatment a source of error since the more treatment steps involved, the more difficult it becomes to define initial conditions. For this reason secondary treatments were not utilized in this experiment.

The study of scattering intensity as a function of time indicates an exponential rate process for fusion. This is supported by scattering at a given time after sonication and by the time rate of change in scattering as a function of pH. The latter is attributed to electrostatic charge which resides on the polar head of the DPC molecules. Knowledge of the exact lipid distribution should enable a precise kinetic analysis of scattering as a function of time. A general method for doing this is given in Eqn. 6.4. A linear rate law was put into Eqn. 6.4. Reasonable agreement with experimental data was observed. This could prove to be a useful method for investigating the fusion of vesicles. Extending this study to different temperatures the activation energy for these processes could be obtained by this method.

Using published data of the refractive index, volume and lipid thickness as a function of temperature Rayleigh-Gans scattering theory predicts a 30 to 39% decrease in scattering intensity between 25°C and 50°C for vesicles prepared in distilled H_2O, in agreement with experiment. K^+ and Ca^{+2} ions have been shown to cause anomalies in this behaviour. K^+ ions are believed to screen charges on the vesicles thus causing fusion or aggregation of vesicles on breaking the internal salt linkage present at pH 6. At pH 10.2 the salt linkage is expected to be broken already by the pH conditions. Ca^{+2} on the other hand, is believed to bind to the lipid between PO_4^- groups. Changes in temperature may change the amount of Ca^{+2} bound, thus causing reorganization of the suspension due to changes in the distributions of charge in the vesicles. This could be tested further by studying scattering at fixed temperatures as a function of time.

CHAPTER 7

GENERAL CONCLUSIONS

The attention in this thesis has been directed towards two basic questions. The first is how does vesicle surface charge affect the fusion or aggregation of vesicles? The second is how do ions of biological importance affect the phase transition behaviour of DPC vesicles as reflected by changes in light scattering.

90^{o} light scattering measurements have provided a method of measuring fusion or aggregation of vesicles through changes in the vesicle size distribution. Variations in the time rate of change of scattering was accounted for by vesicle surface charge. A small rate of change in scattering is obtained when the electrostatic repulsive energy is greater than the thermal energy of the vesicles. The minimum at pH 5.8 is not explained by this rule since the surface charge is low at this pH. The author suggests that internal salt binding lowers the time rate of change of scattering at this pH. Linear rate theory was applied to the data, and was found consistent with the data. However, more complex rates are expected for longer times. Future experiments could extend this analysis to studying S(t) at various temperatures to obtain an estimate of the activation energy. The activation energy in turn should be related to the vesicle charge distribution. The author suspects the activation energy could also be related to vesicle surface charge.

Analysis of Rayleigh-Gans scattering theory predicts a 30 to 39% decrease in scattering intensity between 25°C to 50°C for lipid dispersions prepared in distilled H_2O. K^+ ions in the aqueous media caused anomalous behaviour at pH 6 but not 10.2. The results are explained in terms of internal salt linkage which is expected to be strong at pH 6 but not pH 10.2. The salt linkage may be dissociated thermally at approximately 34°C. The dissociation of the salt linkage is followed by aggregation or fusion of vesicles. Ca^{+2} is believed to bind to lipid polar groups, one Ca^{+2} binding to two PO_4^- groups. Two phenomena are predicted in this case. First, T_c is expected to increase with Ca^{+2} binding. No change was observed in the data which is accounted for in terms of low surface charge. For a measureable change in T_c a charge of nearly one per lipid molecule is expected. The presence of Ca^{+2} does change the magnitude of the phase transition. The amount of Ca^{+2} bound should be temperature dependent. The anomalies observed with Ca^{+2} are believed to be indicative of Ca^{+2} bonds being broken thermally.

APPENDIX 1

Computer Calculations For The Single Lecithin Shell Model

The computation was carried out for six values of t (ratio of aqueous core radius to the outer radius of the vesicle). The maximum vesicle size considered was about the wavelength of incident light. $P(\theta)$ was first calculated using the expression in Eqn. 5.9 for various values of R and the quantities $S(90^{o})/c$, Q, β, and τ/c were calculated for various values of the size parameter. $S(90^{o})/c$ and τ/c are specific values normalized for a lecithin concentration of 0.1 mg/ml and 1 mg/ml respectively. The computed values for the wavelength of 366 nm are given in Table A1.1 to A1.5 and graphical plots are shown in Fig. A1.1 to Fig. A1.5. Note that in Fig. 1,3,4 the origins of the curves for different core radii are shifted.

Table A1.1 Scattering factor as a function of kR

WAVE LENGTH IS 3660.

K*R	RATIO OF INNER/OUTER RADIUS: 0.0	0.20	0.40	0.60	0.80	0.90
0.2136	0.99090	0.99083	0.99040	0.98931	0.98757	0.98627
0.4694	0.95676	0.95643	0.95431	0.94926	0.94076	0.93516
0.7251	0.89947	0.89871	0.89388	0.88241	0.86332	0.85089
0.9808	0.82274	0.82144	0.81314	0.79364	0.76164	0.74109
1.2365	0.73140	0.72949	0.71737	0.68923	0.64395	0.61546
1.4922	0.63094	0.62843	0.61256	0.57626	0.51931	0.48442
1.7480	0.52705	0.52399	0.50485	0.46189	0.39668	0.35806
2.0037	0.42511	0.42162	0.40006	0.35277	0.28396	0.24498
2.2594	0.32979	0.32605	0.30315	0.25442	0.18725	0.15141
2.5151	0.24477	0.24095	0.21796	0.17089	0.11047	0.08081
2.7708	0.17247	0.16878	0.14696	0.10446	0.05508	0.03373
3.0266	0.11409	0.11070	0.09120	0.05574	0.02026	0.00814
3.2823	0.06960	0.06668	0.05043	0.02374	0.00334	0.00004
3.5380	0.03800	0.03566	0.02330	0.00622	0.00029	0.00426
3.7937	0.01751	0.01582	0.00766	0.00014	0.00650	0.01532
4.0494	0.00593	0.00491	0.00091	0.00207	0.01734	0.02820
4.3052	0.00088	0.00050	0.00034	0.00860	0.02880	0.03899
4.5609	0.00009	0.00029	0.00340	0.01675	0.03789	0.04522
4.8166	0.00161	0.00229	0.00793	0.02421	0.04280	0.04594
5.0723	0.00392	0.00495	0.01230	0.02941	0.04295	0.04156
5.3280	0.00596	0.00723	0.01549	0.03163	0.03880	0.03348
5.5838	0.00718	0.00856	0.01699	0.03082	0.03157	0.02364
5.8395	0.00738	0.00877	0.01676	0.02748	0.02284	0.01404
6.0952	0.00669	0.00799	0.01510	0.02243	0.01422	0.00633
6.3509	0.00539	0.00654	0.01248	0.01665	0.00708	0.00155
6.6066	0.00383	0.00478	0.00945	0.01102	0.00228	0.00000
6.8623	0.00233	0.00305	0.00648	0.00625	0.00014	0.00130
7.1181	0.00113	0.00163	0.00393	0.00277	0.00046	0.00455
7.3738	0.00036	0.00065	0.00201	0.00072	0.00260	0.00861
7.6295	0.00002	0.00013	0.00077	0.00001	0.00571	0.01234
7.8852	0.00006	0.00000	0.00015	0.00033	0.00891	0.01483
8.1409	0.00033	0.00015	0.00000	0.00130	0.01142	0.01559
8.3967	0.00069	0.00042	0.00013	0.00251	0.01273	0.01454
8.6524	0.00102	0.00069	0.00038	0.00361	0.01266	0.01203
8.9081	0.00122	0.00087	0.00060	0.00437	0.01132	0.00868
9.1638	0.00126	0.00091	0.00072	0.00465	0.00905	0.00523
9.4195	0.00114	0.00082	0.00071	0.00445	0.00635	0.00235
9.6753	0.00091	0.00063	0.00060	0.00388	0.00374	0.00054
9.9310	0.00063	0.00040	0.00042	0.00306	0.00166	0.00000
10.1867	0.00036	0.00019	0.00024	0.00217	0.00038	0.00065
10.4424	0.00015	0.00005	0.00009	0.00135	0.00000	0.00217
10.6981	0.00003	0.00000	0.00001	0.00069	0.00043	0.00406
10.9539	0.00000	0.00004	0.00001	0.00025	0.00142	0.00583
11.2096	0.00005	0.00014	0.00006	0.00004	0.00267	0.00706
11.4653	0.00015	0.00028	0.00015	0.00001	0.00385	0.00747
11.7210	0.00025	0.00042	0.00023	0.00009	0.00469	0.00701
11.9767	0.00034	0.00052	0.00029	0.00023	0.00503	0.00583
12.2325	0.00038	0.00057	0.00031	0.00037	0.00483	0.00421
12.4882	0.00037	0.00055	0.00028	0.00045	0.00416	0.00253
12.7439	0.00032	0.00048	0.00022	0.00047	0.00318	0.00111
12.9996	0.00024	0.00038	0.00014	0.00043	0.00210	0.00024
13.2553	0.00015	0.00026	0.00006	0.00035	0.00113	0.00001
13.5111	0.00007	0.00015	0.00001	0.00025	0.00041	0.00040
13.7668	0.00002	0.00007	0.00000	0.00015	0.00005	0.00125
14.0225	0.00000	0.00002	0.00003	0.00007	0.00004	0.00230
14.2782	0.00001	0.00000	0.00008	0.00002	0.00033	0.00328
14.5339	0.00004	0.00001	0.00016	0.00000	0.00081	0.00395
14.7897	0.00008	0.00004	0.00024	0.00000	0.00133	0.00418
15.0454	0.00012	0.00007	0.00030	0.00002	0.00178	0.00392
15.3011	0.00015	0.00009	0.00034	0.00003	0.00205	0.00325
15.5568	0.00015	0.00010	0.00034	0.00004	0.00209	0.00234
15.8125	0.00014	0.00009	0.00032	0.00004	0.00191	0.00138
16.0682	0.00011	0.00007	0.00026	0.00003	0.00157	0.00059
16.3240	0.00008	0.00004	0.00019	0.00001	0.00113	0.00011
16.5797	0.00004	0.00002	0.00012	0.00000	0.00069	0.00001
16.8354	0.00002	0.00000	0.00006	0.00000	0.00032	0.00027
17.0911	0.00000	0.00000	0.00002	0.00001	0.00008	0.00079

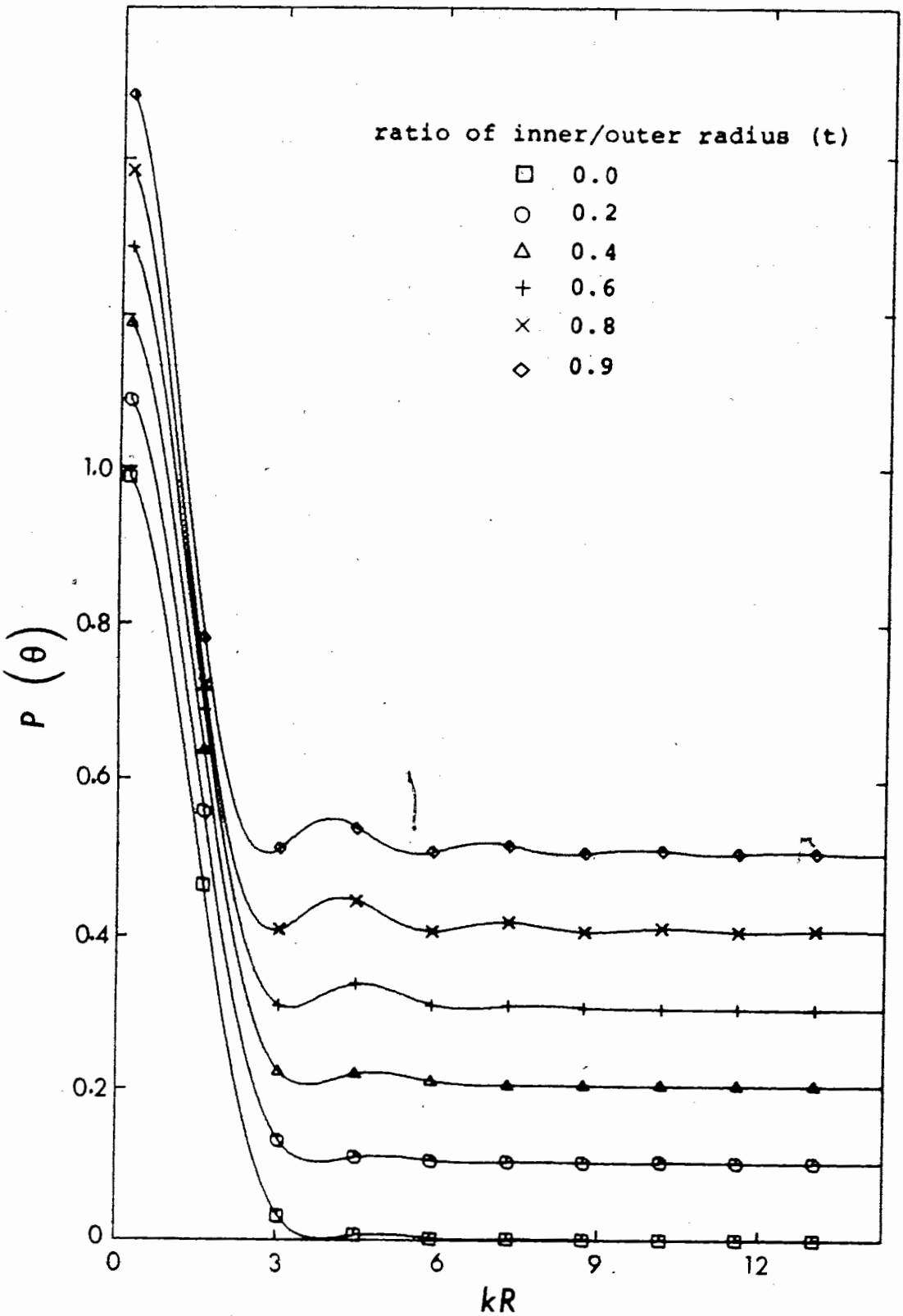

Fig. A1.1 Plot of the scattering factor P(θ) as a function of kR for single lecithin shell vesicles. Note that the baselines of the curves are displaced 0.1 unit from one another.

Table A1.2 Specific scattering as a function of size parameter

I * (10**6) VERSUS N*R/LAMBDA

	RATIO OF INNER/OUTER RADIUS:					
N*R/LAMBDA	0.0	0.20	0.40	0.60	0.80	0.90
0.0184	0.003	0.003	0.002	0.002	0.001	0.001
0.0404	0.027	0.026	0.025	0.021	0.013	0.007
0.0625	0.095	0.094	0.089	0.074	0.045	0.025
0.0845	0.223	0.221	0.207	0.171	0.104	0.057
0.1065	0.418	0.414	0.387	0.317	0.190	0.103
0.1285	0.676	0.669	0.623	0.504	0.297	0.159
0.1506	0.982	0.971	0.899	0.718	0.413	0.217
0.1726	1.314	1.298	1.192	0.937	0.522	0.270
0.1946	1.643	1.620	1.475	1.134	0.610	0.307
0.2166	1.936	1.906	1.717	1.286	0.660	0.322
0.2387	2.164	2.127	1.889	1.369	0.663	0.310
0.2607	2.303	2.257	1.971	1.371	0.616	0.273
0.2827	2.336	2.281	1.951	1.287	0.523	0.214
0.3047	2.258	2.196	1.828	1.125	0.397	0.144
0.3268	2.077	2.009	1.613	0.903	0.258	0.076
0.3488	1.809	1.737	1.329	0.650	0.129	0.024
0.3708	1.481	1.408	1.006	0.399	0.036	0.000
0.3928	1.126	1.055	0.681	0.186	0.000	0.016
0.4149	0.778	0.713	0.389	0.044	0.037	0.075
0.4369	0.470	0.414	0.164	0.001	0.154	0.176
0.4589	0.227	0.186	0.030	0.070	0.346	0.310
0.4810	0.069	0.045	0.004	0.254	0.597	0.463
0.5030	0.002	0.000	0.086	0.541	0.882	0.616
0.5250	0.024	0.045	0.267	0.906	1.168	0.748
0.5470	0.121	0.167	0.526	1.313	1.422	0.841
0.5691	0.270	0.343	0.833	1.721	1.610	0.880
0.5911	0.447	0.544	1.153	2.087	1.707	0.858
0.6131	0.622	0.742	1.451	2.370	1.698	0.776
0.6351	0.770	0.910	1.693	2.539	1.581	0.644
0.6572	0.871	1.026	1.855	2.576	1.368	0.480
0.6792	0.911	1.076	1.921	2.477	1.086	0.308
0.7012	0.887	1.056	1.886	2.250	0.771	0.154
0.7232	0.804	0.971	1.757	1.923	0.465	0.045
0.7453	0.674	0.833	1.549	1.530	0.211	0.000
0.7673	0.517	0.661	1.288	1.113	0.047	0.033
0.7893	0.353	0.476	1.000	0.717	0.001	0.144
0.8113	0.204	0.302	0.715	0.382	0.086	0.324
0.8334	0.088	0.158	0.458	0.141	0.297	0.554
0.8554	0.018	0.057	0.250	0.016	0.615	0.805
0.8774	0.001	0.006	0.103	0.014	1.005	1.045
0.8994	0.034	0.006	0.021	0.128	1.421	1.242
0.9215	0.109	0.049	0.000	0.338	1.813	1.368
0.9435	0.214	0.124	0.029	0.614	2.133	1.405
0.9655	0.329	0.213	0.092	0.920	2.340	1.344
0.9876	0.438	0.300	0.169	1.217	2.407	1.194
1.0096	0.525	0.370	0.244	1.471	2.325	0.973
1.0316	0.576	0.411	0.301	1.652	2.101	0.712
1.0536	0.586	0.417	0.331	1.741	1.764	0.448
1.0757	0.553	0.387	0.329	1.732	1.355	0.219
1.0977	0.483	0.327	0.296	1.628	0.925	0.061
1.1197	0.387	0.247	0.241	1.445	0.531	0.000
1.1417	0.279	0.161	0.173	1.204	0.221	0.050
1.1638	0.173	0.083	0.104	0.934	0.039	0.209
1.1858	0.085	0.026	0.046	0.663	0.007	0.461
1.2078	0.025	0.001	0.010	0.419	0.133	0.775
1.2298	0.000	0.013	0.000	0.221	0.402	1.111
1.2519	0.013	0.062	0.019	0.084	0.782	1.424
1.2739	0.059	0.143	0.061	0.012	1.227	1.674
1.2959	0.129	0.247	0.120	0.003	1.680	1.824
1.3179	0.213	0.360	0.186	0.046	2.087	1.853
1.3400	0.297	0.468	0.247	0.125	2.395	1.756
1.3620	0.369	0.558	0.293	0.221	2.567	1.544
1.3840	0.417	0.617	0.316	0.316	2.582	1.245
1.4061	0.435	0.640	0.312	0.395	2.437	0.901
1.4281	0.422	0.622	0.282	0.446	2.151	0.559
1.4501	0.378	0.569	0.230	0.463	1.760	0.268
1.4721	0.312	0.486	0.165	0.445	1.313	0.072

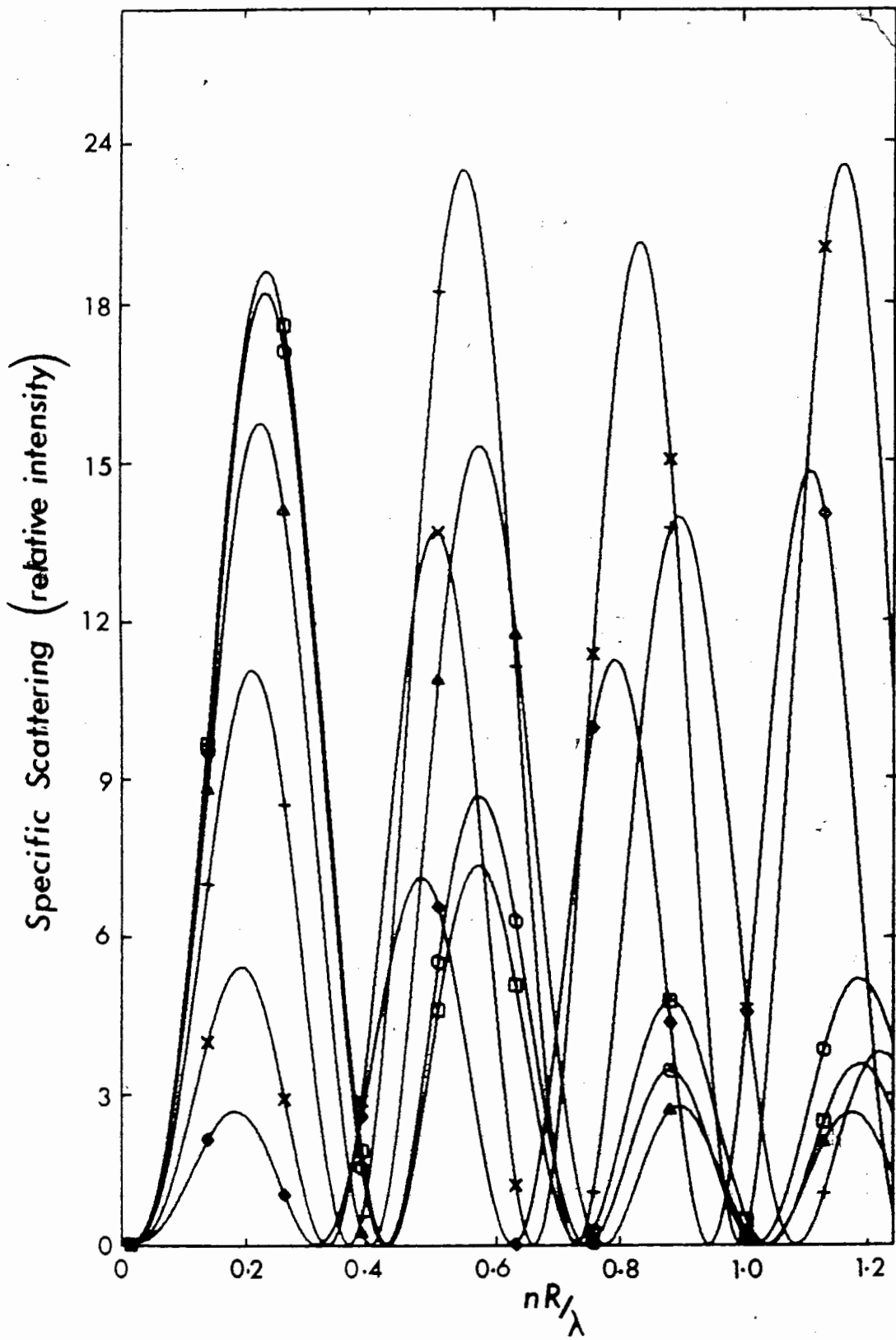

Fig.A1.2 Plot of specific scattering as a function of size parameter for single lecithin shell vesicles. (Refer to Fig. A1.1 for the legend.)

Table A1.3 Dissipation factor as a function of size parameter

Q VERSUS N*R/LAMBDA

N*R/LAMBDA	RATIO OF INNER/OUTER RADIUS: 0.0	0.20	0.40	0.60	0.80	0.90
0.0184	0.994	0.994	0.994	0.993	0.992	0.990
0.0404	0.975	0.974	0.973	0.970	0.965	0.962
0.0625	0.941	0.940	0.937	0.930	0.919	0.912
0.0845	0.895	0.894	0.889	0.877	0.858	0.845
0.1065	0.839	0.838	0.830	0.813	0.785	0.767
0.1285	0.776	0.775	0.765	0.742	0.705	0.682
0.1506	0.709	0.707	0.695	0.667	0.623	0.597
0.1726	0.641	0.639	0.624	0.592	0.543	0.514
0.1946	0.574	0.571	0.555	0.520	0.469	0.439
0.2166	0.510	0.507	0.490	0.454	0.402	0.373
0.2387	0.451	0.448	0.431	0.394	0.345	0.319
0.2607	0.398	0.395	0.378	0.343	0.298	0.275
0.2827	0.352	0.349	0.332	0.300	0.260	0.241
0.3047	0.312	0.309	0.294	0.264	0.231	0.215
0.3268	0.278	0.275	0.261	0.236	0.208	0.196
0.3488	0.249	0.247	0.235	0.213	0.191	0.181
0.3708	0.225	0.223	0.213	0.195	0.177	0.169
0.3928	0.205	0.204	0.195	0.181	0.166	0.158
0.4149	0.188	0.187	0.180	0.168	0.155	0.147
0.4369	0.174	0.172	0.167	0.157	0.145	0.136
0.4589	0.161	0.160	0.155	0.147	0.135	0.126
0.4810	0.149	0.148	0.144	0.137	0.125	0.116
0.5030	0.139	0.138	0.135	0.128	0.115	0.106
0.5250	0.129	0.129	0.126	0.119	0.106	0.098
0.5470	0.120	0.120	0.117	0.111	0.098	0.090
0.5691	0.112	0.112	0.109	0.103	0.091	0.084
0.5911	0.105	0.104	0.102	0.096	0.085	0.079
0.6131	0.098	0.098	0.095	0.090	0.080	0.075
0.6351	0.092	0.092	0.089	0.084	0.076	0.072
0.6572	0.087	0.086	0.084	0.079	0.072	0.068
0.6792	0.082	0.081	0.079	0.074	0.069	0.065
0.7012	0.077	0.077	0.075	0.070	0.066	0.062
0.7232	0.073	0.073	0.070	0.067	0.063	0.059
0.7453	0.069	0.069	0.067	0.064	0.060	0.056
0.7673	0.066	0.065	0.063	0.061	0.057	0.053
0.7893	0.062	0.062	0.060	0.058	0.054	0.050
0.8113	0.059	0.059	0.057	0.055	0.051	0.048
0.8334	0.056	0.056	0.054	0.052	0.049	0.045
0.8554	0.054	0.053	0.052	0.050	0.046	0.043
0.8774	0.051	0.051	0.049	0.048	0.044	0.042
0.8994	0.049	0.049	0.047	0.045	0.042	0.040
0.9215	0.047	0.046	0.045	0.043	0.041	0.039
0.9435	0.045	0.044	0.043	0.042	0.039	0.037
0.9655	0.043	0.043	0.041	0.040	0.038	0.036
0.9876	0.041	0.041	0.040	0.038	0.036	0.035
1.0096	0.039	0.039	0.038	0.037	0.035	0.033
1.0316	0.038	0.038	0.037	0.035	0.033	0.031
1.0536	0.036	0.036	0.035	0.034	0.032	0.030
1.0757	0.035	0.035	0.034	0.032	0.031	0.028
1.0977	0.033	0.033	0.032	0.031	0.029	0.027
1.1197	0.032	0.032	0.031	0.030	0.028	0.026
1.1417	0.031	0.031	0.030	0.029	0.027	0.025
1.1638	0.030	0.029	0.029	0.027	0.025	0.024
1.1858	0.028	0.028	0.028	0.026	0.024	0.023
1.2078	0.027	0.027	0.027	0.025	0.023	0.023
1.2298	0.026	0.026	0.026	0.024	0.023	0.022
1.2519	0.025	0.025	0.025	0.023	0.022	0.022
1.2739	0.025	0.024	0.024	0.022	0.021	0.021
1.2959	0.024	0.024	0.023	0.022	0.021	0.021
1.3179	0.023	0.023	0.022	0.021	0.021	0.021
1.3400	0.022	0.022	0.022	0.021	0.021	0.021
1.3620	0.022	0.021	0.021	0.020	0.020	0.022
1.3840	0.021	0.021	0.020	0.020	0.020	0.022
1.4061	0.021	0.020	0.020	0.019	0.021	0.022
1.4281	0.020	0.020	0.020	0.019	0.021	0.023
1.4501	0.020	0.020	0.019	0.019	0.021	0.023
1.4721	0.019	0.019	0.019	0.019	0.021	0.023

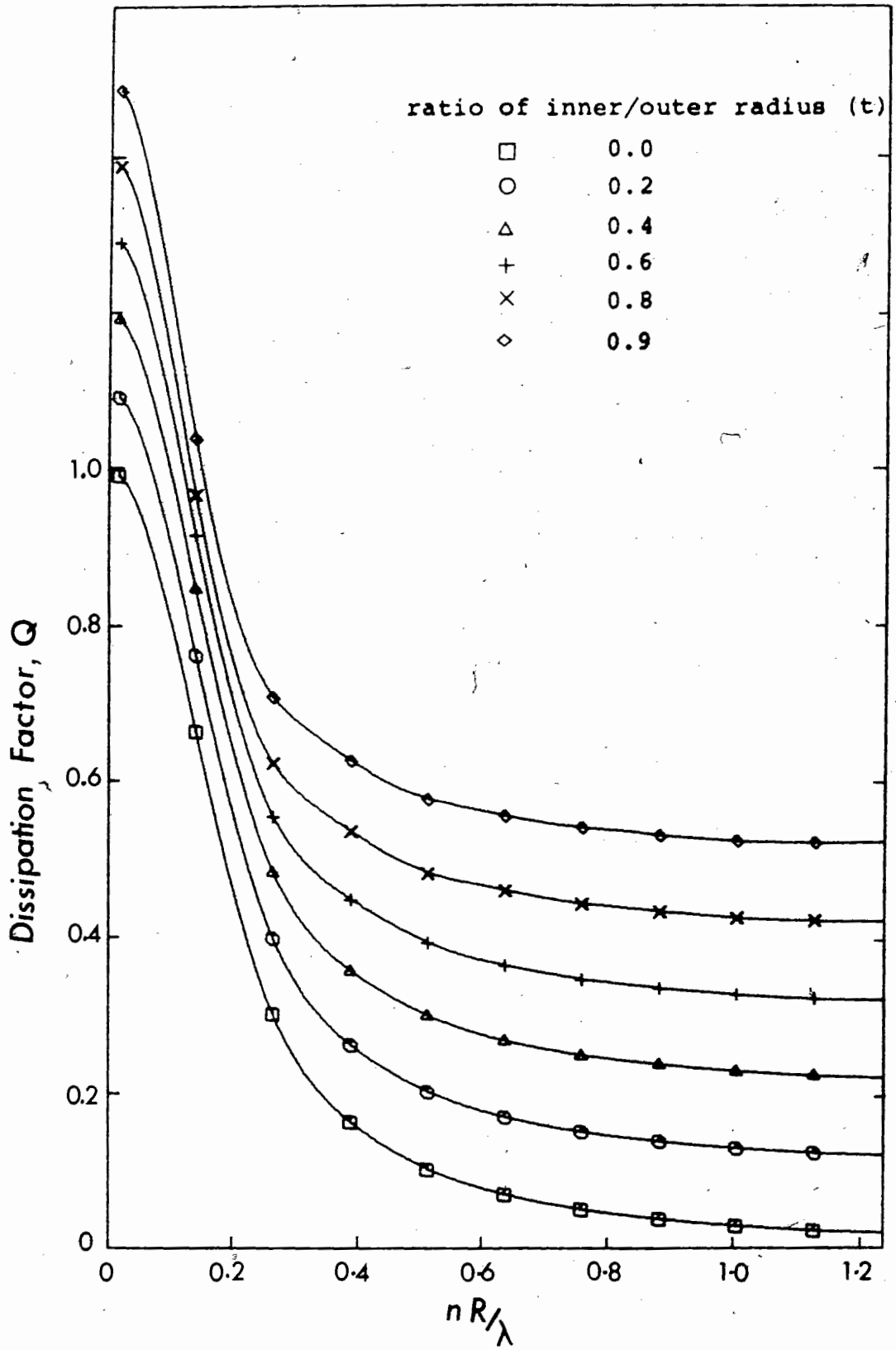

Fig.A1.3 Plot of dissipation factor as a function of size parameter for single lecithin shell vesicles. Note that that the baselines of the curves are displaced 0.1 unit from one another.

Table A1.4 Power factor as a function of size parameter

BETA VERSUS N*R/LAMBDA

N*R/LAMBDA	RATIO OF INNER/OUTER RADIUS: 0.0	0.20	0.40	0.60	0.80	0.90
0.0184	0.07	0.07	0.07	0.07	0.20	0.18
0.0404	0.04	0.04	0.04	0.04	0.06	0.04
0.0625	0.12	0.12	0.12	0.15	0.15	0.16
0.0845	0.22	0.22	0.23	0.26	0.30	0.33
0.1065	0.34	0.35	0.36	0.40	0.47	0.52
0.1285	0.49	0.49	0.52	0.58	0.67	0.74
0.1506	0.65	0.66	0.69	0.77	0.89	0.97
0.1726	0.83	0.84	0.88	0.97	1.12	1.21
0.1946	1.01	1.02	1.07	1.17	1.33	1.41
0.2166	1.18	1.19	1.25	1.36	1.51	1.58
0.2387	1.34	1.35	1.41	1.52	1.63	1.67
0.2607	1.48	1.49	1.54	1.63	1.68	1.66
0.2827	1.58	1.58	1.63	1.67	1.64	1.57
0.3047	1.64	1.64	1.67	1.66	1.53	1.42
0.3268	1.66	1.67	1.66	1.59	1.40	1.29
0.3488	1.66	1.66	1.62	1.50	1.27	1.17
0.3708	1.63	1.62	1.57	1.40	1.19	1.15
0.3928	1.60	1.59	1.51	1.33	1.19	1.22
0.4149	1.57	1.56	1.47	1.30	1.25	1.35
0.4369	1.56	1.55	1.46	1.32	1.38	1.52
0.4589	1.57	1.56	1.48	1.39	1.54	1.71
0.4810	1.60	1.59	1.52	1.49	1.71	1.86
0.5030	1.64	1.63	1.58	1.61	1.84	1.94
0.5250	1.69	1.68	1.66	1.72	1.93	1.94
0.5470	1.74	1.73	1.73	1.82	1.94	1.86
0.5691	1.77	1.77	1.79	1.88	1.89	1.71
0.5911	1.80	1.80	1.83	1.90	1.77	1.54
0.6131	1.81	1.81	1.85	1.89	1.64	1.40
0.6351	1.81	1.82	1.85	1.85	1.51	1.33
0.6572	1.80	1.81	1.85	1.79	1.42	1.34
0.6792	1.79	1.81	1.83	1.74	1.40	1.42
0.7012	1.79	1.80	1.82	1.69	1.44	1.56
0.7232	1.79	1.80	1.81	1.66	1.53	1.72
0.7453	1.80	1.81	1.81	1.67	1.65	1.85
0.7673	1.81	1.82	1.82	1.69	1.78	1.94
0.7893	1.83	1.84	1.83	1.73	1.88	1.95
0.8113	1.85	1.85	1.84	1.78	1.93	1.89
0.8334	1.86	1.86	1.85	1.82	1.92	1.77
0.8554	1.87	1.86	1.85	1.85	1.87	1.63
0.8774	1.87	1.86	1.85	1.87	1.79	1.51
0.8994	1.87	1.86	1.85	1.88	1.70	1.46
0.9215	1.87	1.86	1.85	1.87	1.63	1.49
0.9435	1.87	1.86	1.85	1.87	1.60	1.59
0.9655	1.88	1.86	1.86	1.87	1.63	1.76
0.9876	1.89	1.87	1.88	1.88	1.71	1.97
1.0096	1.91	1.89	1.90	1.89	1.84	2.17
1.0316	1.93	1.92	1.93	1.92	1.98	2.32
1.0536	1.96	1.95	1.96	1.97	2.13	2.41
1.0757	1.99	1.99	1.99	2.02	2.26	2.42
1.0977	2.02	2.02	2.02	2.07	2.35	2.35
1.1197	2.05	2.05	2.05	2.12	2.39	2.21
1.1417	2.07	2.08	2.08	2.16	2.37	2.04
1.1638	2.09	2.10	2.09	2.19	2.30	1.84
1.1858	2.10	2.11	2.11	2.21	2.18	1.64
1.2078	2.10	2.11	2.11	2.21	2.02	1.42
1.2298	2.10	2.11	2.10	2.19	1.83	1.18
1.2519	2.08	2.08	2.08	2.14	1.62	0.89
1.2739	2.04	2.05	2.04	2.05	1.36	0.55
1.2959	1.99	1.99	1.98	1.94	1.08	0.18
1.3179	1.92	1.92	1.90	1.78	0.77	-0.21
1.3400	1.83	1.83	1.80	1.60	0.44	-0.57
1.3620	1.73	1.73	1.69	1.40	0.12	-0.83
1.3840	1.62	1.61	1.56	1.18	-0.17	-0.95
1.4061	1.51	1.50	1.42	0.97	-0.40	-0.90
1.4281	1.40	1.39	1.30	0.77	-0.53	-0.65
1.4501	1.31	1.29	1.18	0.61	-0.54	-0.22
1.4721	1.23	1.21	1.09	0.49	-0.43	0.38

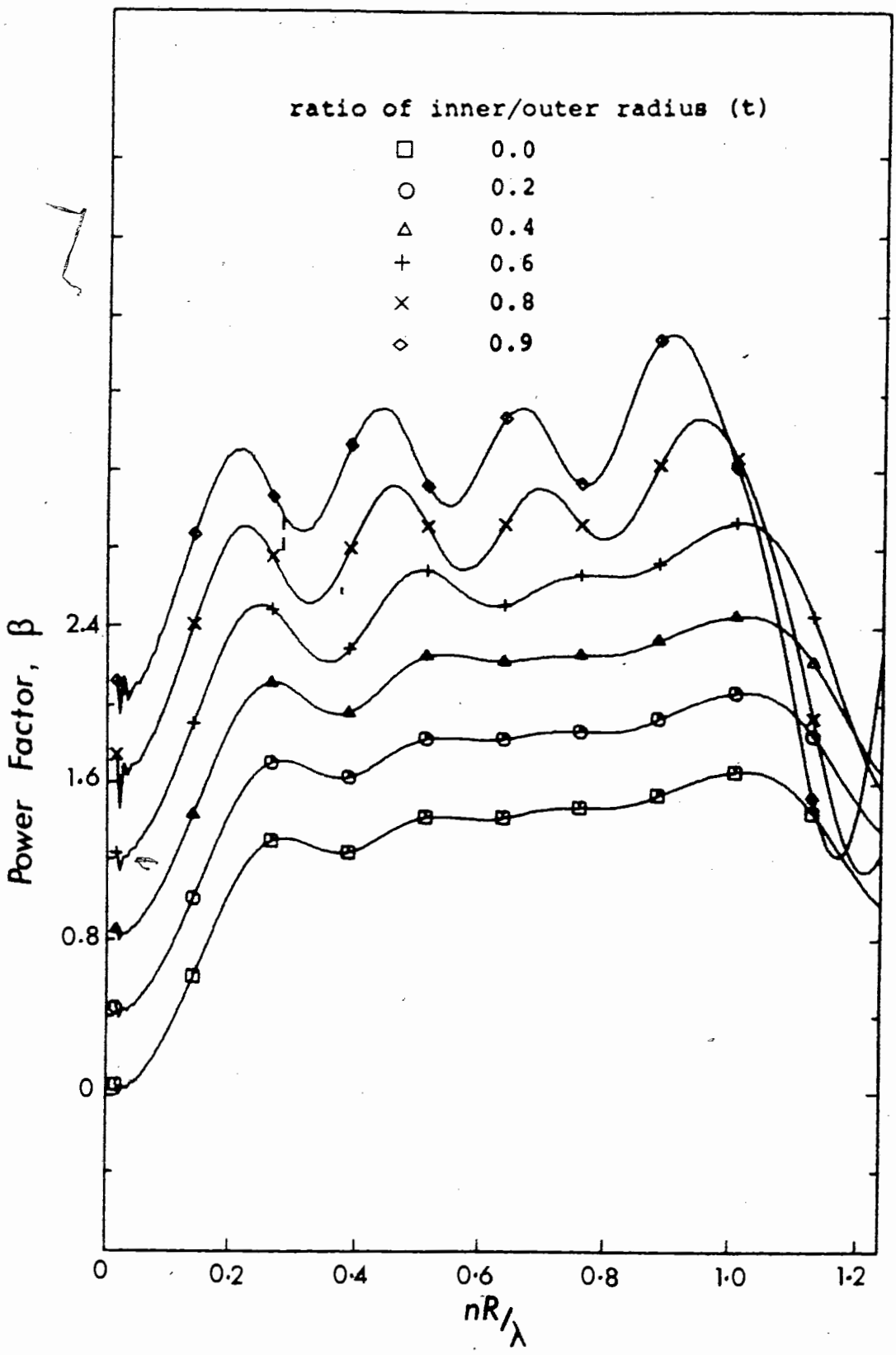

Fig. A1.4 Plot of the power factor as a function of size parameter for single lecithin shell vesicles.

Table A1.5 Specific turbidity as a function of size parameter

T * (10**5) VERSUS N*R/LAMBDA

N*R/LAMBDA	RATIO OF INNER/OUTER RADIUS: 0.0	0.20	0.40	0.60	0.80	0.90
0.0184	0.00	0.00	0.00	0.00	0.00	0.00
0.0404	0.04	0.04	0.04	0.03	0.02	0.01
0.0625	0.16	0.16	0.15	0.12	0.08	0.04
0.0845	0.37	0.37	0.35	0.29	0.18	0.10
0.1065	0.70	0.70	0.65	0.53	0.32	0.17
0.1285	1.14	1.13	1.05	0.86	0.51	0.27
0.1506	1.68	1.66	1.54	1.24	0.72	0.38
0.1726	2.29	2.26	2.08	1.66	0.95	0.50
0.1946	2.94	2.90	2.66	2.09	1.17	0.61
0.2166	3.60	3.55	3.24	2.51	1.38	0.71
0.2387	4.26	4.20	3.80	2.92	1.59	0.81
0.2607	4.90	4.82	4.35	3.31	1.79	0.92
0.2827	5.51	5.43	4.88	3.69	1.99	1.02
0.3047	6.12	6.02	5.40	4.07	2.21	1.15
0.3268	6.72	6.61	5.92	4.48	2.46	1.29
0.3488	7.33	7.21	6.47	4.93	2.75	1.44
0.3708	7.97	7.84	7.05	5.42	3.06	1.62
0.3928	8.63	8.50	7.67	5.96	3.40	1.80
0.4149	9.33	9.19	8.33	6.54	3.75	1.97
0.4369	10.04	9.90	9.02	7.13	4.09	2.14
0.4589	10.78	10.63	9.73	7.73	4.41	2.29
0.4810	11.51	11.36	10.44	8.32	4.70	2.42
0.5030	12.25	12.09	11.14	8.88	4.97	2.54
0.5250	12.96	12.81	11.82	9.40	5.21	2.66
0.5470	13.67	13.51	12.47	9.88	5.44	2.78
0.5691	14.36	14.19	13.09	10.34	5.68	2.92
0.5911	15.03	14.85	13.70	10.78	5.94	3.08
0.6131	15.71	15.52	14.29	11.22	6.23	3.26
0.6351	16.38	16.18	14.88	11.68	6.55	3.45
0.6572	17.07	16.85	15.48	12.16	6.91	3.65
0.6792	17.76	17.52	16.08	12.67	7.28	3.86
0.7012	18.46	18.20	16.70	13.20	7.66	4.05
0.7232	19.16	18.89	17.32	13.76	8.02	4.22
0.7453	19.87	19.58	17.95	14.32	8.37	4.37
0.7673	20.57	20.27	18.58	14.88	8.68	4.51
0.7893	21.27	20.95	19.21	15.43	8.97	4.65
0.8113	21.96	21.63	19.84	15.97	9.25	4.79
0.8334	22.64	22.30	20.46	16.49	9.52	4.94
0.8554	23.32	22.97	21.09	17.00	9.79	5.12
0.8774	24.00	23.65	21.71	17.50	10.09	5.31
0.8994	24.68	24.32	22.34	17.99	10.41	5.51
0.9215	25.36	25.01	22.97	18.49	10.76	5.72
0.9435	26.05	25.69	23.60	18.99	11.12	5.92
0.9655	26.73	26.38	24.23	19.49	11.48	6.10
0.9876	27.42	27.06	24.85	19.99	11.83	6.26
1.00996	28.09	27.73	25.47	20.49	12.15	6.39
1.0316	28.75	28.39	26.07	20.98	12.43	6.49
1.0536	29.40	29.03	26.66	21.45	12.68	6.57
1.0757	30.03	29.65	27.23	21.90	12.89	6.65
1.0977	30.64	30.26	27.78	22.33	13.07	6.74
1.1197	31.23	30.84	28.31	22.73	13.23	6.83
1.1417	31.80	31.40	28.83	23.11	13.39	6.95
1.1638	32.37	31.95	29.33	23.48	13.56	7.10
1.1858	32.92	32.49	29.83	23.83	13.76	7.27
1.2078	33.47	33.03	30.33	24.18	14.00	7.48
1.2298	34.02	33.56	30.82	24.53	14.28	7.71
1.2519	34.57	34.11	31.33	24.90	14.61	7.99
1.2739	35.15	34.67	31.85	25.30	15.01	8.32
1.2959	35.75	35.26	32.40	25.75	15.48	8.72
1.3179	36.39	35.89	32.99	26.25	16.05	9.18
1.3400	37.08	36.58	33.63	26.84	16.71	9.72
1.3620	37.84	37.32	34.34	27.52	17.48	10.33
1.3840	38.66	38.13	35.12	28.30	18.37	11.00
1.4061	39.55	39.02	35.97	29.18	19.36	11.71
1.4281	40.52	39.99	36.91	30.18	20.43	12.41
1.4501	41.57	41.03	37.94	31.28	21.57	13.07
1.4721	42.68	42.14	39.03	32.47	22.74	13.64

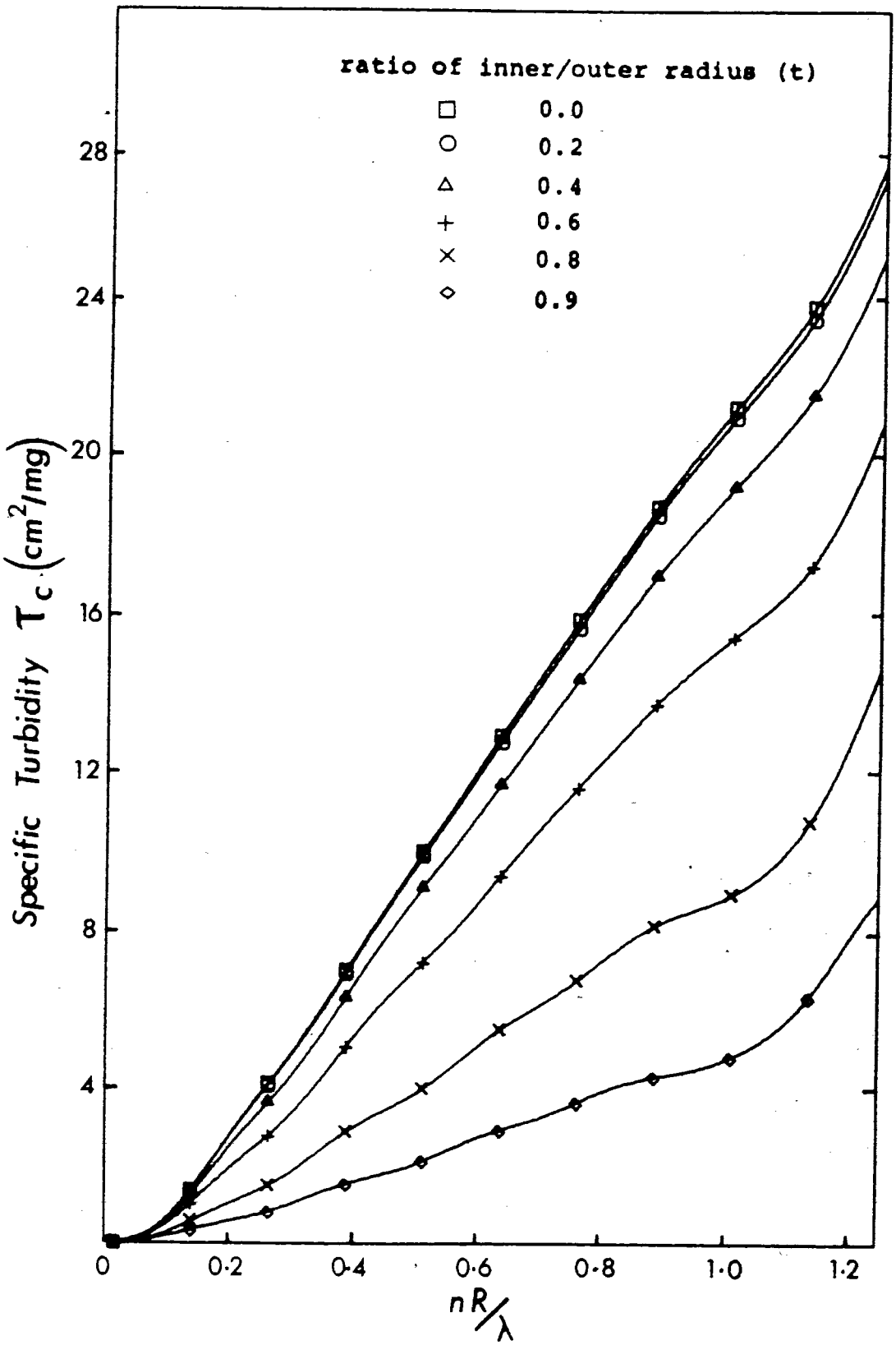

Fig. A1.5 Plot of specific turbidity as a function of size parameter for single lecithin shell vesicles.

APPENDIX 2

Computer Calculations for the Multilammelar Model

The computations are limited to 6 aqueous core radii and 50 concentric lecithin bilayers. The water layer thickness used was w = 25 Å and the lipid thickness l used was 45 Å. The computation starts with the form factor f using Eqn. 5.12. The calculated values of $P(\theta)$, $I(90^{o})/c$, Q, β and τ/c for the wavelength 366 nm are in Tables A2.1 to A2.5 and the plots are shown in Fig. A2.1 to Fig. A2.5. In the Tables, under each of the six values of R_o (inner aqueous core radius), the first column gives either kR or the size parameter. The second column shows the calculated values of $P(\theta)$ or the other quantities. Note that in Fig. 1,3, and 4 the origins of the curves for different core radii are displaced with respect to each other.

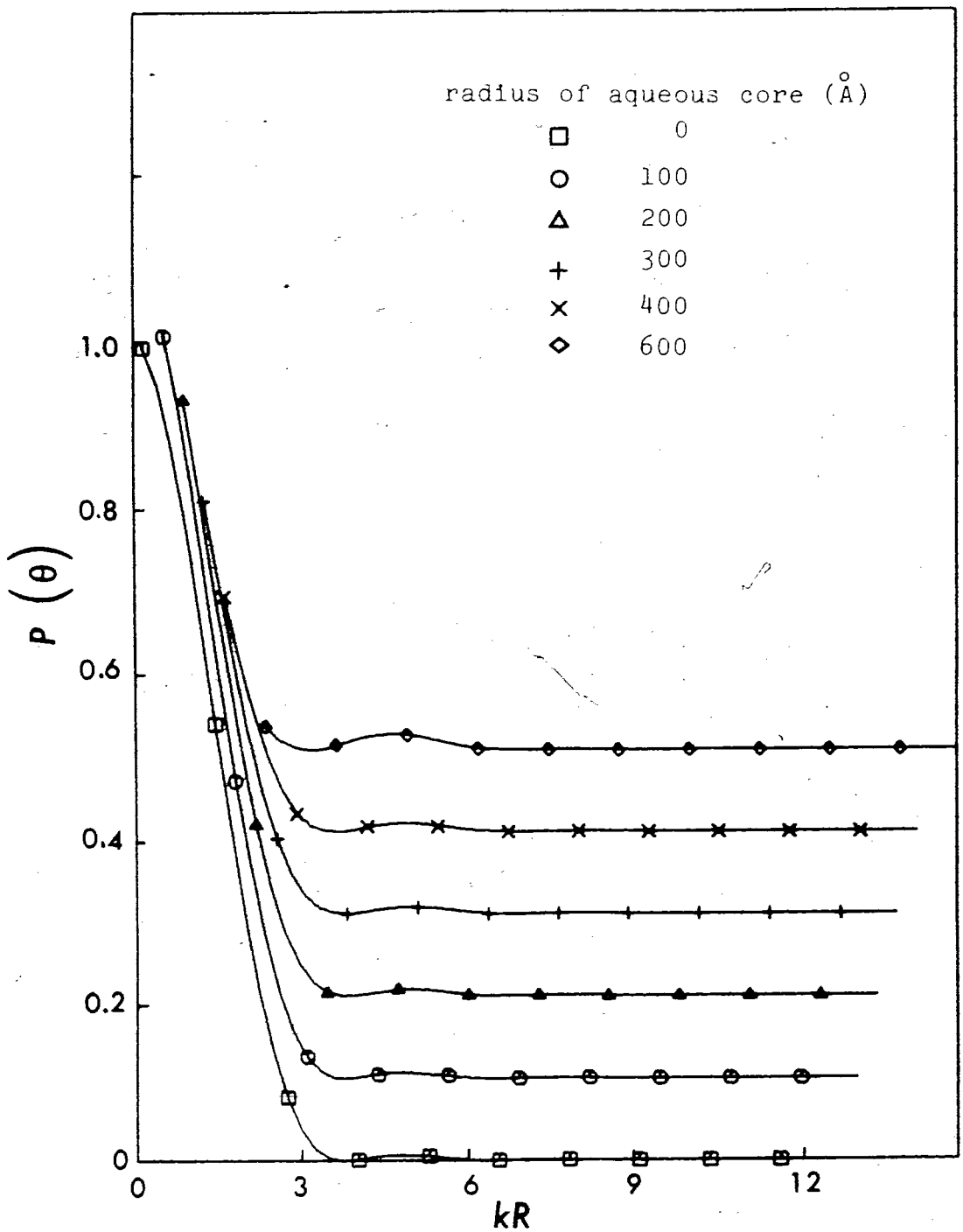

Fig. A2.1 Plot of scattering factor as a function of kR for multilamellar vesicles of different aqueous core radii.

Table A2.1 Scattering factor as a function of kr

WAVE LENGTH IS 366.
INNER RADIUS:

0.0		100.00		200.00		300.00		400.00		600.00	
0.1923	0.99263	0.6196	0.90729	1.0468	0.72893	1.4741	0.50455	1.9014	0.2*861	2.7559	0.03010
0.3914	0.96782	0.9136	0.82295	1.3459	0.62828	1.7732	0.40863	2.2005	0.21412	3.0550	0.01237
0.7905	0.87117	1.2177	0.71706	1.6450	0.51729	2.0723	0.31323	2.4996	0.14739	3.3541	0.00272
1.1896	0.77683	1.5168	0.59902	1.9441	0.40536	2.3714	0.22585	2.7987	0.09241	3.6532	0.00060
1.3887	0.65511	1.8159	0.47814	2.2432	0.30056	2.6705	0.15077	3.0978	0.05106	3.9523	0.00229
1.5877	0.53311	2.1150	0.36235	2.5423	0.20905	2.9696	0.09176	3.3959	0.02327	4.2514	0.00734
1.7868	0.41357	2.4141	0.25964	2.8414	0.13449	3.2687	0.04912	3.6950	0.00740	4.5505	0.01305
2.2859	0.30391	2.7132	0.17365	3.1405	0.07822	3.5678	0.02158	3.9951	0.00079	4.8496	0.01775
2.3850	0.20954	3.0123	0.10642	3.4396	0.03946	3.8669	0.00651	4.2941	0.00039	5.1487	0.02043
2.3841	0.13371	3.3114	0.05804	3.7387	0.01581	4.1660	0.00060	4.5932	0.00327	5.4478	0.02076
3.1832	0.07710	3.6105	0.02660	4.0378	0.00392	4.4651	0.00044	4.8923	0.00703	5.7469	0.01897
3.4823	0.03851	3.9096	0.00895	4.3369	0.00011	4.7642	0.00306	5.1914	0.01003	6.0460	0.01569
3.7814	0.01524	4.2087	0.00134	4.6360	0.00094	5.0632	0.00618	5.4905	0.01145	6.3451	0.01171
4.0805	0.00369	4.5078	0.00010	4.9351	0.00363	5.3623	0.00841	5.7896	0.01114	6.6442	0.00777
4.3796	0.00008	4.8069	0.00212	5.2342	0.00624	5.6614	0.00915	6.0887	0.00948	6.9433	0.00446
4.6787	0.00096	5.1060	0.00474	5.5333	0.00773	5.9605	0.00844	6.3878	0.00705	7.2424	0.00207
4.9778	0.00355	5.4051	0.00678	5.8323	0.00779	6.2596	0.00672	6.6969	0.00452	7.5415	0.00066
5.2769	0.00600	5.7042	0.00750	6.1314	0.00667	6.5587	0.00458	6.9860	0.00237	7.8406	0.00007
5.5760	0.00732	6.0033	0.00691	6.4305	0.00487	6.8578	0.00257	7.2851	0.00089	8.1397	0.00003
5.8751	0.00727	6.3024	0.00542	6.7296	0.00296	7.1569	0.00107	7.5842	0.00015	8.4387	0.00027
6.1742	0.00610	6.6014	0.00357	7.0287	0.00138	7.4560	0.00023	7.8833	0.00001	8.7378	0.00053
6.4733	0.00435	6.9005	0.00188	7.3278	0.00039	7.7551	0.00000	8.1824	0.00024	9.0369	0.00066
6.7724	0.00254	7.1996	0.00067	7.6269	0.00001	8.0542	0.00020	8.4815	0.00060	9.3360	0.00064
7.0715	0.00111	7.4987	0.00008	7.9260	0.00012	8.3533	0.00058	8.7806	0.00088	9.6351	0.00048
7.3706	0.00026	7.7978	0.00004	8.2251	0.00049	8.6524	0.00093	9.0797	0.00098	9.9342	0.00026
7.6696	0.00000	8.0969	0.00034	8.5242	0.00089	8.9515	0.00112	9.3788	0.00089	10.2333	0.00009
7.9687	0.00018	8.3960	0.00076	8.8233	0.00117	9.2506	0.00109	9.6779	0.00066	10.5324	0.00000
8.2678	0.00059	8.6951	0.00111	9.1224	0.00122	9.5497	0.00089	9.9769	0.00038	10.8315	0.00003
8.5669	0.00099	8.9942	0.00127	9.4215	0.00107	9.8488	0.00059	10.2760	0.00015	11.1306	0.00015
8.8660	0.00123	9.2933	0.00119	9.7206	0.00078	10.1479	0.00030	10.5751	0.00002	11.4297	0.00032
9.1651	0.00125	9.5924	0.00095	10.0197	0.00046	10.4470	0.00009	10.8742	0.00001	11.7288	0.00047
9.4642	0.00107	9.8915	0.00062	10.3188	0.00019	10.7460	0.00000	11.1733	0.00010	12.0279	0.00056
9.7633	0.00076	10.1906	0.00031	10.6179	0.00003	11.0451	0.00003	11.4724	0.00024	12.3270	0.00057
10.0624	0.00043	10.4897	0.00009	10.9170	0.00000	11.3442	0.00014	11.7715	0.00037	12.6261	0.00050
10.3615	0.00017	10.7888	0.00000	11.2161	0.00008	11.6433	0.00028	12.0706	0.00045	12.9252	0.00038
10.6606	0.00002	11.0879	0.00003	11.5152	0.00020	11.9424	0.00038	12.3697	0.00046	13.2243	0.00024
10.9597	0.00001	11.3870	0.00014	11.8142	0.00032	12.2415	0.00042	12.6688	0.00039	13.5234	0.00012
11.2588	0.00009	11.6861	0.00026	12.1133	0.00039	12.5406	0.00039	12.9679	0.00029	13.8225	0.00004

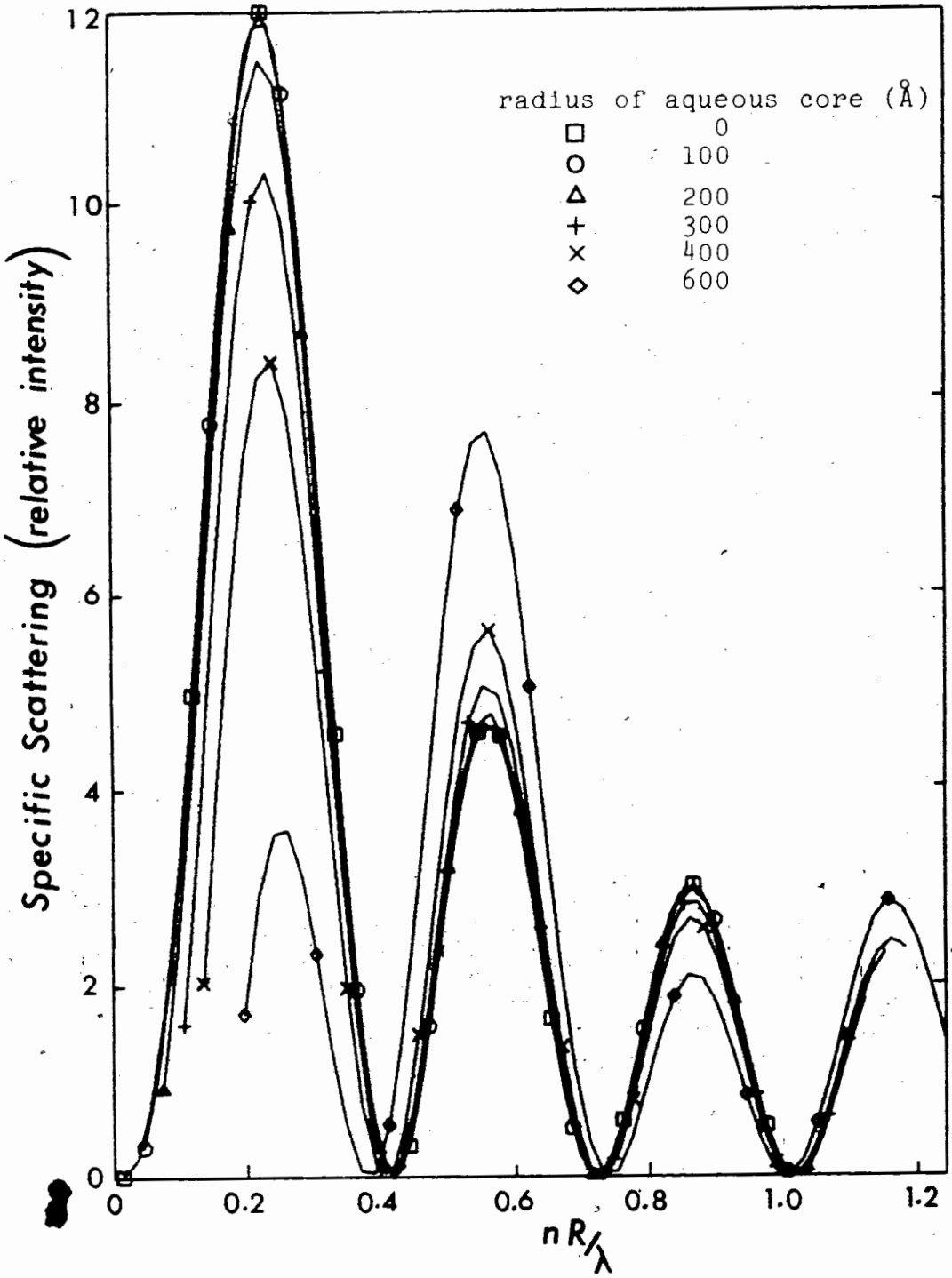

Fig. A2.2 Plot of specific scattering as a function of size parameter for multilamellar vesicles of different aqueous core radii.

Table A2.2 Specific scattering as a function of size parameter

I = (I**6) VERSUS X=R/LAMBDA

INNER RADIUS:

0.0		100.00		200.00		300.00		400.00		600.00	
0.0156	0.002	0.0534	0.040	0.0902	0.116	0.1270	0.198	0.1638	0.253	0.2374	0.212
0.0423	0.025	0.0791	0.131	0.1159	0.290	0.1527	0.437	0.1995	0.513	0.2631	0.344
0.0631	0.093	0.1049	0.250	0.1417	0.513	0.1765	0.694	0.2153	0.749	0.2889	0.443
0.0938	0.216	0.1307	0.413	0.1675	0.763	0.2043	0.938	0.2411	0.932	0.3147	0.446
0.1196	0.398	0.1554	0.724	0.1932	1.012	0.2300	1.136	0.2669	1.039	0.3404	0.390
0.1454	0.625	0.1822	0.976	0.2190	1.227	0.2578	1.262	0.2926	1.056	0.3662	0.289
0.1711	0.876	0.2079	1.207	0.2447	1.378	0.2815	1.299	0.3183	0.985	0.3920	0.173
0.1969	1.120	0.2337	1.365	0.2705	1.443	0.3073	1.242	0.3441	0.842	0.4177	0.071
0.2227	1.324	0.2595	1.458	0.2963	1.413	0.3331	1.100	0.3699	0.649	0.4435	0.010
0.2484	1.469	0.2852	1.491	0.3220	1.290	0.3588	0.895	0.3956	0.439	0.4692	0.006
0.2742	1.507	0.3110	1.461	0.3478	1.091	0.3846	0.657	0.4214	0.246	0.4950	0.068
0.2999	1.456	0.3367	1.226	0.3736	0.845	0.4104	0.420	0.4472	0.097	0.5208	0.191
0.3257	1.315	0.3623	0.949	0.3993	0.594	0.4361	0.217	0.4729	0.014	0.5465	0.357
0.3515	1.100	0.3880	0.723	0.4251	0.348	0.4619	0.073	0.4987	0.006	0.5723	0.543
0.3772	0.842	0.4140	0.454	0.4508	0.156	0.4876	0.005	0.5244	0.068	0.5981	0.721
0.4030	0.575	0.4398	0.243	0.4766	0.038	0.5134	0.015	0.5502	0.185	0.6238	0.864
0.4288	0.333	0.4656	0.087	0.5024	0.000	0.5392	0.091	0.5760	0.333	0.6496	0.949
0.4545	0.146	0.4913	0.009	0.5281	0.037	0.5649	0.214	0.6017	0.483	0.6753	0.964
0.4803	0.033	0.5171	0.010	0.5539	0.133	0.5907	0.356	0.6275	0.609	0.7011	0.909
0.5060	0.000	0.5428	0.060	0.5797	0.264	0.6165	0.469	0.6533	0.686	0.7269	0.793
0.5316	0.042	0.5686	0.196	0.6054	0.399	0.6422	0.588	0.6790	0.708	0.7526	0.635
0.5576	0.141	0.5944	0.330	0.6312	0.513	0.6680	0.636	0.7046	0.666	0.7784	0.457
0.5833	0.271	0.6201	0.456	0.6569	0.596	0.6937	0.625	0.7305	0.572	0.8042	0.287
0.6091	0.403	0.6459	0.547	0.6827	0.631	0.7195	0.559	0.7563	0.443	0.8299	0.146
0.6349	0.512	0.6717	0.598	0.7085	0.606	0.7453	0.452	0.7821	0.302	0.8557	0.049
0.6606	0.575	0.6974	0.572	0.7342	0.473	0.7710	0.322	0.8078	0.170	0.8814	0.004
0.6864	0.584	0.7232	0.504	0.7600	0.356	0.7968	0.194	0.8336	0.069	0.9072	0.008
0.7121	0.538	0.7489	0.399	0.7857	0.230	0.8226	0.089	0.8594	0.012	0.9330	0.049
0.7379	0.447	0.7747	0.276	0.8115	0.116	0.8483	0.021	0.8851	0.002	0.9587	0.113
0.7637	0.329	0.8005	0.158	0.8373	0.036	0.8741	0.000	0.9109	0.036	0.9845	0.180
0.7894	0.206	0.8262	0.064	0.8630	0.002	0.8998	0.024	0.9366	0.101	1.0102	0.233
0.8152	0.100	0.8520	0.010	0.8888	0.012	0.9256	0.064	0.9624	0.180	1.0360	0.261
0.8410	0.028	0.8778	0.002	0.9146	0.061	0.9514	0.164	0.9882	0.255	1.0618	0.257
0.8667	0.000	0.9035	0.038	0.9403	0.135	0.9771	0.247	1.0139	0.310	1.0875	0.224
0.8925	0.018	0.9293	0.106	0.9661	0.224	1.0029	0.314	1.0397	0.334	1.1133	0.170
0.9182	0.074	0.9550	0.192	0.9918	0.302	1.0287	0.353	1.0655	0.322	1.1391	0.106
0.9440	0.155	0.9808	0.275	1.0176	0.354	1.0544	0.356	1.0912	0.279	1.1648	0.049
0.9698	0.241	1.0066	0.341	1.0434	0.373	1.0802	0.323	1.1170	0.212	1.1906	0.011

7

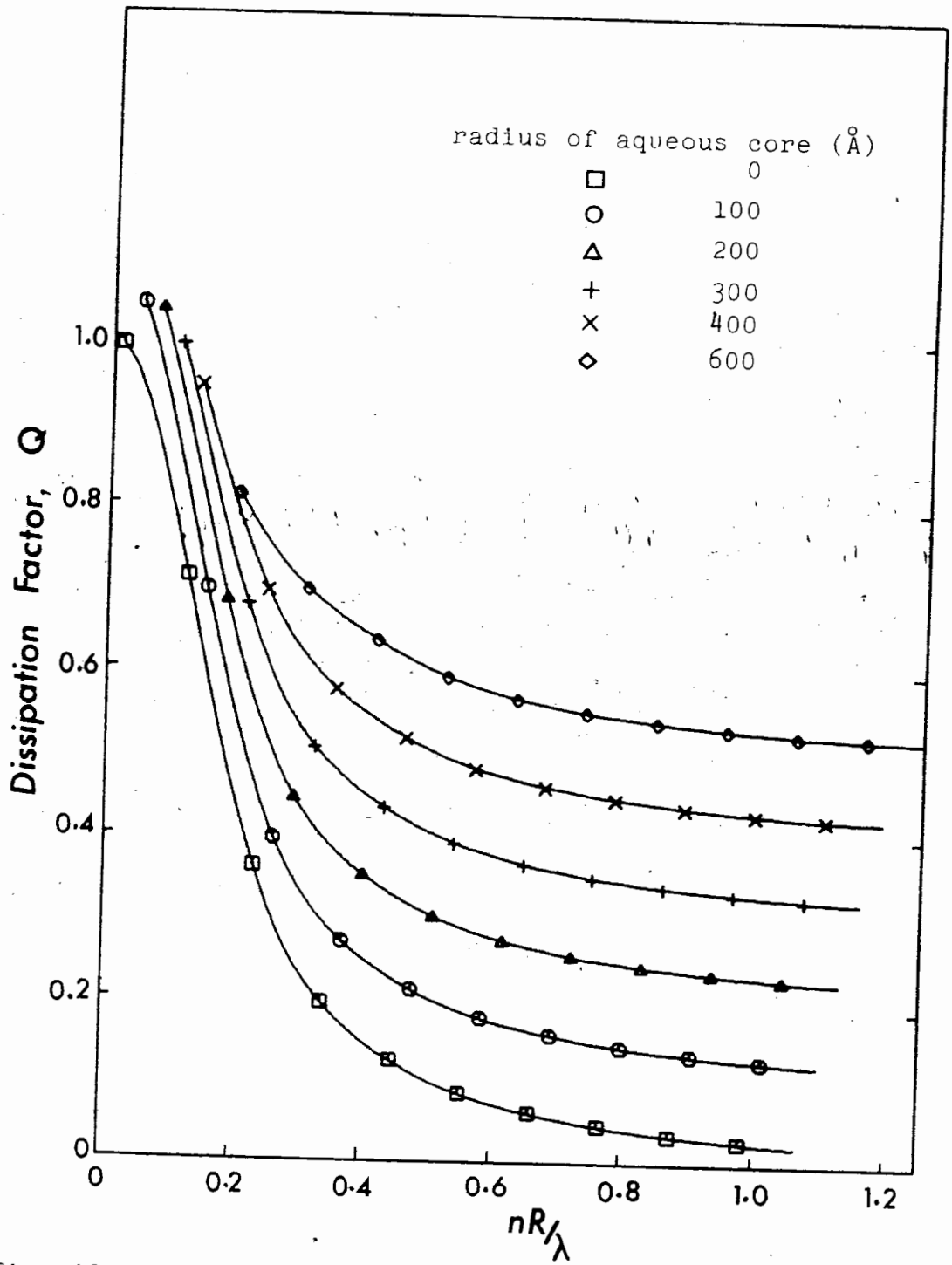

Fig. A2.3 Plot of dissipation factor as a function of size parameter for multilamellar vesicles of different aqueous core radii.

Table A2.3 Dissipation factor as a function of size parameter

Q VERSUS N=R/LAMBDA

INNER RADIUS=

0.0		100.00		200.00		300.00		400.00		600.00	
0.0166	0.9947	0.0534	0.9453	0.0902	0.8376	0.1270	0.6955	0.1638	0.5468	0.2374	0.3137
0.0423	0.9690	0.0791	0.8943	0.1159	0.7748	0.1527	0.6311	0.1895	0.4698	0.2631	0.2835
0.0681	0.9236	0.1049	0.8300	0.1417	0.7033	0.1785	0.5637	0.2153	0.4342	0.2889	0.2567
0.0938	0.8630	0.1307	0.7559	0.1675	0.6230	0.2043	0.4972	0.2411	0.3823	0.3147	0.2337
0.1196	0.7913	0.1564	0.6759	0.1932	0.5532	0.2300	0.4349	0.2668	0.3360	0.3404	0.2140
0.1454	0.7132	0.1822	0.5977	0.2190	0.4925	0.2558	0.3798	0.2926	0.2960	0.3662	0.1972
0.1711	0.6331	0.2079	0.5219	0.2447	0.4385	0.2815	0.3302	0.3183	0.2623	0.3920	0.1826
0.1969	0.5550	0.2337	0.4524	0.2705	0.3824	0.3073	0.2891	0.3441	0.2344	0.4177	0.1695
0.2227	0.4822	0.2595	0.3909	0.2963	0.3149	0.3331	0.2552	0.3699	0.2113	0.4435	0.1575
0.2484	0.4169	0.2852	0.3393	0.3220	0.2754	0.3588	0.2274	0.3956	0.1921	0.4692	0.1462
0.2742	0.3602	0.3110	0.2943	0.3478	0.2433	0.3846	0.2046	0.4214	0.1757	0.4950	0.1355
0.2999	0.3125	0.3367	0.2583	0.3736	0.2171	0.4104	0.1857	0.4472	0.1615	0.5208	0.1254
0.3257	0.2731	0.3625	0.2291	0.3993	0.1956	0.4361	0.1696	0.4729	0.1487	0.5465	0.1160
0.3515	0.2410	0.3883	0.2053	0.4251	0.1777	0.4619	0.1555	0.4987	0.1370	0.5723	0.1073
0.3772	0.2150	0.4140	0.1857	0.4508	0.1623	0.4876	0.1429	0.5244	0.1263	0.5981	0.0993
0.4030	0.1937	0.4398	0.1691	0.4766	0.1489	0.5134	0.1316	0.5502	0.1166	0.6238	0.0922
0.4288	0.1759	0.4656	0.1547	0.5024	0.1368	0.5392	0.1212	0.5760	0.1076	0.6496	0.0858
0.4545	0.1607	0.4913	0.1420	0.5281	0.1259	0.5649	0.1118	0.6017	0.0996	0.6753	0.0801
0.4803	0.1473	0.5171	0.1306	0.5539	0.1160	0.5907	0.1033	0.6275	0.0924	0.7011	0.0750
0.5060	0.1354	0.5428	0.1202	0.5797	0.1071	0.6165	0.0957	0.6533	0.0860	0.7269	0.0703
0.5318	0.1245	0.5686	0.1109	0.6054	0.0991	0.6422	0.0890	0.6790	0.0803	0.7526	0.0661
0.5576	0.1148	0.5944	0.1025	0.6312	0.0920	0.6680	0.0829	0.7048	0.0751	0.7784	0.0623
0.5833	0.1060	0.6201	0.0950	0.6569	0.0856	0.6937	0.0775	0.7305	0.0705	0.8042	0.0588
0.6091	0.0981	0.6459	0.0883	0.6827	0.0799	0.7195	0.0727	0.7563	0.0663	0.8299	0.0555
0.6349	0.0911	0.6717	0.0823	0.7085	0.0748	0.7453	0.0683	0.7821	0.0624	0.8557	0.0525
0.6606	0.0849	0.6974	0.0770	0.7342	0.0702	0.7710	0.0642	0.8078	0.0588	0.8814	0.0497
0.6864	0.0792	0.7232	0.0722	0.7600	0.0660	0.7968	0.0605	0.8336	0.0555	0.9072	0.0472
0.7121	0.0742	0.7489	0.0678	0.7857	0.0622	0.8226	0.0571	0.8594	0.0525	0.9330	0.0448
0.7379	0.0697	0.7747	0.0638	0.8115	0.0586	0.8483	0.0539	0.8851	0.0497	0.9587	0.0427
0.7637	0.0655	0.8005	0.0601	0.8373	0.0553	0.8741	0.0510	0.9109	0.0471	0.9845	0.0406
0.7894	0.0617	0.8262	0.0567	0.8630	0.0523	0.8998	0.0483	0.9366	0.0448	1.0102	0.0387
0.8152	0.0581	0.8520	0.0536	0.8888	0.0495	0.9256	0.0459	0.9624	0.0428	1.0360	0.0369
0.8410	0.0549	0.8778	0.0507	0.9146	0.0469	0.9514	0.0436	0.9882	0.0405	1.0618	0.0352
0.8667	0.0519	0.9035	0.0480	0.9403	0.0446	0.9771	0.0415	1.0139	0.0386	1.0875	0.0336
0.8925	0.0491	0.9293	0.0456	0.9661	0.0424	1.0029	0.0395	1.0397	0.0368	1.1133	0.0320
0.9182	0.0466	0.9550	0.0433	0.9918	0.0403	1.0287	0.0376	1.0655	0.0351	1.1391	0.0306
0.9440	0.0443	0.9808	0.0412	1.0176	0.0384	1.0544	0.0358	1.0912	0.0335	1.1648	0.0292
0.9698	0.0421	1.0066	0.0392	1.0434	0.0366	1.0802	0.0342	1.1170	0.0319	1.1906	0.0279

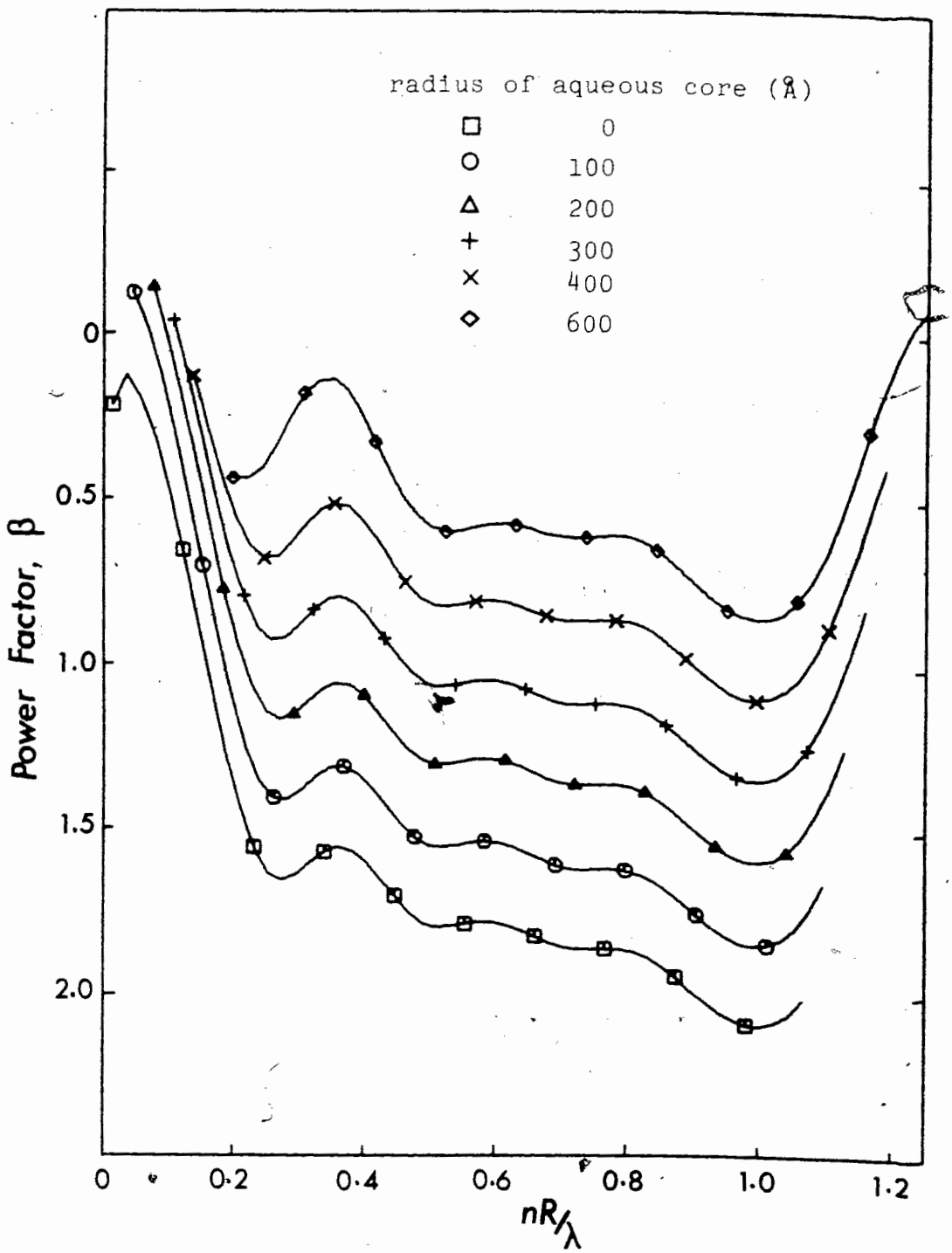

Fig. A2.4 Plot of power factor as a function of size parameter for multilamellar vesicles of different aqueous core radii.

Table A2.4 Power factor as a function of size parameter

BET. VERSUS N*R/LAMBDA

INNER RADIUS:

0.0		100.00		200.00		300.00		400.00		600.00	
0.0166	-0.201	0.0534	-0.114	0.0902	-0.344	0.1270	-0.696	0.1638	-1.113	0.2374	-1.678
0.0423	-0.110	0.0791	-0.217	0.1159	-0.497	0.1527	-0.866	0.1895	-1.272	0.2631	-1.678
0.0581	-0.132	0.1049	-0.363	0.1417	-0.672	0.1765	-1.051	0.2153	-1.424	0.2889	-1.641
0.0938	-0.300	0.1307	-0.540	0.1675	-0.869	0.2043	-1.239	0.2411	-1.546	0.3147	-1.570
0.1196	-0.460	0.1564	-0.735	0.1932	-1.073	0.2300	-1.403	0.2565	-1.633	0.3404	-1.489
0.1454	-0.648	0.1822	-0.944	0.2190	-1.268	0.2558	-1.538	0.2926	-1.673	0.3662	-1.417
0.1711	-0.852	0.2079	-1.153	0.2447	-1.431	0.2815	-1.634	0.3183	-1.667	0.3920	-1.376
0.1969	-1.063	0.2337	-1.342	0.2705	-1.559	0.3073	-1.672	0.3441	-1.623	0.4177	-1.372
0.2227	-1.259	0.2595	-1.500	0.2963	-1.639	0.3331	-1.685	0.3699	-1.569	0.4435	-1.409
0.2484	-1.427	0.2852	-1.605	0.3220	-1.666	0.3588	-1.626	0.3956	-1.525	0.4692	-1.477
0.2742	-1.557	0.3110	-1.656	0.3478	-1.649	0.3846	-1.581	0.4214	-1.504	0.4950	-1.566
0.2999	-1.635	0.3367	-1.659	0.3736	-1.613	0.4104	-1.547	0.4472	-1.513	0.5208	-1.657
0.3257	-1.659	0.3625	-1.633	0.3993	-1.575	0.4361	-1.539	0.4729	-1.554	0.5465	-1.738
0.3515	-1.642	0.3883	-1.594	0.4251	-1.555	0.4619	-1.562	0.4987	-1.616	0.5723	-1.795
0.3772	-1.605	0.4140	-1.565	0.4508	-1.550	0.4876	-1.610	0.5244	-1.682	0.5981	-1.830
0.4030	-1.572	0.4398	-1.559	0.4766	-1.593	0.5134	-1.667	0.5502	-1.745	0.6238	-1.842
0.4288	-1.555	0.4656	-1.590	0.5024	-1.644	0.5392	-1.725	0.5760	-1.790	0.6496	-1.838
0.4545	-1.567	0.4913	-1.624	0.5281	-1.699	0.5649	-1.774	0.6017	-1.813	0.6753	-1.826
0.4803	-1.601	0.5171	-1.679	0.5539	-1.750	0.5907	-1.804	0.6275	-1.819	0.7011	-1.818
0.5061	-1.652	0.5428	-1.732	0.5797	-1.785	0.6165	-1.815	0.6533	-1.814	0.7269	-1.816
0.5318	-1.706	0.5686	-1.774	0.6054	-1.802	0.6422	-1.810	0.6790	-1.805	0.7526	-1.824
0.5576	-1.754	0.5944	-1.799	0.6312	-1.803	0.6680	-1.802	0.7048	-1.799	0.7784	-1.836
0.5833	-1.786	0.6201	-1.806	0.6569	-1.795	0.6937	-1.795	0.7305	-1.803	0.8042	-1.849
0.6091	-1.799	0.6459	-1.801	0.6827	-1.786	0.7195	-1.796	0.7563	-1.816	0.8299	-1.858
0.6349	-1.798	0.6717	-1.793	0.7085	-1.784	0.7453	-1.805	0.7821	-1.832	0.8557	-1.862
0.6606	-1.791	0.6974	-1.788	0.7342	-1.790	0.7710	-1.823	0.8078	-1.847	0.8814	-1.860
0.6864	-1.783	0.7232	-1.790	0.7600	-1.806	0.7968	-1.841	0.8336	-1.860	0.9072	-1.854
0.7121	-1.782	0.7489	-1.803	0.7857	-1.825	0.8226	-1.858	0.8594	-1.866	0.9330	-1.853
0.7379	-1.791	0.7747	-1.821	0.8115	-1.844	0.8483	-1.867	0.8851	-1.864	0.9587	-1.859
0.7637	-1.807	0.8005	-1.841	0.8373	-1.858	0.8741	-1.871	0.9109	-1.863	0.9845	-1.875
0.7894	-1.828	0.8262	-1.859	0.8630	-1.865	0.8998	-1.868	0.9366	-1.862	1.0102	-1.899
0.8152	-1.846	0.8520	-1.870	0.8888	-1.865	0.9256	-1.866	0.9624	-1.866	1.0360	-1.934
0.8410	-1.861	0.8778	-1.875	0.9146	-1.864	0.9514	-1.869	0.9882	-1.881	1.0618	-1.975
0.8667	-1.867	0.9035	-1.872	0.9403	-1.864	0.9771	-1.881	1.0139	-1.907	1.0875	-2.014
0.8925	-1.867	0.9293	-1.871	0.9661	-1.871	1.0029	-1.902	1.0397	-1.942	1.1133	-2.050
0.9182	-1.864	0.9550	-1.875	0.9918	-1.887	1.0287	-1.931	1.0655	-1.979	1.1391	-2.079
0.9440	-1.865	0.9808	-1.887	1.0176	-1.914	1.0544	-1.965	1.0912	-2.016	1.1648	-2.101
0.9698	-1.874	1.0066	-1.908	1.0434	-1.948	1.0802	-2.002	1.1170	-2.051	1.1906	-2.110

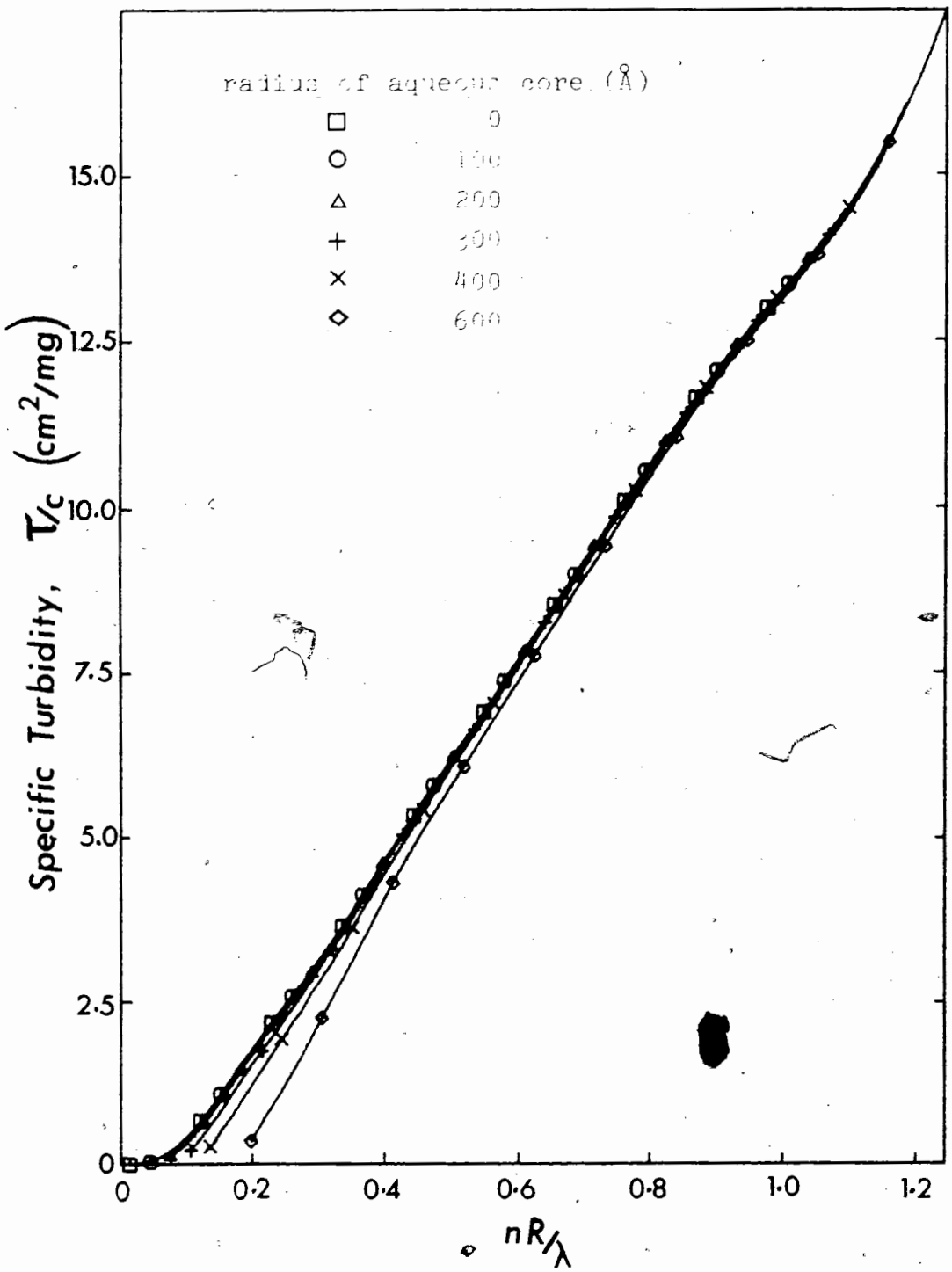

Fig. A2.5 Plot of specific turbidity as a function of size parameter for multilamellar vesicles of different aqueous core radii.

Table A2.5 Specific turbidity as a function of size parameter

T = 1.0-0.5I VERSUS X=R/LAMBDA

INNER RADIUS:

0.0		100.00		200.00		300.00		400.00		600.00	
0.0166	0.003	0.0534	0.067	0.102	0.194	0.1270	0.338	0.1638	0.456	0.2374	0.568
0.0423	0.043	0.0791	0.219	0.1179	0.490	0.1527	0.702	0.1995	0.964	0.2631	1.146
0.0681	0.155	0.1049	0.471	0.1437	0.877	0.1785	1.244	0.2153	1.496	0.2889	1.737
0.0938	0.364	0.1307	0.820	0.1675	1.332	0.2043	1.756	0.2411	2.032	0.3147	2.338
0.1196	0.672	0.1564	1.247	0.1932	1.826	0.2300	2.273	0.2668	2.560	0.3404	2.955
0.1454	1.068	0.1822	1.724	0.2190	2.332	0.2558	2.781	0.2926	3.080	0.3662	3.594
0.1711	1.526	0.2079	2.223	0.2447	2.859	0.2815	3.274	0.3183	3.599	0.3920	4.254
0.1969	2.020	0.2337	2.725	0.2705	3.310	0.3073	3.798	0.3441	4.125	0.4177	4.929
0.2227	2.52	0.2594	3.241	0.2963	3.776	0.3331	4.245	0.3599	4.674	0.4435	5.607
0.2484	3.058	0.2852	3.665	0.3220	4.238	0.3588	4.746	0.3956	5.243	0.4692	6.277
0.2742	3.677	0.3110	4.115	0.3478	4.710	0.3846	5.270	0.4214	5.831	0.4950	6.926
0.2999	3.933	0.3367	4.578	0.3736	5.201	0.4104	5.817	0.4472	6.429	0.5208	7.546
0.3257	4.356	0.3625	5.049	0.3993	5.718	0.4361	6.353	0.4729	7.027	0.5465	8.136
0.3515	4.850	0.3883	5.547	0.4251	6.259	0.4619	6.957	0.4987	7.613	0.5723	8.701
0.3772	5.336	0.4140	6.070	0.4508	6.814	0.4876	7.527	0.5244	8.180	0.5981	9.247
0.4030	5.848	0.4398	6.614	0.4766	7.374	0.5134	8.086	0.5502	8.726	0.6238	9.785
0.4288	6.354	0.4656	7.159	0.5024	7.928	0.5392	8.628	0.5760	9.255	0.6496	10.323
0.4545	6.934	0.4913	7.722	0.5281	8.469	0.5649	9.153	0.6017	9.774	0.6753	10.864
0.4803	7.489	0.5171	8.265	0.5539	8.995	0.5907	9.678	0.6275	10.289	0.7011	11.411
0.5060	8.037	0.5428	8.795	0.5797	9.509	0.6165	10.178	0.6533	10.809	0.7269	11.961
0.5318	8.572	0.5686	9.311	0.6054	10.017	0.6422	10.691	0.6790	11.334	0.7526	12.511
0.5576	9.094	0.5944	9.820	0.6312	10.526	0.6680	11.210	0.7046	11.867	0.7784	13.057
0.5833	9.604	0.6201	10.327	0.6569	11.040	0.6937	11.737	0.7305	12.402	0.8042	13.599
0.6091	10.111	0.6459	10.838	0.6827	11.552	0.7195	12.268	0.7563	12.937	0.8299	14.136
0.6349	10.621	0.6717	11.356	0.7085	12.091	0.7453	12.801	0.7821	13.468	0.8557	14.671
0.6606	11.135	0.6974	11.882	0.7342	12.622	0.7710	13.330	0.8078	13.993	0.8814	15.207
0.6864	11.656	0.7232	12.412	0.7600	13.152	0.7968	13.854	0.8336	14.515	0.9072	15.745
0.7121	12.186	0.7489	12.942	0.7857	13.677	0.8226	14.373	0.8594	15.033	0.9330	16.285
0.7379	12.717	0.7747	13.469	0.8115	14.195	0.8483	14.888	0.8851	15.553	0.9587	16.824
0.7637	13.246	0.8005	13.989	0.8373	14.709	0.8741	15.402	0.9109	16.075	0.9845	17.359
0.7894	13.769	0.8262	14.504	0.8630	15.220	0.8998	15.918	0.9366	16.599	1.0102	17.884
0.8152	14.286	0.8520	15.013	0.8888	15.733	0.9256	16.436	0.9624	17.123	1.0360	18.396
0.8410	14.798	0.8778	15.526	0.9146	16.247	0.9514	16.956	0.9882	17.643	1.0618	18.889
0.8667	15.308	0.9035	16.035	0.9403	16.764	0.9771	17.474	1.0139	18.154	1.0875	19.364
0.8925	15.820	0.9293	16.554	0.9661	17.281	1.0029	17.986	1.0397	18.682	1.1133	19.820
0.9182	16.334	0.9550	17.070	0.9918	17.794	1.0287	18.466	1.0655	19.133	1.1391	20.260
0.9440	16.850	0.9808	17.534	1.0176	18.297	1.0544	18.972	1.0912	19.597	1.1648	20.668
0.9698	17.365	1.0066	18.091	1.0434	18.738	1.0802	19.441	1.1170	20.044	1.1906	21.107

REFERENCES

Abramson, M.B. (1971) Biochim. Biophys. Acta 225, 167

Abramson, M.B. and Pisetsky, D. (1972) Biochim. Biophys. Acta 282, 80

Apostolov, K. and Poste, G. (1972) Microbiol 6, 247-261

Ashe, G.B. and Steim, J.M. (1971) Biochim. Biophys. Acta 233, 810

Atwood, D. and Saunders, L. (1965) Biochim. Biophys. Acta 225, 167

Badzhinyan, S.A., Dunin-Barkovskii, V.L., Kovalev, S.A. and Chailakhyan, L.M. (1971) Bio. Fizika 16, 1019

Bangham, A.D. (1968) Progress Biophys. and Mol. Biol., 18, 29

Bangham, A.D. and Horne, R.W. (1964) J. Mol. Biol. 8, 660

Barker, R.W., Bell, J.D., Radda, G.K. and Richards, R.E. (1972) Biochim. Biophys. Acta 260, 161

Batzri, S. and Korn, E.D. (1973) Biochim. Biophys. Acta 298, 1015

Benson, A.A. (1966) Journal of American Oil Chemical Society 43, 265

Blazyk, J.F. and Steim, J.M. (1972) Biochim. Biophys. Acta 266, 737

Blodgett, K.B. (1935) J. Am. Chem. Soc. 57, 1007

Bottcher, C.J.F. (1952) Theory of Electric Polarization, Elsevier, Amsterdam

Brooks, D.E. (1973) J. Coll. Int. Sci. 43, 714

Capaldi, R.A. (1974) Scientific American, p 27-33

Chapman, D., Fluck, D.J., Penkett, S.A. and Shipley, G.G. (1968) Biochim. Biophys. Acta 163, 255

Chapman, D., Williams, R.M. and Ladbrooke, B.D. (1967) Chem. Phys. Lipids 1, 445

Chong, C.S. (1975) Phd. Thesis, Simon Fraser University, Burnaby, B.C., Canada

Christensen, H.N. and Hastings, A.B. (1940) J. Biol. Chem. 136, 387

Colbow, K. (1973) Biochim. Biophys. Acta 318, 4-9

Curtis, A.S.G. (1962) Biological Reviews 37, 82

Danielli, J.F. and Davson, H. (1935) Journal of Cellular Compounds Physiology 5, 495-508

Debye, P. (1909) Ann. Physik 30, 57

Debye, P. (1915) Ann. Physik 46, 809

Drachev, L.A., Jasaltis, A.A., Kaulen, A.D., Kondrashin, A.A., Liberman, E.A., Nemecek, I.B., Ostromov, S.A., Semondv, A.Yu and Skulachev, V.P. (1974) Nature 249, 321

Doty, P. and Steiner, R.F. (1950) J. Chem. Phys. 18, 1211

Engleman, D.M. (1970) J. Mol. Biol. 47, 115

Gans, R. (1925) Ann. Physik 76, 29

Gorter, E. and Grendal, F. (1925) Journal of Experimental Medicine, p 439-443

Green, D.E. (1972) Mol. Basis Electron Trans., Proc. Miami Winter Symp. Acad., New York, 1-44

Green, D.E. and Perdue, J.F. (1966) Proc. of Natl. Acad. of Sci. of U.S., 55, 1295

Hanai, T., Haydon, D.A. and Taylor, J. (1965) Journal of Theoretical Biology, Vol 9, 278-296

Harris, H. (1970) Cell Fusion, Clarendon Press, Oxford

Hendler, R.W. (1971) Physiol. Rev. 51, 66

Henkert, P., Humphreys, S. and Humphreys, T. (1973) Biochemistry 12, 3045

Hinz, H. and Sturtevant, J.M. (1972) J. Mol. Chem. 247, 6071

Hirano, H., Parkhouse, B., Nicholson, G.L., Lennox, E.S. and Singer, S.J. (1972) Proc. Natl. Acad. Sci. U.S. 69, 2945

Huang, C. (1969) Biochemistry Vol 8, 344-351

Huang, C. and Thompson, T.E. (1965) Journal of Molecular Biology, Vol 13, 183

Hubbel, W.L. and McConnell, J.M. (1971) J. Amer. Chem. Soc. 93, 314

Hybl, A. and Dorset, D. (1970) Biopys. Soc. Abs. p 49a

Katchalsky, A., Danon, D., Nevd, A. and Vries, D. (1959) Biochim. Biophys. Acta 33, 120

Korn, E.D. (1966) Science 153, 1491-1498

Joos, R.W. and Carr, C.W. (1967) Proc. Soc. Exp. Med. 194, 1268

Kerker, M. (1969) The Scattering of Light, Academic Press, New York

Koch, A.L. (1961) Biochim. Biophys. Acta 51, 429

Koch, W. and Pike, F.H. (1910) J. Pharmacol, 2, 245

Ladbrooke, B.D. and Chapman, D. (1969) Chem. Phys. Lipids 3, 304

Lee, A.G., Bisdall, N.J.M., Levine, Y.K. and Metcalfe, J.C. (1972) Biochim. Biophys. Acta 255, 43

Lenhard, J. and Singer, S.J. (1966) Proc. Natl. Acad. Sci. U.S. 56, 1828

Liberman, Y.A. and Nenashev, V.A. (1972) Bio. Fizika 17, 1017

Lippert, J.L. and Peticolas, W.L. (1971) Proc. Nat. Acad. Sci. U.S. 68, 1572

Lucy, J.A. (1970) Nature 227, 815-817

Lucy, J.A. (1964) Journal of Theoretical Biology 7, 360-373

Luzzati, V. (1968) X-Ray Diffraction Studies of Lipid-Water Systems, Biological Membranes. (Physical Fact and Function) D. Chapman, Academic Press

Maeda, T.S., Ohnishi (1974) Biochemical and Biophysical Research Communications 60, 1509

Melchoir, D.L., Morowitz, H.I., Sturtevant, I.M. and Tsong, T.Y. (1970) Biochim. Biophys. Acta 219, 114

Mie, G. (1908) Ann. Physik 25, 377

Montal, M. and Muller, P. (1972) Proc. Natl. Acad. Sci. U.S. 69, 3561

Mueller, P., Rudin, D.O., Tien, H.T. and Wescott, W.C. (1964) Recent Progress in Surface Science 1, II

Nagasawa, J., Douglas, W.W. and Schulz, R.A. (1970) Nature 227, 407

Nagle, J.F. (1973) Proc. Natl. Acad. Sci. (USA) 70, 3443

Neher, E. (1974) Biochim. Biophys. Acta 373, 327-336

Neugebauer, T. (1943) Ann. Physik 42, 509

Ohki, S. (1969) J. Coll. and Inter. Sci. 30, 413

Oster, G. and Riley, D.P. (1952) Acta Cryst. 5, 1

Overath, P. and Trauble, H. (1973) Biochemistry 12, 2625

Papahadjopoulos, O., Poste, G., Schaeffer, B.E. and Vail, W.J. (1973) Biochim. Biophys. Acta 352, 10

Papahadopoulas, D., Poste, G., Schaeffer, B.E. and Vail, W.J. (1974) Membrane Fusion and Molecular Segregation in Phospholipid Vesicles 352, 10-28

Parsegian, A. (1974) 1974 Summer Institute On The Physics of Biological Membranes, Simon Fraser University

Pohl, G.W., Stark, G. and Trissl, H.W. (1973) Biochim. Biophys. Acta 318, 478

Poste, G. and Allison, A.C. (1971) J. Theor. Biol. 32, 165-184

Poste, G. and Allison, A.C. (1973) Membrane Fusion, Biochim. Biophys. Acta 300, 421-465

Prestegard, J.H. and Fellmeth, B. (1974) Biochem. 13, 1122-1126

Rayleigh, Lord (1914) Proc. Roy. Soc. (London) A90, 219

Reinert, J.C. and Steim, I.M. (1970) Science 168, 1580

Robertson, J.D. (1947) J. of Biophys. and Biochem. Cyt. 3, 1043-1047

Roth, S. (1973) Quarterly Review of Biology 48, 541

Sackmann, E. and Trauble, H. (1972) J. Amer. Chem. Soc. 94, 4482

Seimiya, T. and Ohki, S. (1972) Biochim. Biophys. Acta 298, 546

Seufert, W.D. (1970) Biophysik 7, 60

Shah, D.O. and Schulman, S.H. (1967) (a) J. of Lipid Research 8, 223

(b) J. of Lipid Research 8, 215

(c) J. of Lipid Research 6, 341 (1965)

Sheetz, M.P. and Chan, S. (1972) Biochem. 2, 4573

Singer, S.J. (1971) Structure and Function of Biological Membranes L.I. Rothfield (ed) Academic Press, New York, p 145

Singer, S.J. and Nicholson, G.L. (1972) The Fluid Mosaic of the Structure of Cell Membranes, Science 175, 720

Sjostrand, F.S. (1963a) Nature 199, 1262

Smith, A.D. (1972) Sci. Basis Med. Ann. Rev. 13, 74-102

Steim, J.M., Tourtellotte, M.E., Reinert, I.C., McElhaney, R.N. and Rader, R.L. (1969) Proc. Nat. Acad. Sci. U.S. 63, 104

Steinburg, M.S. (1962) Biological Interactions in Normal and Neoplastic Growth, M.J. Brennan and W.L.S. Simpson (eds), Little, Brown, Boston, p 127

Stoëckenius, W., Schulman, J.H., Prince, L.M. (1960) Kolloid, Z. 169, 170

Taupin, C. and McConnel, H.M. (1972) Mitochondria/Biomembranes. p 219, North-Holland, Amsterdam

Tinker, D.O. (1972) Chem. Phys. Lipids 8, 230

Trauble, H. (1971) Naturwissenschaften 58, 277

Trauble, H. and Eible, H. (1974) Proc. Nat. Acad. Sci. U.S. 71, 214

Trauble, H. and Haynes, D.H. (1971) Chem. Phys. Lipids 7, 324

Vanderkooi, G. (1972) Ann. N.Y. Acad. Sci. 195, 6

Wallach, D.F.H. and Zahler, P.H. (1966) Protein Conformations in Cellular Membranes. Proc. Natl. Acad. Sci. U.S. 56, 1552

Weiss, L. (1967) The Cell Periphery, Metastasis, and Other Contact Phenomena, North-Holland, Amsterdam

Yi, P.N. and MacDonald, R.C. (1973) Chem. Phys. Lipids 11, 114

Zimm, B.H. (1948) J. Chem. Phys. 16, 1099